MULTIPLE WAVE SCATTERING AND CALCULATED EFFECTIVE STIFFNESS AND WAVE PROPERTIES IN UNIDIRECTIONAL FIBER-REINFORCED COMPOSITES

Wenlung Liu

Dissertation submitted to the Faculty of the Virginia Polytechnic Institute and State University in partial fulfillment of the requirements for the degree of

DOCTOR OF PHILOSOPHY
in
Engineering Mechanics

Ronald D. Kriz, chair
Edmund G. Henneke
Robert A. Heller
John C. Duke
Robert L. West

May 13, 1997
Blacksburg, Virginia

Key words: wave propagation, multiple scattering, interphase, interfacial cracks, fiber-reinforced composites, quasi-crystalline approximation.

MULTIPLE WAVE SCATTERING AND CALCULATED EFFECTIVE STIFFNESS AND WAVE PROPERTIES IN UNIDIRECTIONAL FIBER-REINFORCED COMPOSITES

Wenlung Liu

(ABSTRACT)

Analytic methods of elastic wave scattering in fiber-reinforced composite materials are investigated in this study to calculate the effective static stiffness (axial shear modulus, μ) and wave properties (axially shear wave speed, B and attenuation, Ψ) in composites. For simplicity only out-of-plane shear waves are modeled propagating in a plane transverse to the fiber axis. Statistical averaging of a spatially random distribution of fibers is performed and a simultaneous system of linear equations are obtained from which the effective global wave numbers are numerically calculated. The wave numbers, $K=\mathrm{Re}(K)+i\mathrm{Im}(K)$, are complex numbers where the real parts are used to compute the effective axial shear static stiffness and wave speed; the imaginary parts are used to compute the effective axial shear wave attenuation in composites.

Three major parts of this study are presented. The first part is the discussion of multiple scattering phenomena in a successive-events scattering approach. The successive-events scattering approach is proven to be mathematically exact by comparing the results obtained by the many-bodies-single-event approach. Scattering cross-section is computed and comparison of the first five scattering orders is made. Furthermore, the ubiquitous quasi-crystalline approximation theorem is given a justifiable foundation in the fiber-matrix composite context. The second part is to calculate μ, B and Ψ for fiber-reinforced composites with interfacial layers between fibers and matrix. The material properties of the layers are assumed to be either linearly or exponentially distributed between the fibers and matrix. A concise formula is obtained where parameters can be computed using a computationally easy-to-program determinant of a square matrix. The numerical computations show, among other things, that the smoother (more divisional layers), or thinner, the interfacial region the less damped are the composite materials. Additionally composites with exponential order distribution of the interfacial region are more damped than the linear distribution ones. The third part is to calculate μ, B and Ψ for fiber-reinforced composites with interfacial cracks. The procedures and computational techniques are similar to those in the second part except that the singularity near the crack tip needs the Chebychev function as a series expansion to be adopted in the computation.

Both the interfacial layers and interfacial crack cases are analyzed in the low frequency range. The analytic results show that waves in both cases are attenuated and non-dispersive in

the low frequency range. The composites with interfacial layers are transversely isotropic, while composites with interfacial cracks are generally transversely anisotropic.

The author wishes to express gratitude for support provided by Virginia Tech's NSF Science and Technology Center for High performance Polymeric Adhesives and Composite, contract DMR9120004. Also, this work was partially supported by the National Center for Supercomputing Applications under grant number DMR950003N and utilized the computer system Silicon Graphics Power Challenge Array at the National Center for Supercomputing Applications, University of Illinois at Urbana-Champaign.

ACKNOWLEDGEMENT

The author wishes to thank the following for their contributions and invaluable advice during the formation of this work:

- Dr. Ronald D. Kriz for his leading me into this field and his being never discouraged encouraging me when I was overly self-effacing, and Mrs. Kaye Kriz's advice and corrections on the English writing.
- Drs. Edmond G. Henneke, Robert L. Heller, John C. Duke and Robert L. West for their taking time from busy schedule and serving as the committee members.
- Shelia Collins and Paula Lee for their efficiency in setting everything in order at Material Response Group and their kindness when I need more assistance from them.
- Cindy Hopkins of the ESM Department for her impeccable work coordinating the graduate student affair and her patience explaining every rules we need to follow so that we will have no trouble getting graduated.
- past MRG member Dr. Yong Li Xu, Boyt Stevens for the fruitful discussion on FEM work; and Dr. Nirmal Iyengar, Brendan Fabeny and Jyothi Jaganathan for their broad knowledge in answering my questions.
- Blair Russel for his leading me to the scuba diving sports and helping me on editing my resume so that I will be able to get a job easier.
- Mike Pastor for his inviting me to the card games and many occasions of enjoyable debate.
- B. K. Ahn, Hari Reddy, Celine Mahieux, Axinte Ionita and Fred McBagonluri for letting me understand the diversified cultures from all over the world.
- Dr. Scott Case, Stephan Phifer and James Loverich for their being nice MRG partner.
- those bodies from the same land we came from, Taiwan, for their sharing with me some good time and boring time.
- And finally my parents who's only wish is that I will be living happily and successfully.

TABLE OF CONTENTS

LIST OF FIGURES

MULTIPLE WAVE SCATTERING AND CALCULATED EFFECTIVE STIFFNESS AND WAVE PROPERTIES IN UNIDIRECTIONAL FIBER-REINFORCED COMPOSITES

CHAPTER 1. MOTIVATION AND BACKGROUND

Mechanics of wave propagation are used in many areas of research: seismology, biomedical applications, non-destructive evaluation (NDE) of materials, etc. The classical theories of wave propagation were developed extensively in the first half of this century. After WW II many new electronic devices were created that were capable of detecting stress waves in the field and in the laboratory. These devices revived the study of wave phenomena from an experimental viewpoint. In seismology, the study of wave scattering caused by the earth's non-uniform internal structure is a subject of interest for the mining the oil industry. Knowledge of elastic surface wave propagation that models seismic wave propagation across tectonic plates is essential for the assessment of earthquake damage. In biomedical applications, ultrasonic waves are used to display images of internal body organs and to perform prenatal examinations. Severity of osteoporosis, which is characterized by decreased density and enlarged porosity space in human bones, can be examined by ultrasonic equipment. In NDE, the use of scanning acoustic microscopy (SAM) is a perfect example for the nondestructive evaluation of materials. Through SAM, either with transmission microscopy or reflection microscopy, the information of stiffness, wave speed, attenuation and imperfection in materials can be obtained. Whatever the application, the understanding of wave mechanics in materials is essential for observing and reproducing waves and ultimately developing state-of-the-art detecting instruments.

From wave propagation studies in solids, materials are categorized as: 1. Isotropic or anisotropic. 2. Homogeneous or inhomogeneous. Waves in an isotropic, homogeneous medium are simply disturbances that depend on both time and position and that convey (transport) energy [1]. The progression of waves is either in shear mode (SH and SV; SH is the out-of-plane displacement with respect to the plane of propagation, SV is the in-plane shear wave with respect to the plane of propagation), where the wave normal is perpendicular to the polarized direction of particle movement, or in longitudinal mode (P), where the wave normal is parallel to the polarized direction of particle movement. Waves in an anisotropic medium are characterized by non-zero flux deviation angles formed by the energy flow direction and wave normal. Quasi-longitudinal (QL), quasi-transverse (QT) and pure shear (T) are three mode categories for waves in anisotropic media that exist only in principal material planes. Subjects for waves in anisotropic materials were extensively studied based on the knowledge of continuum mechanics and elasticity. Wave surfaces (velocity, slowness and energy) and their utility for interpretation of wave characteristics in polycrystalline and composite materials broaden our understanding of the dynamic properties of these materials [2-3]. Specifically, the physical significance of those analyses is that by measuring the wave speed for various directions across the specimen, the elastic constants and orientations of crystals can be obtained. Another important feature is the hypothesis that, in general, Rayleigh surface waves can be propagated in all directions with dissipation except in some directions where there is no dissipation [4]. More examples include: critical angle for reflection phenomena at a plane boundary between anisotropic media [5] and

wave-surface topological features describing the transverse-longitudinal mode conversion over a single surface [6].

Waves traveling in inhomogeneous media, due to the discontinuity of material properties and boundary geometries, are typically scattered. For plane waves in solids where component materials share common boundaries, reflection, refraction, diffraction and scattering occur. Reflection and refraction problems for inhomogeneous materials usually associate with the calculation of reflection and transmission coefficients and mode conversion and are considered trivial (unless they occur in an anisotropic medium). Problems of scattering or diffraction of plane waves by a single obstacle or many obstacles (elliptical, spherical inclusions or cylinders) have received attention by several researchers. Scattering of plane waves by a single obstacle was investigated and the methods of approaches were variously discussed. Method of separation of variables, for inclusions where the boundaries have strong geometrical symmetries (spherical inclusions or cylinders), is classical [7-8] for deriving expressions for scattered wave function and total scattering energy. For inclusions where strong geometrical symmetries do not exist (elliptic inclusions or cylinders), an alternative approach (such as matched asymptotic expansion- MAE [9]) can be applied. The so-called T-matrix method in wave scattering problems is also popular and can be easily extended to cases of many scatterers. Waterman [10] was the first researcher to introduce a transition matrix formulation for acoustic scattering by an object with arbitrary shape. Following his lead, cases of arbitrary number of scatterers and scattering of elastic waves using the same principle were developed [11-13]. Recently [14-15] a formulation of multi-centered, T-supermatrix approach was developed and then applied to a multi-layered acoustic medium. Finally the integral Equation method was perfected by many authors. Representative research by Pao and Varatharajulu [16] derived the Helmholtz- (for steady state waves) and Kirchhoff-type (for transient waves) integral formulae for elastic waves in isotropic and anisotropic solids. An instructive paper by Twersky [17] also used the integral Equation method for multiple scattering in three dimensions.

Other interesting aspects of wave propagation are: extinction cross-section (the sum of scattering and absorption cross section) which is a measure of attenuation in inhomogeneous media [7,18]; reciprocal relations for amplitudes (or for energy) of transmission and reflection waves for various kinds of interfaces, which is widely used for ultrasonic testing of materials [19-20]; causality and the dispersion relations expressing 1.) the speed as a function of frequency for homogeneous media, and 2.) the real part of a scattering amplitude as an integral involving the imaginary part (attenuation) for inhomogeneous media [21-23].

Theoretically no material is a pure homogeneous medium, since one can always go to the atomic or subatomic level to argue against the existence of one. Yet in the continuum mechanics perspective, particularly with respect to wave propagation, the bulk mechanical behavior of a material can be regarded as a criterion by which the medium is categorized as homogeneous or inhomogeneous. For the concept of homogenizing an inhomogeneous medium, a review paper by Hashin [24] surveyed the general theory for predicting bulk mechanical properties of inhomogeneous materials. Applying the same concept, elastic wave propagation in multi-phase

media can be justifiably homogenized and analyzed as one. For example, for plane waves in particulate- or fiber-matrix composites, effective average waves travel in rectilinear paths. In addition to the principal waves, scattering waves occur as a result of wave interactions between inclusions and matrix. Those waves in the rectilinear paths are commonly called coherent waves, and the scattering waves, which make up the non-constructive part, are the incoherent waves. In wave propagation analyses for composite materials, the media are usually regarded as homogeneous but attenuated as long as the wave length is long compared to the characteristic length of inclusions. It is homogeneous because, for long wave lengths, the waves are less sensitive to the existence of the inclusions, or less able to 'detect' the existence of the inclusions. It is attenuated because the scattering generated by inhomogenity is measured as attenuation.

The homogenization of heterogeneous media inevitably leads to the 'calculated moduli or properties' which are themselves a subject in the application of mechanical analyses. Representative papers by Hashin [25] and Hashin [26] presented an overview of the mechanical behavior of heterogeneous media. Hashin and Rosen [27] calculated the elastic moduli of heterogeneous materials. They also discussed the use of variational theorems of elasticity and calculated the bounds of elastic moduli for fiber-reinforced materials. Other papers by Hashin [28] and Hashin [29] developed the correspondence principle by which the visco-elastic properties of composites can be determined on the basis of analytic expressions for elastic moduli of composites. An alternative method to calculate the average properties (effective elastic moduli for static strength and wave speed and attenuation for dynamic characteristics) of a heterogeneous material is to use wave scattering. A pioneering and exemplary study by Foldy [30] investigated the multiple scattering of scalar waves by a random distribution of isotropic scatterers and calculated the average wave function and average flux carried by the wave. The randomness and configuration averaging concepts were introduced using a statistical ensemble technique. Later Waterman and Truell [31] used the same principle and obtained the forward-amplitude and extinction theorem of multiple scattering in heterogeneous materials. More significantly, an explicit expression for the complex propagation index was derived and shown to include properties for sufficiently low densities of anisotrpic obstacles. About the same time, two instructive and comprehensive papers written by Lax [32-33] dealt with many aspects of multiple wave scattering. They include, among others, coherence and incoherence, multiple scattering and many-bodies problems (topics which are closely related to this dissertation). Finally a review paper on multiple scattering of waves by Twersky [34] reported the root and contemporary activities and included a fairly comprehensive literature survey. Although [31-34] mostly applied to electromagnetics and optics, the philosophies and techniques they employed were evoked by many mechanics (acoustics and elasticity) researchers afterward and are currently used by this dissertation.

One of the catalysts for the renewed interest in wave propagation, indeed for the engineering mechanics discipline as a whole, is the use of composite materials in many industrial products. There are two kinds, among others, of composites: particulate-matrix and fiber-matrix composites [25]. Particulate-matrix composites are those where either spherical- or spheroid-shape inclusions occupy an otherwise matrix material. An example is concrete as a construction

material, where the gravel or pebbles (as inclusions) are s urrounded by the cement matrix. Thus a concrete composite consists of pebbles, cement and water. The water in this case acts as an adhesive agent between the pebbles and cement. The fiber-matrix composites are those with cylindrical fibers embedded in the matrix. While the particulate composites are globally isotropic and their order of strength depends on the volume fractions of the inclusions, the fiber-matrix composites are highly anisotropic; their design and manufacturing are relevant to mechanics analysis. The stiffness of a fiber-matrix composite (with continuous fibers) in the fiber direction is that of the order of fibers and it is the order of matrix in the transverse direction. Thus the laminated structure, where laminate composite slabs with unidirectional fibers are fabricated layer by layer in different orientations, is an improvement and compensates for the weakness in the transverse direction.

For the material characterization of composites, elastic wave propagation methods are indispensably effective. It is well established that multiple wave scattering theory in composite materials, when treated in a macroscopic (or effective global) viewpoint, leads to calculated effective global properties (static strength, wave speed and attenuation) of the composites. Many research papers were published in this concept based on the multiple scattering literature mentioned previously [30-34]. Bose and Mal [35], as the direct reference for this dissertation, studied the axial shear waves in one paper and the longitudinal and transverse shear waves in another for fiber-reinforced composites. In those papers, the so-called quasi-crystalline approximation was used and a correlation function was introduced to obtain the average propagation relationship. A recursive multiple scattering formula in terms of the displacement wave function was then obtained by which a homogeneous linear system of equations was derived and the average wave number--hence the static stiffness and dynamic propagation properties--could be calculated. Their procedures and principles are closely followed in our study. A similar methodology using various approaches was adopted in different cases by others [36-37]. Other methodologies worth mentioning include: the variational method [38]; the forward amplitude theorem outlined in [31], also used in [39], and in [40] where it was combined with the self consist model (GSCM) first introduced by Christensen [41] for the calculation of static elastic constants. The common feature of all those approaches is that they all lead to the same static bounds, thus confirming their applicability for waves in composites. Other than calculating effective moduli and wave properties, wave theories in fiber-reinforced composites take on many important aspects. Using various analysis techniques for numerous problem definitions, dynamic equation of motion and dispersion relations were studied from which certain mechanical properties could be drawn [42-51].

Wave methods applied in composites have been studied extensively. In spite of that, we shall, in the fiber-reinforced composites context, revisit some theories and lay out some new procedures. In this study, only fiber-matrix composites with identical, uni-directionally aligned and spatially random-distributed fibers are discussed. There will be three parts. The first part is the multiple elastic wave scattering aspect in fiber-reinforced composites. Multiple elastic wave scattering phenomena in fiber-reinforced composites are reexamined in order to lay out, as a prerequisite condition for material system homogenization, the quasi-crystalline approximation

from which a statistical technique can be suitably applied. This approximation was then used in the ensemble average procedure for the gradient-interface and interfacial cracks studies. Twersky [52-56] extensively studied multiple scattering of radiation by parallel cylinders for acoustics and eletromagnetics. His studies on multiple wave scattering and a 'self consistent field approach' are valuable references for this dissertation. The method therein of obtaining a formal solution of the scattering function—in the context of successive scattering orders expressed recursively in terms of previous orders—is modified in our study. This successive wave scattering concept was later used to justify the use of the quasi-crystalline approximation. In the successive-events approach, the boundary conditions (continuity of displacement and stress across the interface between fiber and matrix) are to be satisfied for each scattering event. The scattering wave functions are then summed for each fiber and for each consecutive scattering event to obtain the wave function in the composite field. An alternative method to calculate the scattering wave function in the composite field is the many-bodies approach for which the boundary conditions are to be satisfied simultaneously for all fiber-matrix interfaces. The result of this approach is a recursive formulation which can be expanded to obtain the same analytic expression as in the successive-events approach. The many-bodies formulation is the basis for constructing the ensemble average procedure which is used for calculation of global effective material properties for composites with interfacial layers and with interfacial cracks in the second and third part of this dissertation.

For the many-bodies approach, the procedure starts with the Helmholtz equation for harmonic waves in a steady state condition, followed by the application of the eigenfunction expansion of wave fields (displacements in our case). Then by setting up the boundary conditions for the multiple wave scattering problem, scattering coefficients can be obtained in a recursive fashion. Based on this recursive formula, configuration averaging of random distribution of fibers is performed. Finally the effective global wave number in the composites, at low frequencies range, can be extracted from a linear system of equations. For a fiber-reinforced composite, the average wave number is a complex number for which the average wave speed and attenuation can be deduced. Throughout this study, mainly the axially shear wave phase speed and attenuation are to be calculated. The axially shear modulus of the composites is just a by-product of the wave methods as the wave frequency goes to the static limit.

The second part is the study of waves in fiber-reinforced composites with gradient interfaces. For fiber-matrix composites, the interface between the fiber and matrix may play an important role in determining the overall properties of the system. An important study for the effect of interfacial zone on mechanical behavior of fiber-reinforced composites was given by Achenbach and Zhu [57]. For a static model, a spring-like discontinuous displacement mechanism for the interfacial area, combined with the numerical boundary integral method, was used by the authors to investigate the pronounced changes in stress distribution caused by variation of the interphase parameters. Later Xu and Datta [58] used a hybrid method combining the finite-element and eigenfunction expansions to study the characteristics of the fiber-matrix interface by guided waves. They showed the reduction of interfacial bond stiffness had a significant effect on the leaky waves. On the use of the NDE method to characterize interfacial

properties, Chu and Rokhlin [59], using the well established Christoffel equation and experimental data, devised a self-reference bulk wave model to characterize effective elastic properties of the interphase and the composites. In another paper [60], the same authors reported a method for the inverse determination of effective elastic moduli of the fiber-matrix interphase from experimentally measured composite moduli. The multiple-phase generalized self-consistent (MGSC) model is the theoretical basis for obtaining the analytic expression for the transverse shear modulus of a composite with multi-layered fibers. Huang et al [61] studied the fiber-matrix interphases effects on the scattering of elastic waves. This can be used for the relationship of attenuation of composites and the elastic properties of the interphases. In this study, we will employ (instead of the spring model of [57]) the continuous displacement and stress model for the interphase area between fiber and matrix. Further, instead of using the total transfer matrix method of [60], we will derive an analytic expression for the axially transverse shear modulus for our composites with multi-layered fibers using an alternative matrix method. The interfacial material properties depend on how the fiber and matrix were bonded. Usually the interphase is a chemical coating layer as a bonding agent. Yet for the sake of demonstrating the multiphase feature of our analyses, we will assume gradient characteristics for the interfacial region. That is, we will assume that the material properties of the interface is between fiber and matrix and that the elastic properties are continuously distributed—thus guaranteeing the continuity of stress and displacement through the interfacial regions. Two kinds of gradient functions are possible: linearly and exponentially gradient. The fact that the mechanical properties of the interphase might be visco-elastic can be assayed by using the correspondence principle, by which elastic properties of interface should be replaced by visco-elastic ones to obtain the overall effective quantities.

The third part of the dissertation is the wave method application on fiber-reinforced composites with interfacial cracks. The interfacial cracks may occur in components at the manufacturing stage or after use over time. The micro-defects in a fiber-matrix composite may be cracks in one or more of the three regions: matrix, fibers and matrix-fiber interface. In our case only debonds between fibers and matrix are to be analyzed, and only the circumferential cracks are considered. Furthermore, to make analysis simple, the cracks are infinitely extended along the fiber axis direction and each fiber has the same crack parameters (crack length and orientation).

Basic interfacial circular crack problems in static state have been studied by many researchers. Tamate and Yamada [62] applied the cylindrical axially transverse loads at an infinite distance away form the circular inclusion. Toya [63] studied the same problem except that the loads are applied under biaxial loads which are longitudinally transverse to the inclusions. The basic properties such as the stress in the vicinity of the crack and the stress intensity factors offer valuable basic information for wave propagation problems in cracked media. Research of elastic wave propagation interacting with cracks in solids starts with simple cases as a line crack in a media. Freund [64] studied elastic waves due to normal impact loading of equal but opposite concentrated normal forces on the crack faces in an unbounded elastic solid. The time dependent stress intensity factor was discussed in detail and generalized for

spatially-distributed and time-varying normal impact loads. Angel [65] demonstrated that the harmonic wave propagation by cracks can be reduced to systems of singular equations of the Cauchy type by either the Fourier integral transform technique or by the Green function method. These two methods provide us with insightful information on how a crack problem can be modeled and mathematically solved. Later Itou [66] used the Fourier integral transform method on a wave problem where three-dimensional waves in a cracked elastic solid are considered. The application then extended to layered composites where cracks exist between two different materials. Love waves and bulk waves scattered by a stress-free crack with finite width of layered composite were studied by Neerhoff [67]. Again the integral equation method was employed and an infinite system of linear equations obtained. An important feature of [67] regarding the satisfaction of the edge condition for expansion functions (Chebyshev functions) is adopted in our study. In a similar problem, Bostrom [68] also used the integral equation method and Chebyshev polynomials to construct the matrix equations. For waves scattered by a circular or penny-shaped crack, Krenk and Schmidt [69], using the direct integral equation method, developed a solution-method based on expansion of stresses and displacements on the crack surfaces in terms of trigonometric functions and orthogonal polynomials. This method was not restricted by any assumptions of symmetry. Tsai [70], using the Hankel transform method, studied longitudinal harmonic waves scattered by a penny-shaped crack in a transversely isotropic material. The results showed that the dynamic stress intensity factor has different maximum values at different wave frequencies. As direct references for the method we employed in this study, Norris and Yang [71] and Yang and Norris [72] studied elastic waves scattered by a partially-bonded fiber embedded in the matrix. In [71] the unknown stresses are represented by a series expansion of Chebyshev functions whose coefficients were to be determined by boundary conditions, while in [72] they use unknown displacements (COD) to perform a similar derivation. We will closely follow the formulation in [72] for the construction of boundary conditions. For NDE applications on a cracked medium, an inverse methodology was presented by Achenbach et al [73] to characterize a planar crack of general shape contained in an elastic solid. They showed that, for a given scattered field, the inverse problem can be formulated as a nonlinear optimization problem. Particularly, at low frequencies its solution gives the location of cracks, the orientation of the crack-plane, and the crack-opening volumes. About the same time Sotiropoulos and Achenbach [74] studied the ultrasonic wave reflection and transmission by planar crack distribution. Reflection and transmission coefficients were derived for incident longitudinal and transverse time-harmonic plane waves. For low frequencies, a closed form expression was given in terms of geometric parameters, the material constants, and the incident wave field. Deterministic and statistical distributions of planer cracks were also considered. The application in recent years extended to the study of fiber-reinforced composites with cracks or defects. Coussy [75] studied the scattering of elastic SH waves from a fiber imperfectly bonded to a matrix. By means of the perturbation method associated with a homogenization procedure, the analysis was extended to fiber-reinforced composites with interfacial cracks. The results he obtained, that the composites behave like anisotropic visco-elastic materials, are expected in our study. Aboudi [76] presented a continuum theory for elastic wave propagation in three-dimensional composite materials with imperfect bonding between the phases. It provided the dispersion relations for harmonic waves and the dynamic

response of the composite to impulsive loading. Perfect contact, perfect lubrication and complete debonding of the constituents were discussed. Mal et al [77] developed ultrasonic nondestructive methods using guided waves in undamaged as well as damaged fiber-reinforced composite laminates. A systematic inversion scheme of dispersion data was applied to determine the reduction in stiffness due to transverse cracks in the off-axis plies of damaged, multi-orientation laminates. Recently Angel and Koba [78], by invoking Kramers-Kronig relations, determined analytically the speed and attenuation of antiplane waves in an elastic solid containing a dilute distribution of parallel or randomly oriented cracks. The linearity, passivity, and causality based Kramers-Kronig relations constitute a resourcefully analytic avenue for investigating dynamic properties of composites.

The main objectives of this study are to calculate the effective static strength (out of plane shear moduli) and dynamic wave properties (shear wave speed and attenuation) of fiber-reinforced composites with interphase (between fibers and matrix) and interfacial cracks and where the fibers are randomly and spatially distributed in the matrix. Before those can be done, we will highlight a frequently used theorem (quasi-crystalline approximation) in multiple scattering in composites by showing its validity using the successive-events scattering approach. Then by the many-bodies approach, combined with statistical procedures, the average wave properties for composites with the two cases just mentioned will be investigated. Parametric computations will be performed to study the general trend as functions of interphase and crack variables.

CHAPTER 2. MULTIPLE WAVE SCATTERING IN FIBER-REINFORCED COMPOSITES: MICROMECHANICAL VIEWPOINT

2.1 Introduction

While the multiple wave scattering problems in composites in a statistical-average sense have been investigated thoroughly [35,37], the micromechanical perspective of the same problem has received limited attention. In references [35,37], the focus was on the calculated elastic constants using the multiple wave scattering approach. In quantum-mechanics or electromagnetics, the calculation of the index of refraction (a propagation constant) can be achieved by using a spatial statistical-averaging technique. Only in studies of the more general aspects of wave scattering phenomena is the micro-mechanism of multiple scattering investigated [52-56]. As the studies in [52-56] were concentrated on the micromechanical aspects, we attempt, in the same spirit, to calculate the transferability of energy from one scattering event to the next in a fiber-reinforced composite material system and to validate one of the theorems (quasi-crystalline approximation) on which the spatial statistical-averaging technique is based. For simplicity, only shear waves are considered to demonstrate the micro-mechanical physics of the multiple scattering phenomena.

We define "wave scattering" as the redistribution of radiation from the wave source in the presence of an obstacle or obstacles (the term 'scatterer' is also used). Wave scattering in solids is the collection of reflection, refraction and diffraction occurring in a non-homogeneous medium. The term 'multiple wave scattering' is used when, in a medium, two or more obstacles are present. For a single-body scattering problem, radiation from the obstacle, combined with the wave source, is the effective field in the medium. For many-bodies problems, multiple scattering events occur consecutively between those obstacles. The effective field for a many-body problem is the combination of all those events and the wave source. Whenever a scattering event occurs, the energy radiation from a particular scatterer is incident upon other scatterers, which in turn serve the source for the next scattering event. Thus "primary scattering" is defined as the scattering from the obstacles on which the incident wave impinges. "Secondary scattering" is the scattering from the obstacles upon which the primary wave impinges. The "tertiary" and the fourth-order of multiple scattering are defined accordingly.

The mechanics of wave scattering is governed by the wave equation. There are coordinate systems for which the wave equations are separable [79]. In situations where the scatterer's boundary surface coincides with this class of coordinate systems, an eigenfunction expansion can be used where a series solution of special functions is employed to express the wave field. Specifically, trigonometric functions are used for the rectilinear Cartesian Coordinate system, Bessel functions for the cylindrical coordinate system, and the spherical Bessel and Legendre functions for spherical coordinate systems. For scatterers whose surfaces coincide with coordinate systems for which the wave equation cannot be separated, the computational integral equation method [10] or perturbation method is often used [80]. Since the scatterers in a

fiber-reinforced composite system are unidirectionally parallel fibers spatially distributed in the composite, we will employ the cylindrical coordinate system in which the Bessel and Hankel functions are used.

For wave scattering, the effective field for a single-scatterer problem is the combination of both the incident wave source and the scattered radiation. For a many-scatterers problem, one seeks to combine the effects of all the scattering events and the incident wave source. Two approaches can be used to calculate the effective wave field. First, the domain can be treated from a many-bodies-single-event perspective (Figure 1). From this, interactions of waves in a system of inclusions are seen as a single event. The boundary conditions for this system must be satisfied simultaneously for all the inclusions when an attempt is made to obtain solutions of the wave equation. Using this method, the solutions are functions of themselves and are implicit solutions. Secondly, the wave interactions between the obstacles can be thought of as consecutive events of waves reflecting between the scatterers and refracting incessantly (Figure. 2). For primary scattering, the boundary value problem consists of a single scatterer and a wave source (incident waves) from the far field. For the secondary and higher order of scattering, it consists of a single scatterer and a wave source emitted from one of the other scatterers. The boundary conditions needed to be satisfied are the boundary of that specific single scatterer and that particular event. Thus, one needs to keep track of the wave fields for each order of scattering and for each scatterer. With this method, the total wave field induced by all wave interactions of scattering is accounted for and summed. The results thus obtained are explicit solutions, since the solutions are explicitly expressed as functions of the scatterers' location, material properties of both the scatterers and matrix, and the dynamic input of the incident waves. Theoretically, the two approaches described above should lead to the same results in the linear range [55-56]. It is our intention, after proving that these two approaches lead to the same results for a fiber-reinforced composite system, to study the energy transferability of the multiple scattering phenomena between fibers in the composite system.

In addition, the quasi-crystalline approximation for the wave theory in fiber-reinforced composites can be validated using the consecutive-events approach. Twersky's discussions [55] on planar random distributions of parallel cylinders encouraged a closer look at this approximation. In [55], the parallel cylinders are located on the y-axis only. For our case, the fibers are distributed in a 2-D (x-y) plane. As in [55], we will use the average scattering coefficients ($A_0, A_1, A_{-1}\ldots$) as the parameters for discussions.

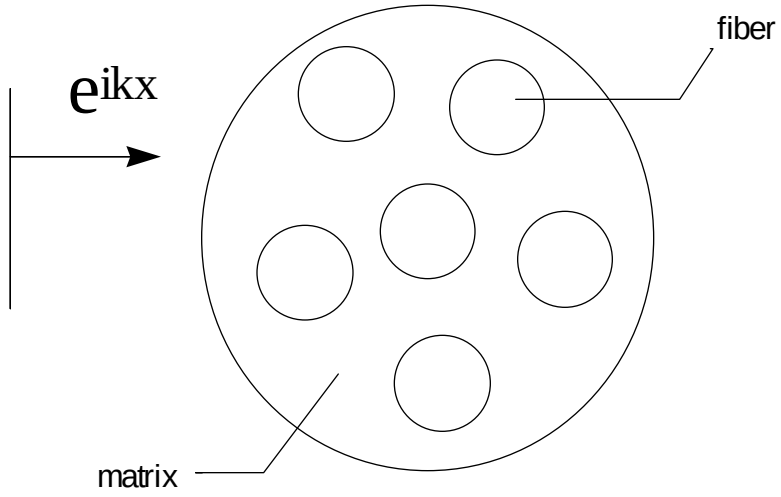

Figure 1. Schematic representation of the many-body-single-event approach.

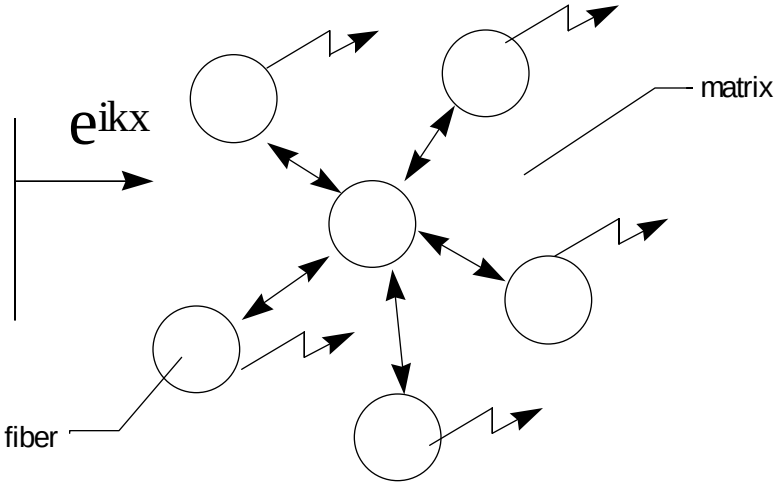

Figure 2. Schematic representation of the consecutive-events approach.

2.2 General consecutive-events approach for multiple wave scattering

In this study we use the consecutive-events approach (Figure 2.) of multiple scattering to investigate shear wave scattering phenomena in a fiber-matrix composite system. The composite system consists of randomly-distributed isotropic parallel fibers embedded in an isotropic homogeneous matrix. Following Waterman and Truell [31], let $\psi_i^E\left(\mathbf{r_i}|\mathbf{R_1},\mathbf{R_2},\ldots\ldots\ldots\mathbf{R_n}\right)$ be the shear displacement exciting field acting on the fiber '*i*'. Then

$$\psi_i^E\left(\mathbf{r_i}|\mathbf{R_1},\mathbf{R_2},\ldots\ldots\ldots\mathbf{R_n}\right)$$
$$= e^{ik_1x} + \sum_{j\neq i}^{n} T^1(r_j)e^{ik_1x} + \sum_{j\neq i}^{n} T^1(r_j)\sum_{k\neq j}^{n} T^1(r_k)e^{ik_1x} + \sum_{j\neq i}^{n} T^1(r_j)\sum_{k\neq j}^{n} T^1(r_k)\sum_{l\neq k}^{n} T^1(r_l)e^{ik_1x} + \cdots, \tag{2.1}$$

where e^{ik_1x} represents the far field incident wave (the incident wave amplitude u_0 is normalized for simplicity) and $T^1(r_j)$ represents the linear operator that operates on scatterer j with respect to the scattering field in the matrix. The superscript '1' indicates that it is referring to the scattering field in the matrix. The exciting field $\psi_i^E\left(\mathbf{r_i}|\mathbf{R_1},\mathbf{R_2},\ldots\ldots\ldots\mathbf{R_n}\right)$, a scalar of shear displacement in only one coordinate dimension (z-component for our case), is apparently a function of the geometrical distribution of all the fibers and the position vector relative to fiber '*i*' (Figure 3). Note that the vector $\mathbf{R_i}$ represents the global position of fiber '*i*' and $\mathbf{r_i}$ represents the field point (*p*) position relative to fiber '*i*'. Therefore the total field in the matrix is

$$\psi^1(r) = e^{ik_1x} + \sum_{i=1}^{n} T^1(r_i)\psi_i^E\left(\mathbf{r_i}|\mathbf{R_1},\mathbf{R_2},\ldots\ldots\ldots\mathbf{R_n}\right)$$
$$= e^{ik_1x} + \sum_{i=1}^{n} T^1(r_i)e^{ik_1x} + \sum_{i=1}^{n} T^1(r_i)\sum_{j\neq i}^{n} T^1(r_j)e^{ik_1x} + \sum_{i=1}^{n} T^1(r_i)\sum_{j\neq i}^{n} T^1(r_j)\sum_{k\neq j}^{n} T^1(r_k)e^{ik_1x}$$
$$+\sum_{i=1}^{n} T^1(r_i)\sum_{j\neq i}^{n} T^1(r_j)\sum_{k\neq j}^{n} T^1(r_k)\sum_{l\neq k}^{n} T^1(r_l)e^{ik_1x} + \cdots, \tag{2.2}$$

and the total field in the fiber '*i*' is

$$\psi_i^2(r) = T^2(r_i)\psi_i^E\left(\mathbf{r_i}|\mathbf{R_1},\mathbf{R_2},\ldots\ldots\ldots\mathbf{R_n}\right)$$
$$= T^2(r_i)e^{ik_1x} + T^2(r_i)\sum_{j\neq i}^{n} T^1(r_j)e^{ik_1x} + T^2(r_i)\sum_{j\neq i}^{n} T^1(r_j)\sum_{k\neq j}^{n} T^1(r_k)e^{ik_1x}$$
$$+T^2(r_i)\sum_{j\neq i}^{n} T^1(r_j)\sum_{k\neq j}^{n} T^1(r_k)\sum_{l\neq k}^{n} T^1(r_l)e^{ik_1x} + \cdots, \tag{2.3}$$

where $T^2(r_i)$ represents the linear operator that operates on fiber '*i*' with respect to the scattering field in the fiber. The superscript '2' indicates that it is referring to the scattering field in the fiber. In Equations (2.2) and (2.3), $\sum_{i=1}^{n} T^1(r_i)e^{ik_1x}$ and $T^2(r_i)e^{ik_1x}$ are the primary scattering waves in the matrix and fiber '*i*', respectively. The secondary scattering waves are $\sum_{i=1}^{n} T^1(r_i)\sum_{j\neq i}^{n} T^1(r_j)e^{ik_1x}$ (matrix) and $T^2(r_i)\sum_{j\neq i}^{n} T^1(r_j)e^{ik_1x}$ (fibers). Tertiary and higher orders of scattering

can be recognized in the same fashion. All of the terms in Equations (2.2) and (2.3) can be obtained by solving boundary value problems for the consecutive events as developed in the next section.

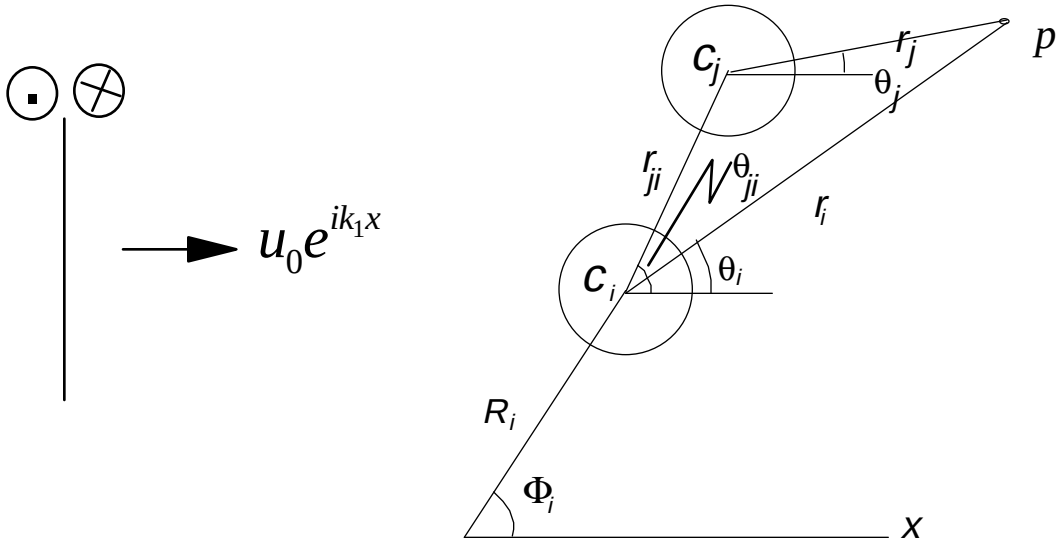

Figure 3. Representative fibers '*i*' and '*j*', the incident waves, and the coordinate system.

2.3 Boundary value problems of multiple SH wave scattering in the fiber-matrix composite

We follow the consecutive events approach laid out in the previous section to solve the boundary value problems and obtain, for each event, the displacement field in the composite. Also, we assume that the displacement of a planar, harmonic, axially shear incident wave u^{in} is generated at infinity and is propagating in the x-axis direction (Figure 3). The composite consists of identical parallel fibers (with radius '*a*' for each fiber extending infinitely in the z-direction) embedded in a matrix. As stated in the last section, we label the fields associated with the matrix with '1', and those associated with the fibers with '2'. The frequency ω of the incident wave is such that $k_1=\omega/c_1$ (also $k_2=\omega/c_2$), where k is the wave number, c is the wave speed. Note that $c_1=\sqrt{\mu_1/\rho_1}$ and $c_2=\sqrt{\mu_2/\rho_2}$, where μ and ρ are the shear modulus and material density, respectively. The amplitude of the incident wave is assumed to be u_0. The time factor e^{-iwt} can be omitted for all quantities involved in the wave equation for the steady state condition. The displacement u^{in} can be expanded as the summation of cylindrical functions as

$$u^{in} = u_0 e^{ik_1 x} = u_0 e^{ik_1(R_i\cos\Phi_i + r_i\cos\theta_i)} = u_0 e^{ik_1 R_i\cos\Phi_i} \sum_{m=-\infty}^{\infty} i^m J_m(k_1 r_i) e^{im\theta_i} \quad . \tag{2.4}$$

In the equation above, the incident wave is satisfied as a solution of the wave equation $\nabla^2 u + k_1^2 u = 0$. Also note that (R_i, Φ_i) are the global polar coordinates of fiber '*i*' and (r_i, θ_i) are the local polar coordinates as referred to fiber '*i*'.

The primary event consists of the incident wave (Equation (2.4)) generated in the far field, the reflecting (scattering) wave in the matrix u_i^1, and the refracting (transmitting) wave in the fiber u_i^2 (Figure 4). Then

$$u_i^1 = T^1(r_i) e^{ik_1 x} = \sum_{m=-\infty}^{\infty} A_{mi} H_m(k_1 r_i) e^{im\theta_i} \quad . \tag{2.5}$$

$$u_i^2 = T^2(r_i) e^{ik_1 x} = \sum_{m=-\infty}^{\infty} B_{mi} J_m(k_2 r_i) e^{im\theta_i} \quad . \tag{2.6}$$

In the equations above, J_m is the Bessel function of the first kind and H_m is the Hankel function of the first kind. A_{mi} and B_{mi} are the scattering coefficients. Both u_i^1 and u_i^2 are solutions of the wave equation.

The displacement and stress boundary conditions for the primary scattering event are

$$\left(u^{in} + u_i^1\right)_{|r_i=a} = u_i^2{}_{|r_i=a} \qquad \text{and} \qquad \mu_1 \frac{\partial}{\partial r_i}\left(u^{in} + u_i^1\right)_{|r_i=a} = \mu_2 \frac{\partial u_i^2}{\partial r_i}{}_{|r_i=a} \quad , \tag{2.7}$$

respectively.

Substitute Equations (2.4), (2.5) and (2.6) into the boundary conditions given above, then multiply both sides by $e^{-in\theta_i}$ and integrate from 0 to 2π over θ_i, Equation (2.7) then becomes

$$u_0 e^{ik_1 R_i\cos\Phi_i} i^m J_m(k_1 a) + A_{mi} H_m(k_1 a) = B_{mi} J_m(k_2 a) \qquad \text{and}$$

$$\frac{\mu_1 k_1}{\mu_2 k_2}\left[u_0 e^{ik_1 R_i\cos\Phi_i} i^m J_m'(k_1 a) + A_{mi} H_m'(k_1 a)\right] = B_{mi} J_m'(k_2 a) \, . \tag{2.8}$$

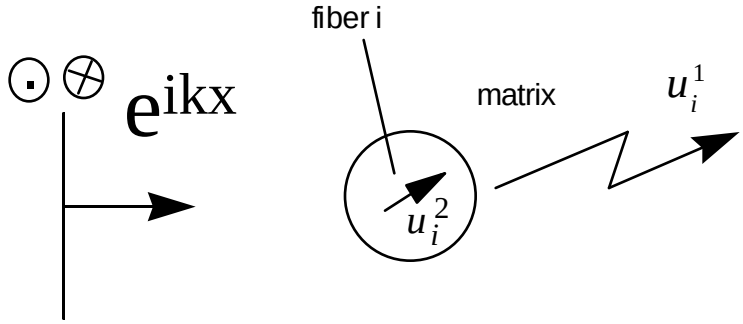

Figure 4. Schematic representation of the primary scattering event associated with fiber '*i*'.

From Equation (2.8), we solve the scattering coefficient A_{mi} and B_{mi} :

$$A_{mi} = u_0 e^{ik_1 R_i \cos\Phi_i} i^m \frac{E_m}{D_m}, \quad B_{mi} = 2u_0 e^{ik_1 R_i \cos\Phi_i} i^{m+1} \frac{1}{\pi k_1 a D_m}. \tag{2.9}$$

Where

$$\begin{aligned} E_m &= zJ_m(k_1 a)J_m'(k_2 a) - J_m(k_2 a)J_m'(k_1 a) \\ D_m &= J_m(k_2 a)H_m'(k_1 a) - zJ_m'(k_2 a)H_m(k_1 a) \\ z &= \frac{\mu_2 k_2}{\mu_1 k_1}. \end{aligned} \tag{2.10}$$

Note that E_m and D_m are even functions with respect to 'm', i.e., $E_m=E_{-m}$ and $D_m=D_{-m}$. And that $A_{-mi}=(-1)^m A_{mi}$, $B_{-mi}=(-1)^m B_{mi}$.

The foregoing treatment is for the primary scattering event. Next we calculate, as a representative formula, the secondary scattering waves in the composite by considering waves reflected from fiber c_j and incident upon fiber c_i (Figure 5). Let u_j^1 be the displacement wave reflected from c_j and incident upon c_i, that is,

$$u_j^1 = T^1(r_j)e^{ik_1 x} = \sum_{m=-\infty}^{\infty} A_{mj} H_m(k_1 r_j) e^{im\theta_j}. \tag{2.11}$$

Let u_{ij}^1 be the secondary wave reflected from fiber i, then

$$u_{ij}^1 = T^1(r_i)u_j^1 = T^1(r_i)T^1(r_j)e^{ik_1 x} = \sum_{m=-\infty}^{\infty} A_{mij} H_m(k_1 r_i) e^{im\theta_i}, \tag{2.12}$$

and let u_{ij}^2 be the secondary refracting wave in fiber i,

$$u_{ij}^2 = T^2(r_i)u_j^1 = T^2(r_i)T^1(r_j)e^{ik_1 x} = \sum_{m=-\infty}^{\infty} B_{mij} J_m(k_2 r_i) e^{im\theta_i}. \tag{2.13}$$

The boundary conditions for the secondary scattering event are

$$\left(u_j^1 + u_{ij}^1\right)_{|r_i=a} = u_{ij}^2{}_{|r_i=a} \qquad \text{and} \qquad \mu_1 \frac{\partial}{\partial r_i}\left(u_j^1 + u_{ij}^1\right)_{|r_i=a} = \mu_2 \frac{\partial u_{ij}^2}{\partial r_i}_{|r_i=a}.$$

Applying the boundary conditions in the same fashion as in the primary scattering case, we have

$$\sum_{m=-\infty}^{\infty}\left[A_{mj}H_m(k_1r_j)e^{im\theta_j}+A_{mij}H_m(k_1r_i)e^{im\theta_i}\right]_{|r_i=a}=\sum_{m=-\infty}^{\infty}\left[B_{mij}J_m(k_2r_i)e^{im\theta_i}\right]_{|r_i=a}\qquad\text{and}$$

$$\sum_{m=-\infty}^{\infty}\mu_1\frac{\partial}{\partial r_i}\left[A_{mj}H_m(k_1r_j)e^{im\theta_j}+A_{mij}H_m(k_1r_i)e^{im\theta_i}\right]_{|r_i=a}=\sum_{m=-\infty}^{\infty}\mu_2\frac{\partial}{\partial r_i}\left[B_{mij}J_m(k_2r_i)e^{im\theta_i}\right]_{|r_i=a}. \tag{2.14}$$

Note that the variables r_j and θ_j in the above equation are referring to the local polar coordinate system of fiber 'j'. They need to be translated to the coordinate system of fiber 'i' using the addition theorem of Hankel functions, which is

$$e^{im\theta_i}H_m(kr_i)=e^{im\theta_{ji}}(-1)^m\sum_{p=-\infty}^{\infty}(-1)^pJ_p(kr_j)H_{p-m}(kr_{ji})e^{ip(\theta_j-\theta_{ji})}. \tag{2.15}$$

Indices i and j need to be interchanged in (2.15) so that the relevant terms in (2.14) apply. Thus

$$\begin{aligned}&J_n(k_1a)\sum_{m=-\infty}^{\infty}A_{m+n,j}H_m(k_1r_{ij})e^{im\theta_{ij}}+A_{nij}H_n(k_1a)=B_{nij}J_n(k_2a)\\&J_n'(k_1a)\sum_{m=-\infty}^{\infty}A_{m+n,j}H_m(k_1r_{ij})e^{im\theta_{ij}}+A_{nij}H_n'(k_1a)=zB_{nij}J_n'(k_2a).\end{aligned} \tag{2.16}$$

Therefore, solving A_{mij} and B_{mij} from the above equations, the secondary scattering coefficients are

$$\begin{aligned}A_{mij}&=\frac{E_m}{D_m}\sum_{p=-\infty}^{\infty}A_{p+m,j}H_p(k_1r_{ij})e^{ip\theta_{ij}}\\B_{mij}&=\frac{1}{D_m}\frac{2i}{\pi k_1a}\sum_{p=-\infty}^{\infty}A_{p+m,j}H_p(k_1r_{ij})e^{ip\theta_{ij}}.\end{aligned} \tag{2.17}$$

Substitute the above equations into (2.12) and (2.13) for the secondary scattering fields

$$\begin{aligned}u_{ij}^1&=T^1(r_i)T^1(r_j)e^{ik_1x}=u_0e^{ik_1R_j\cos\Phi_j}\sum_{m=-\infty}^{\infty}\sum_{p=-\infty}^{\infty}i^{p+m}\frac{E_m}{D_m}\frac{E_{p+m}}{D_{p+m}}H_p(k_1r_{ij})H_m(k_1r_i)e^{i(p\theta_{ij}+m\theta_i)}\\u_{ij}^2&=T^2(r_i)T^1(r_j)e^{ik_1x}=\frac{2u_0e^{ik_1R_j\cos\Phi_j}}{\pi k_1a}\sum_{m=-\infty}^{\infty}\sum_{p=-\infty}^{\infty}i^{p+m+1}\frac{1}{D_m}\frac{E_{p+m}}{D_{p+m}}H_p(k_1r_{ij})J_m(k_2r_i)e^{i(p\theta_{ij}+m\theta_i)}.\end{aligned} \tag{2.18}$$

Using the same procedure as in the foregoing treatment, we can obtain the tertiary scattering fields both in the matrix and in the fiber 'i' as

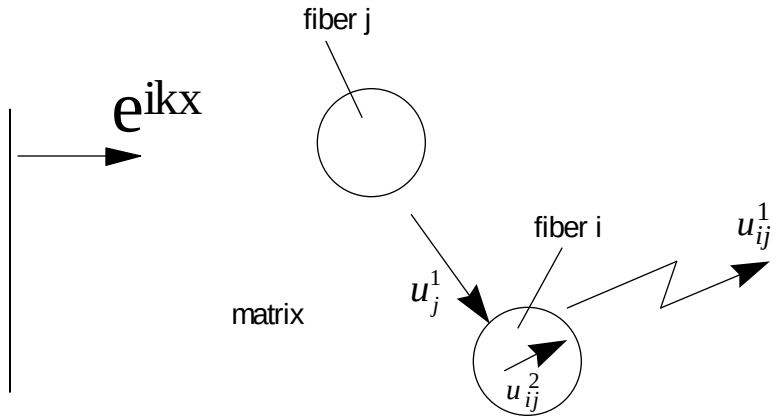

Figure 5. Schematic representation of the secondary scattering event associated with fibers '*i*' and '*j*'. The far field wave first incident upon fiber '*j*', the reflecting wave in the matrix interact with fiber '*i*' to induce the secondary event.

$$u_{ijk}^{1}=T^{1}(r_i)T^{1}(r_j)T^{1}(r_k)e^{ik_1x}=\sum_{m=-\infty}^{\infty}\sum_{p=-\infty}^{\infty}\sum_{q=-\infty}^{\infty}u_0e^{ik_1R_k\cos\Phi_k}i^{p+q+m}\frac{E_m}{D_m}\frac{E_{p+m}}{D_{p+m}}\frac{E_{p+q+m}}{D_{p+q+m}}\times$$
$$H_q(k_1r_{jk})H_p(k_1r_{ij})H_m(k_1r_i)e^{i\left(q\theta_{jk}+p\theta_{ij}+m\theta_i\right)}$$
$$u_{ijk}^{2}=T^{2}(r_i)T^{1}(r_j)T^{1}(r_k)e^{ik_1x}=\frac{2u_0e^{ik_1R_k\cos\Phi_k}}{\pi k_1a}\sum_{m=-\infty}^{\infty}\sum_{p=-\infty}^{\infty}\sum_{q=-\infty}^{\infty}i^{p+q+m+1}\frac{1}{D_m}\frac{E_{p+m}}{D_{p+m}}\frac{E_{p+q+m}}{D_{p+q+m}}\times \quad (2.19)$$
$$H_q(k_1r_{jk})H_p(k_1r_{ij})J_m(k_2r_i)e^{i\left(q\theta_{jk}+p\theta_{ij}+m\theta_i\right)}.$$

The subscript 'ijk' in the tertiary scattering represents three succeeding events starting from the primary wave emitting from fiber k, then the secondary wave from fiber j, and finally the tertiary wave from fiber '*i*'. Scattering paths for higher order scattering fields can be interpreted in the same fashion.

As the scattering shear displacement fields for each scattering event are readily obtained, we are ready to apply the general approach as stated in Equations (2.2) and (2.3). Assuming the number of fibers in the matrix to be n, the total primary scattering fields in the matrix and in the fiber '*i*' are

$$u_p^{1^{total}}=\sum_{i=1}^{n}T^{1}(r_i)e^{ik_1x}=\sum_{i=1}^{n}u_i^{1}=u_1^{1}+u_2^{1}+u_3^{1}+\cdots$$
$$=\sum_{i=1}^{n}\sum_{m=-\infty}^{\infty}u_0e^{ik_1R_i\cos\Phi_i}i^{m}\frac{E_m}{D_m}H_m(k_1r_i)e^{im\theta_i} \quad \text{and}$$
$$u_{ip}^{2}=T^{2}(r_i)e^{ik_1x}=\frac{2u_0e^{ik_1R_i\cos\Phi_i}}{\pi k_1a}\sum_{m=-\infty}^{\infty}\frac{i^{m+1}}{D_m}J_m(k_2r_i)e^{im\theta_i}. \quad (2.20)$$

respectively. Note that in the first equation of (2.20), the terms of each primary scattered wave (associated with each fiber) are summed. Therefore the coordinate variables r_i and θ_i for those individual terms are referring to the coordinate systems associated with each fiber. In the second equation, the primary scattering wave in the fiber i is simply the refracting wave for the primary scattering event. The total secondary scattering fields both in the matrix and in fiber '*i*' are

$$u_2^{1^{total}}=\sum_{i=1}^{n}\sum_{j\neq i}^{n}T^{1}(r_i)T^{1}(r_j)e^{ik_1x}=\sum_{i=1}^{n}\sum_{j\neq i}^{n}u_{ij}^{1}$$
$$=\sum_{i=1}^{n}\sum_{j\neq i}^{n}\sum_{m=-\infty}^{\infty}\sum_{p=-\infty}^{\infty}u_0e^{ik_1R_j\cos\Phi_j}i^{p+m}\frac{E_m}{D_m}\frac{E_{p+m}}{D_{p+m}}H_p(k_1r_{ij})H_m(k_1r_i)e^{i\left(p\theta_{ij}+m\theta_i\right)} \quad \text{and}$$

$$u_{i2}^{2^{total}} = \sum_{j\neq i}^{n} T^2(r_i)T^1(r_j)e^{ik_1 x} = \sum_{j\neq i}^{n} u_{ij}^2$$
$$= \sum_{j\neq i}^{n}\sum_{m=-\infty}^{\infty}\sum_{p=-\infty}^{\infty} \frac{2u_0 e^{ik_1 R_j \cos\Phi_j}}{\pi k_1 a}\frac{i^{p+m+1}}{D_m}\frac{E_{p+m}}{D_{p+m}} H_p(k_1 r_{ij}) J_m(k_2 r_i) e^{i\left(p\theta_{ij}+m\theta_i\right)}. \quad (2.21)$$

For the total tertiary and fourth scattering field:

$$u_3^{1^{total}} = \sum_{i=1}^{n}\sum_{j\neq i}^{n}\sum_{k\neq j}^{n} T^1(r_i)T^1(r_j)T^1(r_k)e^{ik_1 x} = \sum_{i=1}^{n}\sum_{j\neq i}^{n}\sum_{k\neq j}^{n} u_{ijk}^1$$
$$= \sum_{i=1}^{n}\sum_{j\neq i}^{n}\sum_{k\neq j}^{n}\sum_{m=-\infty}^{n}\sum_{p=-\infty}^{\infty}\sum_{q=-\infty}^{\infty} u_0 e^{ik_1 R_k\cos\Phi_k} i^{p+q+m}\frac{E_m}{D_m}\frac{E_{p+m}}{D_{p+m}}\frac{E_{p+q+m}}{D_{p+q+m}}\times$$
$$H_q\left(k_1 r_{jk}\right)H_p\left(k_1 r_{ij}\right)H_m\left(k_1 r_i\right)e^{i\left(q\theta_{jk}+p\theta_{ij}+m\theta_i\right)}$$

$$u_{i3}^{2^{total}} = \sum_{j\neq i}^{n}\sum_{k\neq j}^{n} T^2(r_i)T^1(r_j)T^1(r_k)e^{ik_1 x} = \sum_{j\neq i}^{n}\sum_{k\neq j}^{n} u_{ijk}^2$$
$$= \sum_{j\neq i}^{n}\sum_{k\neq j}^{n}\sum_{m=-\infty}^{\infty}\sum_{p=-\infty}^{\infty}\sum_{q=-\infty}^{\infty} \frac{2u_0 e^{ik_1 R_k\cos\Phi_k}}{\pi k_1 a}\frac{i^{p+q+m+1}}{D_m}\frac{E_{p+m}}{D_{p+m}}\frac{E_{p+q+m}}{D_{p+q+m}}\times$$
$$H_q(k_1 r_{jk})H_p(k_1 r_{ij})J_m(k_2 r_i)e^{i\left(q\theta_{jk}+p\theta_{ij}+m\theta_i\right)}$$

$$u_4^{1^{total}} = \sum_{i=1}^{n}\sum_{j\neq i}^{n}\sum_{k\neq j}^{n}\sum_{l\neq k}^{n} T^i(r_i)T^1(r_j)T^1(r_k)T^1(r_k)e^{ik_1 x} = \sum_{i=1}^{n}\sum_{j\neq i}^{n}\sum_{k\neq j}^{n}\sum_{l\neq k}^{n} u_{ijkl}^1$$
$$= \sum_{i=1}^{n}\sum_{j\neq i}^{n}\sum_{k\neq j}^{n}\sum_{l\neq k}^{n}\sum_{m=-\infty}^{n}\sum_{p=-\infty}^{\infty}\sum_{q=-\infty}^{\infty}\sum_{r=-\infty}^{\infty} u_0 e^{ik_1 R_l\cos\Phi_l} i^{p+q+r+m}\frac{E_m}{D_m}\frac{E_{p+m}}{D_{p+m}}\frac{E_{p+q+m}}{D_{p+q+m}}\frac{E_{p+q+r+m}}{D_{p+q+r+m}}\times$$
$$H_r\left(k_1 r_{kl}\right)H_q\left(k_1 r_{jk}\right)H_p\left(k_1 r_{ij}\right)H_m\left(k_1 r_i\right)e^{i\left(r\theta_{kl}+q\theta_{jk}+p\theta_{ij}+m\theta_i\right)}$$

$$u_{i4}^{2^{total}} = \sum_{j\neq i}^{n}\sum_{k\neq j}^{n}\sum_{l\neq k}^{n} T^2(r_i)T^1(r_j)T^1(r_k)T^1(r_k)e^{ik_1 x} = \sum_{j\neq i}^{n}\sum_{k\neq j}^{n}\sum_{l\neq k}^{n} u_{ijkl}^2$$
$$= \sum_{j\neq i}^{n}\sum_{k\neq j}^{n}\sum_{l\neq k}^{n}\sum_{m=-\infty}^{\infty}\sum_{p=-\infty}^{\infty}\sum_{q=-\infty}^{\infty}\sum_{r=-\infty}^{\infty} \frac{2u_0 e^{ik_1 R_l\cos\Phi_l}}{\pi k_1 a}\frac{i^{p+q+r+m+1}}{D_m}\frac{E_{p+m}}{D_{p+m}}\frac{E_{p+q+m}}{D_{p+q+m}}\frac{E_{p+q+r+m}}{D_{p+q+r+m}}\times . \quad (2.22)$$
$$H_r(k_1 r_{kl})H_q(k_1 r_{jk})H_p(k_1 r_{ij})J_m(k_2 r_i)e^{i\left(r\theta_{kl}+q\theta_{jk}+p\theta_{ij}+m\theta_i\right)}$$

Observing Equations (2.20), (2.21) and (2.22), a regular pattern of the scattering fields for each scattering order can be found. Thus, by induction, the displacement field of each order of scattering can be deduced.

The total shear displacement fields in the matrix and in each particular fiber i are simply the summation of the corresponding quantities for each scattering event. Therefore the shear scattering waves in the matrix (w) and in fiber i (w_i) are

$$w = e^{ik_1 x} + u_p^{1\,total} + u_2^{1\,total} + u_3^{1\,total} + u_4^{1\,total} + \cdots$$
$$w_i = u_{ip}^{2\,total} + u_{i2}^{2\,total} + u_{i3}^{2\,total} + u_{i4}^{2\,total} + \cdots. \tag{2.23}$$

To show that the shear displacements fields obtained from the consecutive-events approach lead to the same results as those obtained from the single-event-many-bodies approach, we resort to expanding the latter into a series summation and matching each summation term with those obtained from the consecutive-events approach. A shear displacement scattering wave in fiber-reinforced composite was obtained by Bose and Mal [35] using the many-body-single-event approach. From [35], we have

$$w = e^{ik_1 x} + \sum_{i=1}^{n} \sum_{m=-\infty}^{\infty} A_{(mi)} H_m(k_1 r_i) e^{im\theta_i} \quad \text{and}$$
$$w_i = \sum_{m=-\infty}^{\infty} B_{(mi)} J_m(k_2 r_i) e^{im\theta_i}, \tag{2.24}$$

where

$$A_{(mi)} = u_0 \frac{E_m}{D_m} F_{mi}$$
$$B_{(mi)} = \frac{2u_0 i}{\pi k_1 a} \frac{1}{D_m} F_{mi} \tag{2.25}$$
$$F_{mi} = i^m e^{ik_1 R_i \cos\Phi_i} + \sum_{j \neq i}^{n} \sum_{p=-\infty}^{\infty} \frac{E_{p+m}}{D_{p+m}} F_{p+m,j} H_p(k_1 r_{ij}) e^{ip\theta_{ij}}.$$

In the third equation of (2.25), F_{mi} is a function of itself. By substituting $F_{p+m,j}$ with the function itself, a much larger equation with extended subscripts results. Performing the same substitution for the new F terms incessantly, a series summation can be obtained which renders the results of Equation (2.24) exactly the same as those in Equation (2.23). Thus we prove that the results of the many-body-single-event approach are the same as those obtained from the consecutive-events approach.

2.4 Energy considerations

As stated at the beginning of this chapter and proven mathematically exact in the last section, the wave scattering in the composite can be seen as a series of multiple scattering events. Physically it must be a converging series of events, i.e. the redistributed energy of the succeeding orders must be diminishing consecutively. One of the parameters to measure (mathematically at least) the diminishing scattering effect is the extinction cross-section for each scattering order. By definition [18-19,81-82], the extinction cross-section σ^{ex} is the addition of the scattering cross-section σ^{sc} and the absorption cross-section σ^{ab},

$$\sigma^{ex} = \sigma^{sc} + \sigma^{ab}. \tag{2.26}$$

Simply put: the scattering cross-section can be associated with scattering in the matrix phase and the absorption cross-section is associated with the fiber phase. σ^{sc} and σ^{ab} are defined as

$$\sigma^{sc} = \frac{\overline{E}^{sc}}{\overline{E}^{in}} \qquad \text{and} \qquad \sigma^{ab} = \frac{\overline{E}^{ab}}{\overline{E}^{in}} \tag{2.27}$$

respectively, where $\overline{E}$ is the average power flux over a period and

$$\overline{E} = \frac{1}{T}\int_0^T \int_s \mathrm{Re}\left[\tau_{ij} e^{-i\omega t}\right] \mathrm{Re}\left[-i\omega u_i e^{-i\omega t}\right] n_j \, ds \, dt \,. \tag{2.28}$$

In (2.28) above, T is the period, Re is designated as the real part of a complex number, τ_{ij} is the stress tensor, u_i is the displacement tensor and n_j is the unit normal pointing outwardly to the boundary surface 's'. $\overline{E}$ can be rewritten as

$$\overline{E} = -\frac{1}{2}\mathrm{Re}\left[i\omega \int_s \tau_{ij} u_i^* n_j \, ds\right] \tag{2.29}$$

where u_i^* is the complex conjugate of u_i.

For an incident shear wave, $u_0 e^{ik_1 x}$ (u_0 is the amplitude), the average power flux per unit area is

$$\begin{aligned} \overline{E}^{in} &= -\frac{1}{2}\mathrm{Re}\left[i\omega \int_s \tau_{xz} u_z^* n_x \, ds\right] \\ &= -\frac{1}{2}\mathrm{Re}\left[i\omega \int_s u_0^2 \mu_1 i k_1 n_x \, ds\right] \\ &= \frac{1}{2} u_0^2 \mu_1 k_1 \omega. \end{aligned} \tag{2.30}$$

In the equation above, the integration surface is assigned to be the unit area with the unit normal in the same direction as the positive x-axis. Therefore the energy flux per unit area for the incident wave, or intensity of the power flux, is

$$\overline{E}^{in} = \frac{1}{2} u_0^2 \rho \omega^2 c_s \ , \tag{2.31}$$

where c_s is the shear wave phase velocity in the matrix. The power flux, as an important feature, is proportional to the square of the frequency.

Next consider the scattered power of the primary scattering wave of the fiber i, which can be written as

$$\overline{E}_1^{sc} = -\frac{1}{2}\mathrm{Re}\left[i\omega \int_s \tau_{rz} u_z^* n_r \, ds\right], \tag{2.32}$$

where the boundary 's' is the surface of fiber i and $n_r \, ds = r_i \, d\theta_i$. Substitute the relevant terms (2.5) into (2.32), then

$$\overline{E}_1^{sc} = -\pi \,\mathrm{Re}\left[i\omega\mu_1 k_1 \sum_{p=-\infty}^{\infty} A_{pi}^* A_{pi} H_p^*(k_1 r_i) H_p'(k_1 r_i) r_i \right] \ . \tag{2.33}$$

For a lossless medium, the scattering power can be asymptotically calculated by the far field energy flux, i.e., as $R \to \infty$, $\overline{E}_1^{sc}$ can be evaluated asymptotically (Figure 6). Therefore, substituting the asymptotic value (appendix A) of the Hankel function as the variable r_i in Equation (2.33) goes to infinity, (2.33) becomes

$$\overline{E}_1^{sc} \sim -\pi \,\mathrm{Re}\left[i\omega\mu_1 k_1 \sum_{p=-\infty}^{\infty} A_{pi}^* A_{pi} i \frac{2}{\pi k_1} \right]$$

$$= 2\mu_1 \omega \sum_{p=-\infty}^{\infty} A_{pi}^* A_{pi} \tag{2.34}$$

$$= 2\mu_1 \omega u_0^2 \sum_{p=-\infty}^{\infty} \frac{E_p^* E_p}{D_p^* D_p}.$$

The average power absorbed by the fiber over a period can be evaluated in the same manner. It can be easily shown that the quantity $\overline{E}_1^{ab}$ becomes zero for our case. It is physically consistent with the fact that, for an elastic medium, the rate at which energy flows into a closed surface is exactly the same as the rate at which it flows out of the closed surface. If the medium in which the waves travel is a non-elastic material (viscous or plastic), the power absorbed by the scatterer cannot be zero. Thus the primary scattering cross section is

$$\sigma_1^{sc} = \overline{E}_1^{sc} \Big/ \overline{E}^{in} = \frac{4}{k} u_0^2 \sum_{p=-\infty}^{\infty} \frac{E_p^* E_p}{D_p^* D_p} \quad , \tag{2.35}$$

and the primary absorption cross section is zero. Therefore

$$\sigma_1^{ex} = \sigma_1^{sc} + \sigma_1^{ab} = \sigma_1^{sc} = \frac{4}{k} u_0^2 \sum_{p=-\infty}^{\infty} \frac{E_p^* E_p}{D_p^* D_p} \quad . \tag{2.36}$$

Similarly

$$\sigma_2^{ex} = \sigma_2^{sc}$$

$$= \overline{E}_2^{sc} \Big/ \overline{E}^{in} \tag{2.37}$$

$$= \frac{4}{k} \sum_{p=-\infty}^{\infty} A_{pij}^* A_{pij}.$$

Note that in (2.37), the extinction cross section for the secondary order of scattering is defined as the average power scattering per unit power of the incident wave. Normally the extinction cross section for a higher order of scattering is defined as the average power scattering of the present order per unit power of the previous order, as it should be $\sigma_2^{ex} = \overline{E}_2^{sc} \Big/ \overline{E}_1^{sc}$ in (2.37). Yet to conveniently measure the diminishing power effect, we resort to the incident wave as the common input for all orders of scattering. The same approach can be used to compute the energy scattering for tertiary and higher orders: (see appendix B for the list of the coefficients $A_{pij\ldots}$ for the first five orders of scattering.)

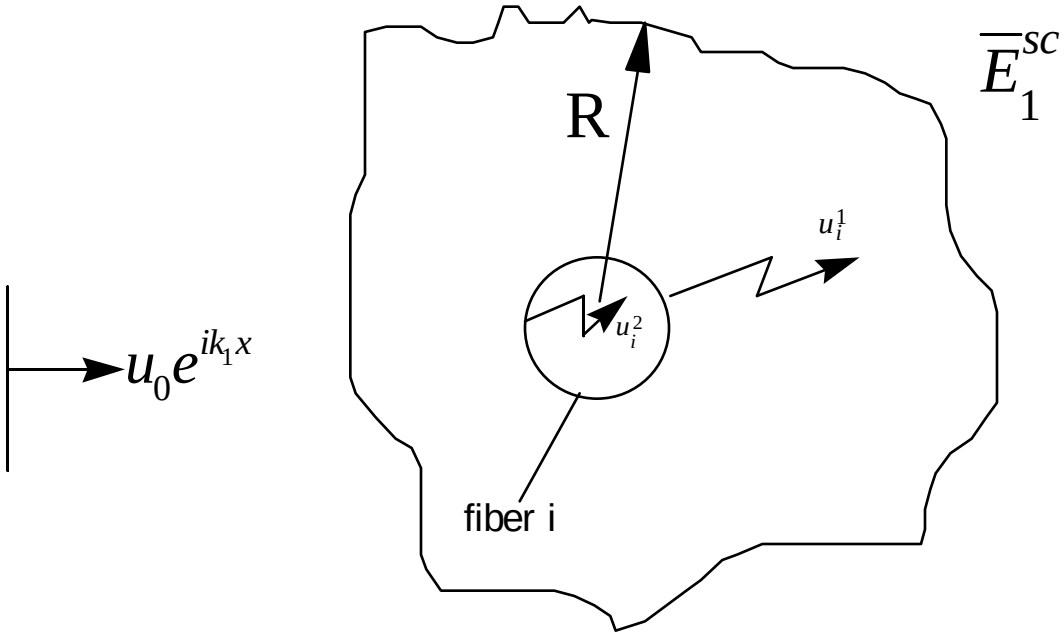

Figure 6. Far field schematic presentation of the primary scattering cross-section.

$$\sigma_3^{ex} = \frac{4}{k}\sum_{p=-\infty}^{\infty} A_{pijk}^* A_{pijk}$$

$$\sigma_4^{ex} = \frac{4}{k}\sum_{p=-\infty}^{\infty} A_{pijkl}^* A_{pijkl} \qquad (2.38)$$

$$\sigma_5^{ex} = \frac{4}{k}\sum_{p=-\infty}^{\infty} A_{pijklh}^* A_{pijklh}$$

$\vdots$

Note that for each order, the quantities inside the summation for the extinction cross-section are the square of absolute values of the corresponding scattering coefficients ($A_{pij}\ldots$). Observing the scattering coefficients in the appendix (Appendix B), the scattering cross-section is proportional to the square of the incident amplitude u_0. Further, there are three geometrical parameters which affect the scattering cross-section: the fiber radius a, fiber separations r_{ij} and the relative angular locations θ_{ij} of the relevant fibers. The only definite statements that we are able to make about the geometrical parameters are: the larger the fiber separations, the less the scattering cross-section will be.

Analytically, it will be promising only to investigate the Rayleigh limit (low frequencies limit, or long wave length limit) of Equations (2.36), (2.37) and (2.38). For simplicity, we intend to study two extreme cases of the separations of fibers, i.e. when the separations are both large and small. Specifically, if the separations are large for the fibers, then $b_{\min} >> \frac{1}{k} >> a$, where b_{min} is the minimum of the fiber separations. If the separations are small, then we assume, in addition to the condition $\frac{1}{k} >> a$, the most extreme case for which $b=2a$ for the adjacent neighborhood of fibers. It is apparent that in both cases, the primary scattering cross-section would yield the same results, since it is independent of the fiber separations. It is also apparent that the case of large fiber-separations is less involved than the case of small-separations.

Considering $ka<<1$ for Equation (2.35) of primary scattering, the minimum power (hence the dominant term) of the series can be shown to be $O(k_1^4 a^4)$. Only three terms survive in the summations of $\frac{E_p^* E_p}{D_p^* D_p}$. Those three terms are when p=0 and p=±1. For large separations such that $b_{\min} >> \frac{1}{k} >> a$, the secondary scattering cross section has the power of $O(k_1^7 a^7)$. Higher order scattering has even higher power terms. Although, individually, the secondary and higher orders of scattering have negligible terms, they may not be ignored if the combined effects of different scattering paths are summed. For example, in the secondary order scattering, there are $n(n-1)$ high order terms with the power of $O(k_1^7 a^7)$. Depending on the wave frequencies, fiber radius and the configuration of the distributions of fibers, the combined effect of secondary scattering cross-

section may be significant. The same statement may be made regarding the higher orders of scattering. Yet asymptotically, we are able to let the quantity of $k_1 a$ become as small as we wish. Therefore as $k_1 a \to \varepsilon$, only the primary scattering is quantitatively significant and higher orders of scattering are legitimately ignored.

For configurations such that $\frac{1}{k} >> a$ and $b=2a$ for the adjacent neighborhood of fibers, more detailed analyses need to be carried out. As stated in the previous paragraph, the cross-section for primary scattering has the magnitude to the order of power $O(k_1^4 a^4)$ in the summations of $\frac{E_p^* E_p}{D_p^* D_p}$. Consequently, for the primary scattering cross-section (2.35), it has the quantity to the order of magnitude $O(k_1^3 a^4)$. Observing the secondary scattering (2.37), given p=1, n=-2, (or p=-1, n=2) and substituting the relevant terms from the asymptotic formula, we have the minimum power of $O(k_1^3 a^4)$. Given p=1, m=-2 and n=2(or p=-1, m=2 and n=-2) for the tertiary scattering (2.38), the minimum power is again $O(k_1^3 a^4)$. Similarly for 4th order scattering it is p=1, m=-2, n=2 and r=-2(or p=-1, m=2, n=-2 and r=2). For 5th order scattering it is p=1, m=-2, n=2, r=-2 and s=2(or p=-1, m=2, n=-2, r=2 and s=-2). Therefore by induction, in the Rayleigh limit, the quantities of the scattering cross section of multiple order are always $O(k_1^3 a^4)$. By the foregoing Rayleigh limit analyses, (2.36-2.38) have the following results for a two-fibers composite system where the fibers are in close contact with each other:

$$
\begin{aligned}
\sigma_1^{ex} &\to \frac{\pi^2}{2} k_1^3 a^4 \left[\left(\frac{\mu_2 - \mu_1}{\mu_2 + \mu_1} \right)^2 + \frac{1}{2} \left(1 - \frac{\rho_2}{\rho_1} \right)^2 \right] \\
\sigma_2^{ex} &\to \frac{\pi^2}{32} k_1^3 a^4 \left(\frac{\mu_2 - \mu_1}{\mu_2 + \mu_1} \right)^4 \\
\sigma_3^{ex} &\to \frac{\pi^2}{512} k_1^3 a^4 \left(\frac{\mu_2 - \mu_1}{\mu_2 + \mu_1} \right)^6 \\
&\vdots \\
\sigma_n^{ex} &\to \frac{\pi^2}{2^{4n-3}} k_1^3 a^4 \left(\frac{\mu_2 - \mu_1}{\mu_2 + \mu_1} \right)^{2n},
\end{aligned}
\qquad (2.39)
$$

for all orders of scattering. Note that in Equation (2.39) the power diminishing factor is $\frac{1}{2^4} \left(\frac{\mu_2 - \mu_1}{\mu_2 + \mu_1} \right)^2$. Apparently, when $\mu_1 = \mu_2$, the diminishing power factor becomes zero. Physically this states that when the shear modulus of the fibers and matrix becomes the same, no re-scattering phenomenon would exist in the composite. Only primary scattering would exist for such situations. As for another case for which $\mu_1 = 0$ and $\mu_2 \neq 0$ (or $\mu_1 \neq 0$ and $\mu_2 = 0$), the power diminishing factor becomes 1/16, which is approximately 6%. For the most dense fiber

configurations, there are six adjacent fibers surrounding any particular one: coordination number, CN=6. Therefore for this situation, about 36% of the power is transferred to the immediately adjacent fibers for each scattering event. Similarly, a significant amount of energy (though less than 36%) is also transferred to the outer layers of fibers and that energy must be taken into account. Overall, the small fiber-separations configuration induced the most multiple scattering phenomenon in the composite.

For higher frequencies we resort to the numerical computation of Equations (2.36), (2.37) and (2.38). Specifically, we arrange a two-fiber-matrix system to investigate the diminishing scattering effect of the shear wave. The results are shown in Figure 7 for a wide range of frequencies. In the Figure, both axes are logarithmic scale, with the first 5 orders of scattering shown. Observe that for the low frequency range, the diminishing effect of the scattering power is apparent. Also for this case, the scattering energy has a linear relationship up to 100MHz. Yet for the high frequency range, the curves tend to coalesce. This implies that for high frequencies, the amount of scattering energy (for the first five orders at least in this particular two fiber-matrix system) tends to be the same order of magnitude.

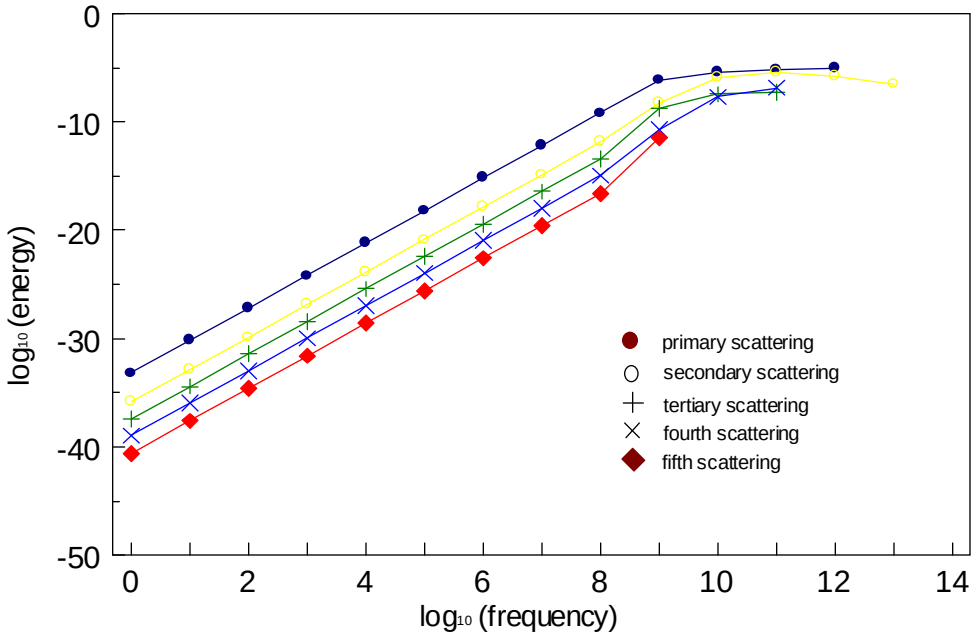

Figure 7. First five orders of extinction cross-section for a two fiber-matrix composite system. $a=2\text{x}10^{-6}$, $r_{12}=2.5a$, $\theta_{12}=30°$, $\rho_1=235.7$, $\rho_2=801$, $\mu_1=1.28\text{x}10$, $\mu_2=8.077\text{x}10$ (all units in SI system).

2.5 Quasi-crystalline (QC) approximation

In this section we intend to prove, from the perspective of the consecutive-events approach, the validity of the quasi-crystalline approximation in the application of wave theory for fiber-reinforced composites. The quasi-crystalline approximation is widely used in wave theory for evaluation of composite material properties. For the derivation of material properties of fiber-reinforced composites, it is used *a priori* to break the statistical hierarchy of spatial averaging procedures [35]. Specifically it states that the spatial average of a field function, when two scatterers are held fixed in space, is equivalent to when only one scatterer is held fixed in space. This can be written as

$$\langle F_{mi}\rangle_{ij} = \langle F_{mi}\rangle_i \qquad i \neq j \qquad , \tag{2.40}$$

where '*i*' and '*j*' represent two different scatterers in the space domain and F_{mi} is a wave function. In Equation (2.40), the bracket (< >) is denoted as the average (or expectation) value of a function. $\langle f \rangle_1$ and $\langle f \rangle_{12}$ are defined as

$$\langle f \rangle_1 = \int \cdots \int_v f \cdot p(\mathbf{R_2} \cdots \mathbf{R_n} | \mathbf{R}_1) d\tau_2 \cdots d\tau_n$$
$$\langle f \rangle_{12} = \int \cdots \int_v f \cdot p(\mathbf{R}_3 \cdots \mathbf{R_n} | \mathbf{R}_1, \mathbf{R}_2) d\tau_3 \cdots d\tau_n . \tag{2.41}$$

In (2.41), $p(\mathbf{R_2} \cdots \mathbf{R_n} | \mathbf{R}_1)$ represents, when the location of scatterer '1' is given at $\mathbf{R_1}$, the joint probability density of locating scatterer '2' at $\mathbf{R_2}$, scatterer '3' at $\mathbf{R_3}$, etc. Similarly, $p(\mathbf{R}_3 \cdots \mathbf{R_n} | \mathbf{R}_1, \mathbf{R}_2)$ represents, when the locations of scatterers '1' and '2' are given at $\mathbf{R_1}$ and $\mathbf{R_2}$, the joint probability density of locating scatterer '3' at $\mathbf{R_3}$, scatterer '4' at $\mathbf{R_4}$, etc. Note that vector $\mathbf{R_i}$ is appropriately regarded as $\mathbf{R_i}=(R_i,\Phi_i)$ for our case (Figure 3), where the polar coordinates are in a global sense in the composite domain. The integration parameter τ_i is regarded as integrating over the defined spatial domain.

For a fiber-reinforced composite for which there are N fibers and the fibers are randomly distributed in the matrix,

$$\begin{aligned} &p(\mathbf{R_1}) = p(\mathbf{R_i}), \quad 1 \le i \le N \\ &p(\mathbf{R_2}|\mathbf{R_1}) = p(\mathbf{R_i}|\mathbf{R_j}), \quad 1 \le i,j \le N,\ i \neq j \\ &p(\mathbf{R_1},\mathbf{R_2},\ldots,\mathbf{R_N}) = p(\mathbf{R_1})p(\mathbf{R_2},\mathbf{R_3},\ldots,\mathbf{R_N}|\mathbf{R_1}) \\ &\qquad\qquad = p(\mathbf{R_1})p(\mathbf{R_2}|\mathbf{R_1})p(\mathbf{R_3},\mathbf{R_4},\ldots,\mathbf{R_N}|\mathbf{R_1},\mathbf{R_2}). \end{aligned} \tag{2.42}$$

The first equation of (2.42) states that the probability that a fiber is located at $\mathbf{R_i}$ is equally probable for all randomly distributed fibers within the domain of the composite. The second equation states that the conditional probability for any two concerned fibers is the same. The third equation is a generalized expansion of the joint probability of all the fibers concerned. Therefore, as the probability density is normalized and the area occupied by a fiber is neglected in a sufficiently large domain, $p(\mathbf{R_i})$ should be equal to $1/s$, where 's' is the cross-sectional area of the composite domain. For definiteness, we have

$$\int_v p(\mathbf{R}_i)d\tau_i = \int_v \frac{1}{s} d\tau_i = \frac{1}{s}\int_v d\tau_i = \frac{1}{s}\times s = 1. \tag{2.43}$$

From the above, the probability that a fiber '*i*' exists in the composite domain is indeed equal to 1. The conditional probability density p($\mathbf{R_i}|\mathbf{R_j}$) can be defined as

$$p(\mathbf{R_i}|\mathbf{R_j}) = \frac{1-f(r_{ij})}{s} \quad , \tag{2.44}$$

where $f(r_{ij})$ is a correlation function, and r_{ij} represents the separation distance of fiber '*i*' and '*j*'. Apparently,

$$\begin{aligned} p(\mathbf{R}_2|\mathbf{R}_1) &= \frac{1}{s}(1-f(r_{12})) \quad , \; r_{12} > 2a \\ &= 0 \qquad\qquad\quad , \; r_{12} \le 2a \; . \end{aligned} \tag{2.45}$$

The first equation of (2.45) shows that if $f(r_{ij})$=0, then there is no correlation between fiber '1' and fiber '2'. Or equivalently, if $f(r_{ij})$=0, then $p(\mathbf{R_2}|\mathbf{R_1})=p(\mathbf{R_2})$=1/s. The second equation simply states that there is no inter-penetration of fibers. For simplicity, the higher order conditional probability will be set equal to $p(\mathbf{R_j}|\mathbf{R_i})$. That is,

$$\begin{aligned} &p(\mathbf{R}_3|\mathbf{R}_1,\mathbf{R}_2) = p(\mathbf{R}_3|\mathbf{R}_2) \\ &p(\mathbf{R}_4|\mathbf{R}_1,\mathbf{R}_2,\mathbf{R}_3) = p(\mathbf{R}_4|\mathbf{R}_3) \\ &\vdots \end{aligned} \tag{2.46}$$

We use the multiple scattering amplitude A_{mi} of Equation (2.25) to demonstrate the validity of quasi-crystalline approximation. From Equation (2.25), the scattering amplitude A_{mi} can be rewritten as

$$A_{m1} = a_m\left(i^m e^{ik_1X_1} + \sum_{j=2}^{N}\sum_{p=-\infty}^{\infty} A_{p+m,j}H_p(k_1r_{1j})e^{ip\theta_{1j}}\right). \tag{2.47}$$

Note that in obtaining (2.47), fiber '1' is chosen as the first parameter of the scattering coefficient and $a_m = \frac{E_m}{D_m}$ (Equation 2.10). Further, let the amplitude u_0 equal to 1. Accordingly, the expectation value $\langle A_{m1}\rangle_1$ is (when the location of fiber '1' is held fixed)

$$\langle A_{m1}\rangle_1 = a_m\left(i^m e^{ik_1X_1} + \sum_{j=2}^{N}\sum_{p=-\infty}^{\infty}\int\cdots\int A_{p+m,j}H_p(k_1r_{1j})e^{ip\theta_{1j}}d\tau_2\cdots d\tau_N \cdot p(\mathbf{R_2}\cdots\mathbf{R_N}|\mathbf{R_1})\right) \quad . \tag{2.48}$$

The parameter '*j*' under the first summation symbol in Equation (2.48) indicates all fibers except fiber '1'. Since the fibers are randomly distributed in the composite, we can chose any fiber 'j' (except fiber '1') to perform the integration without loss of generality. That is, the results of the integration term on the right hand side of (2.48) are independent of the fiber number we chose. Thus if we chose fiber '2' and use Equations (2.40), (2.41), (2.42) and (2.44), then for the integral in (2.48)

$$\int\cdots\int A_{p+m,2}H_p(k_1r_{12})e^{ip\theta_{12}}d\tau_2\cdots d\tau_N p(\mathbf{R_2}\cdots\mathbf{R_N}|\mathbf{R_1})$$
$$=\int\cdots\int A_{p+m,2}H_p(k_1r_{12})e^{ip\theta_{12}}d\tau_2 p(\mathbf{R_2}|\mathbf{R_1})d\tau_3\cdots d\tau_N p(\mathbf{R_3}\cdots\mathbf{R_N}|\mathbf{R_1},\mathbf{R_2})$$
$$=\int H_p(k_1r_{12})e^{ip\theta_{12}}\left\langle A_{p+m,2}\right\rangle_{12}\frac{1-f(r_{12})}{s}d\tau_2 \tag{2.49}$$
$$=\int H_p(k_1r_{12})e^{ip\theta_{12}}\left\langle A_{p+m,2}\right\rangle_{2}\frac{1-f(r_{12})}{s}d\tau_2.$$

Note that in (2.49), the quasi-crystalline approximation (2.40) is applied to obtain the last integral from the third one. By doing this, we assume, *a priori*, that the quasi-crystalline approximation is valid in our case. This assumption will be proven approximately valid by comparing the average scattering coefficients obtained by this assumption with those obtained by the consecutive-events viewpoint. Next we assume that for the scattering coefficients, based upon the randomness distribution of fibers, an average and spatial periodical value exists such that

$$\left\langle A_{mi}\right\rangle_i = i^m A_m e^{ik_1X_i} \quad , \tag{2.50}$$

where X_i is the location of fiber 'i' according to the global coordinate system (Figure 3). Then Equation (2.49) becomes

$$i^{p+m}A_{p+m}e^{ik_1X_1}\int H_p(k_1r_{12})e^{ip\theta_{12}}e^{ik_1r_{12}\cos\theta_{21}}\frac{1-f(r_{12})}{s}d\tau_2$$
$$=i^{p+m}A_{p+m}e^{ik_1X_1}\frac{1}{s}\int_0^{2\pi}\int_{2a}^{\infty}H_p(k_1r_{12})e^{ip\theta_{12}}\sum_{s=-\infty}^{\infty}(-1)^s i^s J_s(k_1r_{12})e^{is\theta_{12}}\left(1-f(r_{12})\right)r_{12}dr_{12}d\theta_{12} \tag{2.51}$$
$$=i^mA_{p+m}e^{ik_1X_1}\frac{2\pi}{s}\int_{2a}^{\infty}H_p(k_1r_{12})J_p(k_1r_{12})\left(1-f(r_{12})\right)r_{12}dr_{12}.$$

Substitute the final result of the integral into Equation (2.48), then

$$i^mA_me^{ik_1X_1}=a_m\left(i^me^{ik_1X_1}+i^mA_{p+m}e^{ik_1X_1}\frac{(N-1)2\pi}{s}\sum_{p=-\infty}^{\infty}\int_{2a}^{\infty}H_p(k_1r_{12})J_p(k_1r_{12})\left(1-f(r_{12})\right)r_{12}dr_{12}\right)$$
$$=a_m\left(i^me^{ik_1X_1}+i^mA_{p+m}e^{ik_1X_1}2\pi n_0\sum_{p=-\infty}^{\infty}\int_{2a}^{\infty}H_p(k_1r_{12})J_p(k_1r_{12})\left(1-f(r_{12})\right)r_{12}dr_{12}\right). \tag{2.52}$$

Note also that in the above equation, the number of fibers 'N' is assumed to be large and the number of fibers per unit area of the cross section is n_0. Then (2.52) becomes

$$A_m=a_m\left(1+A_{p+m}2\pi n_0\sum_{p=-\infty}^{\infty}I_p\right) \quad , \tag{2.53}$$

where $I_p=\int_{2a}^{\infty}H_p(k_1r_{12})J_p(k_1r_{12})\left(1-f(r_{12})\right)r_{12}dr_{12}$. Apparently the average scattering coefficients A_m are the same for each fiber because of the random property of the distribution of fibers. For simplicity, we resort to the low frequency range of a_m to further simplify (2.53). For low frequency, only three terms of a_m are dominant, i.e., a_{-1}, a_0 and a_1. Furthermore, $a_{-1}=a_1$. Therefore Equation (2.53) reduces to a linear system of equations:

$$
\begin{aligned}
&(1-2\pi n_0 a_1 I_0)A_{-1} - 2\pi n_0 a_1 I_1 A_0 - 2\pi n_0 a_1 I_2 A_1 = a_1 \\
&-2\pi n_0 a_0 I_1 A_{-1} + (1-2\pi n_0 a_0 I_0)A_0 - 2\pi n_0 a_0 I_1 A_1 = a_0 \\
&-2\pi n_0 a_1 I_2 A_{-1} - 2\pi n_0 a_1 I_1 A_0 + (1-2\pi n_0 a_1 I_0)A_1 = a_1,
\end{aligned}
\tag{2.54}
$$

where the A's can be solved easily. For brevity, only A_0 will be explicitly calculated for comparison. Thus from (2.54) the scattering coefficient A_0 becomes

$$
\begin{aligned}
A_0 = a_0\Big[&1 + 2\pi n_0(2a_1 I_1 + a_0 I_0) + 4\pi^2 n_0^2(2a_0 a_1 I_0 I_1 + 2a_1^2 I_0 I_1 + 2a_1^2 I_1 I_2 + 2a_0 a_1 I_1^2 + a_0^2 I_0^2) + \\
&8\pi^3 n_0^3(4a_0^2 a_1 I_0 I_1^2 + 4a_0 a_1^2 I_1^3 + 4a_1^3 I_0 I_1 I_2 + 2a_0 a_1^2 I_0 I_1 I_2 + 2a_1^3 I_1 I_2^2 + 2a_1^3 I_0^2 I_1 + \\
&2a_0^2 a_1 I_0^2 I_1 + 2a_0 a_1^2 I_0^2 I_1 + 2a_0 a_1^2 I_0 I_1^2 + 2a_0 a_1^2 I_1^2 I_2 + a_0^3 I_0^3) + \cdots\Big].
\end{aligned}
\tag{2.55}
$$

A_{-1} and A_1 can be obtained similarly.

The forgoing treatment has been to calculate the scattering coefficients A's through the use of the quasi-crystalline approximation (2.40). Next we attempt to achieve the same goal through arguments based upon the successive-events approach. Starting from Equation (2.47), A_{m1} can be expanded into successive-events series summations by re-substituting A_{mi} into the function itself. Then

$$
\begin{aligned}
A_{m1} = a_m\Bigg(&i^m e^{ik_1 X_1} + \sum_{j=2}^{N}\sum_{p=-\infty}^{\infty} a_{p+m} i^{p+m} e^{ik_1 X_j} H_p(k_1 r_{1j}) e^{ip\theta_{1j}} + \\
&\sum_{j=2}^{N}\sum_{k\neq j}^{N}\sum_{p=-\infty}^{\infty}\sum_{q=-\infty}^{\infty} a_{p+m} a_{p+q+m} i^{p+q+m} e^{ik_1 X_k} H_q(k_1 r_{jk}) e^{iq\theta_{jk}} H_p(k_1 r_{1j}) e^{ip\theta_{1j}} + \cdots\Bigg).
\end{aligned}
\tag{2.56}
$$

By taking the expectation value ($\langle A_{m1}\rangle_1$) of the above equation and calculating relevant terms only when m=0, (2.56) becomes

$$
\begin{aligned}
A_0 = a_0\Bigg(&1 + \sum_{j=2}^{N}\sum_{p=-\infty}^{\infty}\left\langle a_p i^p e^{ik_1 r_{1j}\cos\theta_{j1}} H_p(k_1 r_{1j}) e^{ip\theta_{1j}}\right\rangle_1 \\
&+\sum_{j=2}^{N}\sum_{k\neq j}^{N}\sum_{p=-\infty}^{\infty}\sum_{q=-\infty}^{\infty}\left\langle a_p a_{p+q} i^{p+q} e^{ik_1 r_{1k}\cos\theta_{k1}} H_q(k_1 r_{jk}) e^{iq\theta_{jk}} H_p(k_1 r_{1j}) e^{ip\theta_{1j}}\right\rangle_1 + \cdots\Bigg) \quad .
\end{aligned}
\tag{2.57}
$$

Here the beginning term (with magnitude '1') in the parentheses can be recognized as the incident wave, the second term (with double summations) as the incident primary scattering waves, and the third term (with quadruple summations) as the incident secondary scattering waves. The double-summations term can be reduced to $2\pi n_0(2a_1 I_1 + a_0 I_0)$ by using Equations (2.41-2.46). This is exactly the same as that of the second term inside the square bracket of Equation (2.55). The incident secondary scattering wave of (2.57) consists of two distinct categories of the scattering path. One is the repeated routes: the 'follow up' path is the inverse of the leading path. The other is the non-repeated routes: the 'follow up' path is another different path (Figure 8). Specifically, the repeated secondary routes associate with those terms with summations $\left(\sum_{j=2}^{N}\right)_{k=1}$, while the non-repeated secondary routes associate with terms with

summations $\sum_{j=2}^{N}\sum_{k\neq 1\neq j}^{N}$. The summation terms associated with non-repeated secondary routes reduce to $4\pi^2 n_0^2\left(2a_0a_1I_0I_1+2a_1^2I_0I_1+2a_1^2I_1I_2+2a_0a_1I_1^2+a_0^2I_0^2\right)$, which is equivalent to that of the third term inside the square bracket of (2.55). Similarly for the tertiary scattering, the non-repeated routes associate with those terms with summation $\sum_{j=2}^{N}\sum_{k\neq 1\neq j}^{N}\sum_{l\neq 1\neq j\neq k}^{N}$. They too reduce to the fourth term inside the square bracket of (2.55). The same arguments can be applied to higher orders of scattering.

Therefore, by excluding the terms associated with the repeated routes in Equation (2.57), Equation (2.57) reduces to Equation (2.55). That is, for all the terms associated with non-repeated routes in (2.57), they all reduce to those in (2.55) for each order of scattering. Thus, using the quasi-crystalline approximation, Equation (2.40) is equivalent to excluding the effects associated with repeated routes from the consecutive-events viewpoint. The next question which should be asked is 'Are total effects associated with the repeated routes negligible compared to those associated with non-repeated routes?'. Apparently, the primary scattering event is not affected by the use of the QC approximation, only the secondary and higher orders of scattering are. Observing (2.57), there are *(N-1)·(N-1)* terms (counting only the summations with the fiber range) associated with secondary scattering, of which *(N-1)(N-2*) terms are 'non-repeated' and *(N-1)* terms are 'repeated'. Similarly for tertiary scattering, the total number of terms is *(N-1)·(N-1)·(N-1)*, of which *(N-1)·(N-2)·(N-3)* terms are 'non-repeated' and *(N-1)·(3N-5)* terms are 'repeated'. Similar statements can be made for the higher order of scattering. Under the same order of scattering, the magnitude of the scattering coefficients (either 'repeated' or 'non-repeated') is assumed to be the same order for a random distribution of fibers. Consequently for a composite with a large number of fibers and for each order of scattering, judging from the number of terms by which the two categories of scattering routes associate, the wave fields associated with 'repeated' routes are negligible compared to the 'non-repeated' ones. Hence the justification for use of the quasi-crystalline approximation is established.

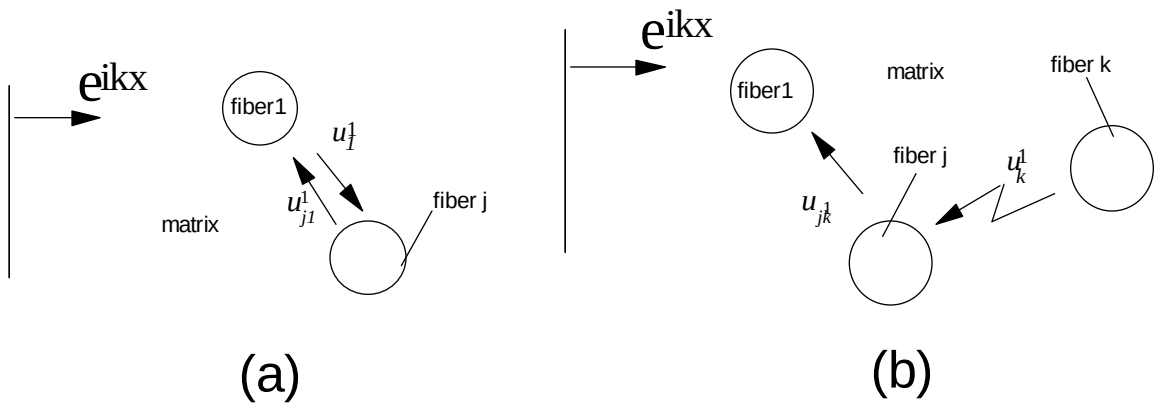

Figure 8. (a) repeated routes of secondary order. (b) non-repeated routes of secondary order.

2.6 Summary

In this study the multiple wave scattering phenomenon in fiber-matrix composites is investigated from a successive-events perspective. Following the multiple scattering approach, the shear wave functions (the particle shear displacement waves for our case) are calculated and summed for the consecutive scattering events. The results thus obtained (an explicit solution) are proved to be the same as those obtained from the many-body approach (an implicit solution) by previous investigators. Proving the mathematical exactness of the multiple scattering approach, we next study the energy transferability by considering the extinction cross-section of each scattering event. Asymptotic analyses are performed for the extinction cross-section for the Rayleigh limit (low frequency limit). The analytical results for the Rayleigh limit show that the shear wave diminishing power factor has a simple relation with the shear modulus, μ, of both the matrix and fiber. And the order of magnitude of the extinction cross-section for each succeeding event is always $O(k_1^3 a^4)$, in which k_1 is the wave number associated with the matrix and a is the fiber radius. Numerical computations are performed for the first five orders of scattering, with a specific arrangement of a two-fibers system and over a wide range of frequencies. The results show that at higher frequencies the quantities of extinction cross-section for the first five scattering orders tend to be in the same order for this particular arrangement of fiber-matrix system. Finally, the widely used quasi-crystalline approximation in the statistical-averaging technique for wave theory is proven to be valid from the successive-events viewpoint.

CHAPTER 3. AXIALLY SHEAR WAVES IN FIBER-REINFORCED COMPOSITES WITH MULTIPLE INTERFACIAL LAYERS BETWEEN FIBER CORE AND MATRIX

3.1 Introduction

The simulation of interfacial zones between fiber core and matrix in a fiber-matrix composite have been studied extensively in the past. The interphase is in most cases created by coating the fiber core. Others may be created by chemical reactions between fiber core and matrix. The interfacial regions, whether they are deliberately made by coatings or inadvertently created by chemical reaction, will affect the performance of a fiber-reinforced composite. Many structural and mechanical models have been built for the interfacial zone to predict it's effect on overall material properties of a composite. For example, a spring model [57] and an effective-fiber model [59, 61] were used to simulate the mechanical behavior of the interfacial zone. By varying the properties of interfacial parameters, pronounced changes in the stress distribution and the overall elastic moduli of the composites were found. Also, guided waves in composite cylinders can be used to characterize the fiber-matrix interphase [58, 83].

As previously intended by many authors, we will investigate the influence of interfacial properties on the overall effective material behavior of a fiber-matrix composite. Neither a spring nor an effective-fiber model will be used, instead a micromechanical model will be built and a statistical approach [35] used. The material properties of the interfacial regions are assumed to have a linear or exponential distribution between the fiber core and matrix to demonstrate the multiple interfacial-layers capability of the model. Effective axial shear modulus (M), axial shear wave phase speed (B) and axial shear wave specific damping capacity (Ψ) are calculated. We start with the eigenfunction (Bessel function) expansion of the wave equation solutions of the displacement fields of a three-phase composite. The scattering coefficients are then obtained by solving the boundary value problems. Then statistical considerations are given and averaging techniques are used to extract the global effective material properties of the composites. Finally the case of three-phase composites are generalized to those of multiphase composites in order to study the effects of arbitrarily varying properties of the interfacial region on the overall effective material properties of the composite media.

3.2 Axial Shear wave scattering in a matrix-fiber composite with an interfacial layer

Before studying the wave scattering in a fiber-reinforced composite, we consider a simple case where waves are scattered by a fiber (with an interfacial layer) imbedded in a matrix. Let this fiber be incident by a plane harmonic axial shear displacement wave u^{in}, which is generated at an infinite distance from the fiber (Figure 9). The domain consists of a matrix (denoted by 1), and a single fiber 'i' (the interfacial region and the fiber core are denoted by 2 and 3 respectively). The incident wave (u^{in}), the scattered wave in the matrix (u_i^1), and in the interface and fiber core (u_i^2 and u_i^3) can be expanded as a series summation of the cylindrical function. Thus

$$u^{in} = e^{ik_1 x} = e^{ik_1 R_i \cos\phi_i} \sum_{m=-\infty}^{\infty} i^m J_m(k_1 r_i) e^{im\theta_i} \tag{3.1}$$

$$u_i^1 = \sum_{m=-\infty}^{\infty} A_{mi} H_m(k_1 r_i) e^{im\theta_i} \tag{3.2}$$

$$u_i^2 = \sum_{m=-\infty}^{\infty} \left(B_{mi} J_m(k_2 r_i) + C_{mi} H_m(k_2 r_i)\right) e^{im\theta_i} \tag{3.3}$$

$$u_i^3 = \sum_{m=-\infty}^{\infty} D_{mi} J_m(k_3 r_i) e^{im\theta_i} \quad . \tag{3.4}$$

In the equations above, the incident and scattering waves are satisfied as solutions of the wave equation $\nabla^2 u + k^2 u = 0$. J_m is the Bessel function of the first kind, H_m is the Hankel function of the first kind. A_{mi}, B_{mi}, C_{mi} and D_{mi} are scattering coefficients which can be solved for by applying the boundary conditions for the system. Note that in Figure 9, similar to Figure 3 in the previous chapter, (R_i ,Φ_i) are the global coordinates of the fiber 'i' and (r_i ,θ_i) are the local coordinates referred to fiber 'i'. The frequency ω of the system is such that $k_1 = \omega/c_1$ (also $k_2 = \omega/c_2$, $k_3 = \omega/c_3$), where k is the wave number, and c is the wave speed. Note that $c_1 = \sqrt{\mu_1/\rho_1}$, $c_2 = \sqrt{\mu_2/\rho_2}$ and $c_3 = \sqrt{\mu_3/\rho_3}$,where μ and ρ are the shear modulus and material density, respectively. The amplitude of the incident wave is assumed to be unity. The time factor $e^{-i\omega t}$ is omitted for all quantities involved in the wave equation for the steady state condition. The boundary conditions are such that the axial shear displacement and shear stress at $r_i = a$ and $r_i = b$ are continuous. Then

$$\begin{aligned}
&\left(u^{in} + u_i^1\right)_{r_i=a} = u_i^2|_{r_i=a} \\
&\mu_1 \frac{\partial}{\partial r_i}\left(u^{in} + u_i^1\right)_{r_i=a} = \mu_2 \frac{\partial}{\partial r_i} u_i^2|_{r_i=a} \\
&u_i^2|_{r_i=b} = u_i^3|_{r_i=b} \\
&\mu_2 \frac{\partial}{\partial r_i} u_i^2|_{r_i=b} = \mu_3 \frac{\partial}{\partial r_i} u_i^3|_{r_i=b},
\end{aligned} \tag{3.5}$$

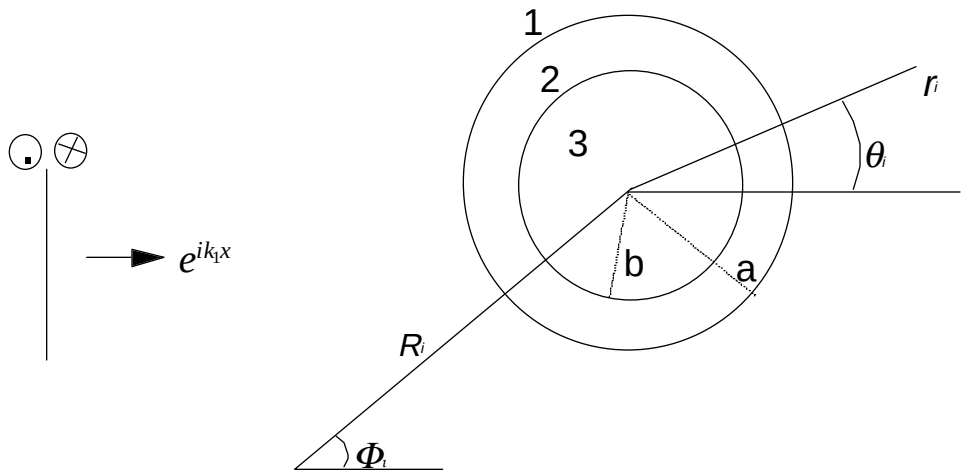

Figure 9. A representative two-phase fiber embedded in the matrix.

The four unknown scattering coefficients can be solved for by substituting the relevant terms, Equations (3.1-3.4), into Equation (3.5). Consequently

$$
\begin{aligned}
A_{mi} &= \frac{e^{ik_1 R_i \cos\phi_i} i^m}{H_m(k_1 a)}\left(\frac{2i\mu_1\left(y_3 H_m(k_2 a) - y_4 J_m(k_2 a)\right)}{\pi a\left(y_2 y_3 - y_1 y_4\right)} - J_m(k_1 a)\right) \\
B_{mi} &= -e^{ik_1 R_i \cos\phi_i} i^m \frac{2i\mu_1}{\pi a}\left(\frac{y_4}{y_2 y_3 - y_1 y_4}\right) \\
C_{mi} &= e^{ik_1 R_i \cos\phi_i} i^m \frac{2i\mu_1}{\pi a}\left(\frac{y_3}{y_2 y_3 - y_1 y_4}\right) \\
D_{mi} &= \frac{e^{ik_1 R_i \cos\phi_i} i^m 2i\mu_1}{J_m(k_3 b)\pi a}\left(\frac{y_3 H_m(k_2 b) - y_4 J_m(k_2 b)}{y_2 y_3 - y_1 y_4}\right),
\end{aligned}
\tag{3.6}
$$

where

$$
\begin{aligned}
y_1 &= \mu_1 k_1 J_m(k_2 a) H_m'(k_1 a) - \mu_2 k_2 J_m'(k_2 a) H_m(k_1 a) \\
y_2 &= \mu_1 k_1 H_m(k_2 a) H_m'(k_1 a) - \mu_2 k_2 H_m'(k_2 a) H_m(k_1 a) \\
y_3 &= \mu_3 k_3 J_m(k_2 b) J_m'(k_3 b) - \mu_2 k_2 J_m'(k_2 b) J_m(k_3 b) \\
y_4 &= \mu_3 k_3 J_m'(k_3 b) H_m(k_2 b) - \mu_2 k_2 J_m(k_3 b) H_m'(k_2 b).
\end{aligned}
\tag{3.7}
$$

For the multiple scattering case in which the number of fibers is N ($N \geq 2$), the solutions of the scattering coefficients in Equations (3.2-3.4) are the same as in Equations (3.6), except that the term $e^{ik_1 R_i \cos\phi_i} i^m$ should be replaced by

$$
e^{ik_1 R_i \cos\phi_i} i^m + \sum_{j \neq i}^{N} \sum_{n=-\infty}^{\infty} A_{n+m,j} H_n(k_1 r_{ij}) e^{in\theta_{ij}} . \tag{3.8}
$$

Therefore rewriting the scattering coefficients for the multiple scattering case, we have

$$
\begin{aligned}
A_{mi} &= F_{mi} a_m \\
B_{mi} &= F_{mi} b_m \\
C_{mi} &= F_{mi} c_m \\
D_{mi} &= F_{mi} d_m,
\end{aligned}
\tag{3.9}
$$

where

$$a_m = \frac{1}{H_m(k_1 a)}\left(\frac{2i\mu_1\left(y_3 H_m(k_2 a) - y_4 J_m(k_2 a)\right)}{\pi a\left(y_2 y_3 - y_1 y_4\right)} - J_m(k_1 a)\right)$$

$$b_m = -\frac{2i\mu_1}{\pi a}\left(\frac{y_4}{y_2 y_3 - y_1 y_4}\right)$$

$$c_m = \frac{2i\mu_1}{\pi a}\left(\frac{y_3}{y_2 y_3 - y_1 y_4}\right) \tag{3.10}$$

$$d_m = \frac{2i\mu_1}{J_m(k_3 b)\pi a}\left(\frac{y_3 H_m(k_2 b) - y_4 J_m(k_2 b)}{y_2 y_3 - y_1 y_4}\right)$$

$$F_{mi} = e^{ik_1 R_i \cos\phi_i} i^m + \sum_{j\neq i}^{N}\sum_{n=-\infty}^{\infty} F_{n+m,j}\, a_{n+m} H_n\left(k_1 r_{ij}\right) e^{in\theta_{ij}}.$$

If the wave length is large compared to the fiber radius, i.e. $ka>>1$, then a_m in Equation (3.10) can be approximated to be

$$a_0 = \frac{\pi i u_0}{4}(k_1 a)^2$$

$$a_m = \frac{\pi i}{m!(m-1)!} u_m \left(\frac{k_1 a}{2}\right)^{2m}, m \geq 1, \tag{3.11}$$

where

$$u_0 = d_2\left(1 - \frac{b^2}{a^2}\right) + d_3 \frac{b^2}{a^2} - 1$$

$$u_m = 2\frac{\left(m_3 - m_2\right)\left(\frac{b^2}{a^2}\right)^m - \left(m_3 + m_2\right)}{\left(1 - m_2\right)\left(m_3 - m_2\right)\left(\frac{b^2}{a^2}\right)^m - \left(1 + m_2\right)\left(m_3 + m_2\right)} - 1$$

$$m_2 = \frac{\mu_2}{\mu_1} \tag{3.12}$$

$$m_3 = \frac{\mu_3}{\mu_1}$$

$$d_2 = \frac{\rho_2}{\rho_1}$$

$$d_3 = \frac{\rho_3}{\rho_1}.$$

3.3 Statistical considerations

3.3.1 Random distribution of the fibers

Here we consider only the spatially random distribution of fibers in a composite system. The geometrical parameters that affect the distribution probability of the fibers in the composite consist of the number of the fibers per unit volume, n_0, and the radius of the fibers '*a*'. Other than these two factors, a statistical parameter, s_t, needs to be determined (will assign a number for this parameter). The definitions of the statistical notation and the probability equation in chapter 2 (2.41-2.45) still apply in this chapter. The following statistical treatments are similar to those in [35], except that the probabilistic correlation term is defined with more explicit geometrical information.

3.3.2 Simulation of the correlation function

The conditional probability $p(\mathbf{R}_2|\mathbf{R}_1)$ will be considered in more detail than in the previous chapter. For r_{12} (the distance between fiber 1 and fiber 2)$\to\infty$, the probability that fiber 2 exists at an infinite distance away from fiber 1 is the same as the probability that any single fiber exists in the composite without considering any other fibers, which is 1/s (section 2.5). Yet for $r_{12} \le 2a$, $p(\mathbf{R}_2|\mathbf{R}_1)=0$ because of the non-penetration condition of fibers. For the case where the fiber radius is smaller and the number of fibers per unit volume n_0 larger, it is more likely to find another fiber at a given distance away from an existing fiber. This corresponds to the steeper slope of the correlation curve in Figure 10. Accordingly, the correlation probability $p(\mathbf{R}_2|\mathbf{R}_1)$ can be simulated as an exponential function of r_{12}. Thus we can rewrite Equation (2.45) with more detail,

$$p(\mathbf{R}_2|\mathbf{R}_1) = \frac{1}{s}\left(1 - f(r_{12})\right) \quad , r_{12} > 2a$$

$$= 0 \quad , r_{12} \le 2a \tag{3.13}$$

where $f(r_{12}) = Ce^{-r_{12}/(a^2/n_0)^{s_t}}$, $0<C<e^{2a/(a^2/n_0)^{s_t}}$.

The above is usually referred to as the 'well-stirred' approximation [37], which is not valid for a high concentrations of scatterers (or for lumpy concentration, in certain part of the composite domain, of scatterers). For a large sample, or for a large domain of the composite, $C\to e^{2a/(a^2/n_0)^{s_t}}$ due to the fact that the number of fibers surrounding the existing fiber is small compared with '*N*' (a large number). Exactly how large a number '*N*' of fibers (or how large n_0) do we need to make the correlation function a reasonable approximation is mostly a statistical issue. We will discuss it in due course. Note that the statistical parameter 's_t' needs to be determined statistically (it is assumed that s_t=0.1 for all the cases). Yet for our computational analyses, a number will be assigned.. Finally the normalization requires that

$$\lim_{R\to\infty} \frac{1}{R^2}\int_{2a}^{R} f(r_{12}) r_{12}\, dr_{12} = 0 .$$

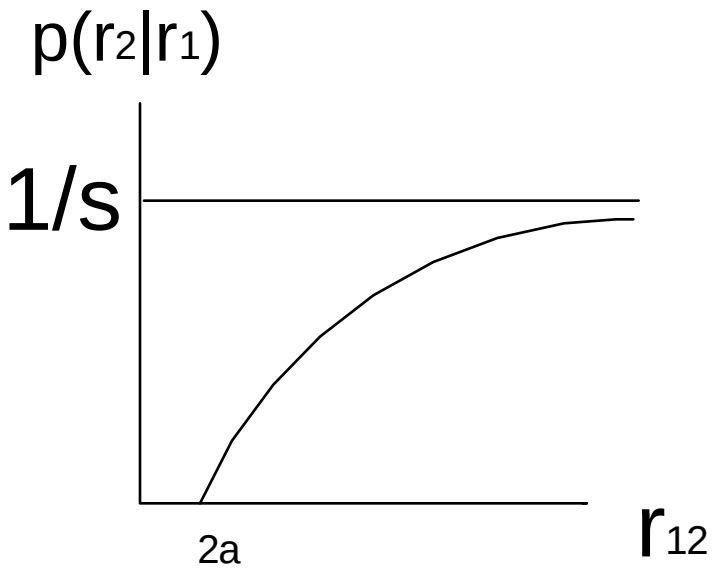

Figure 10. Simulation of the correlation function.

3.4 Averaging technique

From the last equation of (3.10), due to the indistinguishability (2.42) of the fibers, one can chose fiber '1' to investigate the expectation value of F_{mi} without loss of generality. Thus

$$F_{m1} = e^{ik_1 R_1 \cos\phi_1} i^m + \sum_{j=2}^{N} \sum_{n=-\infty}^{\infty} F_{n+m,j} a_{n+m} H_n\left(k_1 r_{1j}\right) e^{in\theta_{1j}} \quad . \tag{3.14}$$

Taking the conditional expectation value of F_{m1}, we have, by using (2.42) and applying the quasi-crystalline approximation (2.40) (which has been proven valid for fiber-reinforced composites in chapter 2),

$$\left\langle F_{m1} \right\rangle_1 = e^{ik_1 R_1 \cos\phi_1} i^m + n_0 \left(1 - \frac{1}{N}\right) \sum_{n=-\infty}^{\infty} a_{n+m} \int_{|\vec{r}_2 - \vec{r}_1| \geq 2a} \left(1 - f\left(r_{12}\right)\right) \left\langle F_{n+m,2} \right\rangle_2 H_n\left(k_1 r_{12}\right) e^{in\theta_{12}} d\tau_2 \quad . \tag{3.15}$$

For a large sample, *1/N* can be ignored. By substituting (3.13) into (3.15), the above equation becomes

$$\left\langle F_{m1} \right\rangle_1 = e^{ik_1 R_1 \cos\phi_1} i^m + n_0 \sum_{n=-\infty}^{\infty} a_{n+m} \int_{|\vec{r}_2 - \vec{r}_1| \geq 2a} \left(1 - e^{2a - r_{12} \Big/ \left(a^2/n_0\right)^{s_t}}\right) \left\langle F_{n+m,2} \right\rangle_2 H_n\left(k_1 r_{12}\right) e^{in\theta_{12}} d\tau_2 \ . \tag{3.16}$$

Assume the existence of an average wave such that

$$\left\langle F_{mi} \right\rangle_i = i^m F_m e^{iKx_i} \quad , \tag{3.17}$$

where K is an effective wave number in the composite system. Then by applying the extinction theorem (the incident waves vanish upon entering the composites [35], or the incident wave is canceled by waves generated at the boundary [31]) and using (3.17), Equation (3.16) becomes

$$\begin{aligned} F_m = 2\pi n_0 \sum_{n=-\infty}^{\infty} a_{n+m} F_{n+m} \Bigg[& \frac{a}{k_1^2 - K^2} \left(J_n(2Ka) \frac{\partial}{\partial a} H_n\left(2k_1 a\right) - H_n\left(2k_1 a\right) \frac{\partial}{\partial a} J_n(2Ka) \right) - \\ & \int_{2a}^{0} e^{\frac{2a - r_{12}}{\left(a^2/n_0\right)^{s_t}}} J_n\left(Kr_{12}\right) H_n\left(k_1 r_{12}\right) r_{12} dr_{12} \Bigg]. \end{aligned} \tag{3.18}$$

For wave lengths that are large compared to the fiber radius, the above equation can be simplified to be

$$F_m = 2\pi n_0 \sum_{n=-\infty}^{\infty} a_{n+m} F_{n+m} \left[\frac{2i}{\pi} \left(\frac{K}{k_1} \right)^{|n|} \frac{1}{k_1^2 - K^2} - \frac{1}{k_1^2} I_n \right] \quad , \tag{3.19}$$

where

$$I_n = \int_{2k_1 a}^{0} e^{\frac{2a - \frac{x}{k_1}}{\left(a^2/n_0\right)^{s_t}}} J_n\left(\frac{K}{k_1} x\right) H_n(x) x dx \quad . \tag{3.20}$$

Apparently I_n becomes zero in the static limit. Equation (3.19) can be considered as three homogeneous equations in F_0, F_{-1} and F_1. For the nontrivial solution of the F terms, the

determinant of the homogeneous equation must be zero. Thus the equation for K can be expressed as

$$\left[\left(cu_1 - 1 - \frac{i\pi}{2}cu_1(I_0 + I_2)\right)\left(\frac{i\pi}{2}cu_0 I_0 + 1\right) - \frac{\pi^2}{4}c^2 u_1 I_1^2 (u_0 + u_1)\right]\left(\frac{K}{k_1}\right)^2$$

$$-\frac{\pi i}{2}c^2 u_1 I_1 (u_1 + 3u_0)\frac{K}{k_1} \qquad (3.21)$$

$$+\frac{\pi^2}{4}c^2 u_1 I_1^2 (u_0 + u_1) + \left(cu_0 + \frac{i\pi}{2}cu_0 I_0 + 1\right)\left(\frac{\pi i}{2}cu_1(I_0 + I_2) + 1 + cu_1\right) = 0.$$

Note that 'c' in (3.21) is the fiber volume fraction in the composite. In the static limit, the above equation reduces to

$$\left(\frac{K}{k_1}\right)^2 = (1 + cu_0)\frac{1 + cu_1}{1 - cu_1} \quad , \qquad (3.22)$$

which can be further simplified to obtain the global shear modulus M. Thus

$$\frac{\mathrm{M}}{\mu_1} = \frac{1 - cu_1}{1 + cu_1} \quad . \qquad (3.23)$$

For low-frequency dynamic case, (K/k_1) cannot be obtained directly from Equation (3.21), since the I_n terms (3.20) are functions of (K/k_1). Therefore to obtain the dynamic quantities, we need to give an initial value of (K/k_1) and substitute it into (3.20) to obtain initial values of I_n terms. Equation (3.21) can then be solved, using the initial values of the I_n terms, to obtain the first approximate value of (K/k_1). This value would substitute back to (3.20) to start another round of computations. By recursively using Equations (3.20) and (3.21), a convergent quantity of (K/k_1) can be obtained. Evidently the static value of (K/k_1) obtained from (3.22) is the best candidate to be the initial value. Note that in the low- frequencies dynamic state, the overall effective wave number K in Equation (3.21) is a complex number,

$$K = \mathrm{Re}(K) + i\,\mathrm{Im}(K) \quad , \qquad (3.24)$$

where $\mathrm{Re}(K) = \frac{\omega}{\mathrm{B}}$. B is the overall effective shear wave phase speed in the composite. The imaginary part of K is a measurement of wave attenuation in the composite. The specific damping capacity, which is defined as $\Psi = 4\pi\frac{\mathrm{Im}(K)}{\mathrm{Re}(K)}$ is widely used for the attenuation measurement.

Observing Equation (3.21), the effective global properties are dependent on the fiber volume fraction ('c'), the I_n terms, and u_0 and u_1. Apparently u_0 and u_1 are functions of the shear modulus and density of the constituents of the composite and their structures. For a composite with multiple interfacial layers, only u_0 and u_1 need to be modified so that Equation (3.21) can be generalized. Since u_0 and u_1 in Equation (3.12) are apparently derived from the scattering coefficient in the matrix region, we will apply the same procedures (as in section 3.2) in the next section to obtain this particular scattering coefficient for the multiple interfacial-layers case.

3.5 Scattering coefficient in the matrix for a fiber-matrix composite with multiple interfacial layers

In this section we study only u_0 and u_1 (as in Equation 3.12) for a fiber-matrix composite with multiple interfacial layers. A representative fiber with multiple interfacial layers is shown in Figure 11. We designate the fiber core region as '0' and the n-layers (starting from inner layer) interfacial regions as '1,2…n'. The material properties (shear modulus, μ, and material density, ρ) for the interfacial regions are given according to the designated numbers. The properties in the matrix are simply μ and ρ. As we did in the section 3.2, a boundary value problem needs to be set up and the solutions need to be obtained for the scattering coefficient in the matrix. The incident harmonic axial shear displacement wave, e^{ikx}, is again

$$u^{in} = e^{ikx} = e^{ikR\cos\Phi} \sum_{m=-\infty}^{\infty} i^m J_m(kr) e^{im\theta}$$

The displacements in the matrix, fiber and each interfacial region can be written as

$$\begin{aligned}
u &= e^{ikR\cos\Phi} \sum_{m=-\infty}^{\infty} i^m J_m(kr) e^{im\theta} + \sum_{m=-\infty}^{\infty} B_m H_m(kr) e^{im\theta}, r \geq a_n \\
&= \sum_{m=-\infty}^{\infty} \left(A_{mn} J_m(k_n r) + B_{mn} H_m(k_n r) \right) e^{im\theta}, a_n \geq r \geq a_{n-1} \\
&= \sum_{m=-\infty}^{\infty} \left(A_{m,n-1} J_m(k_{n-1} r) + B_{m,n-1} H_m(k_{n-1} r) \right) e^{im\theta}, a_{n-1} \geq r \geq a_{n-2} \\
&\vdots \\
&= \sum_{m=-\infty}^{\infty} \left(A_{m1} J_m(k_1 r) + B_{m1} H_m(k_1 r) \right) e^{im\theta}, a_1 \geq r \geq a_0 \\
&= \sum_{m=-\infty}^{\infty} A_{m0} J_m(k_0 r) e^{im\theta}, a_0 \geq r.
\end{aligned} \tag{3.25}$$

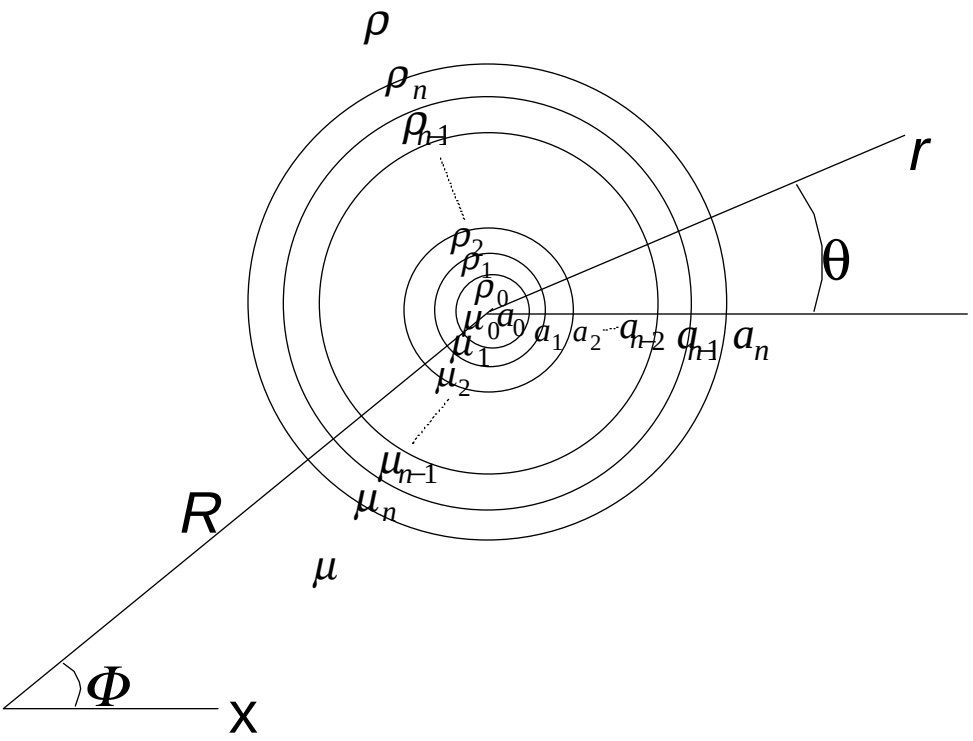

Figure 11. A representative multiphase fiber embedded in the matrix.

Note that in the above, the scattering coefficient in the matrix is B_m in the first equation of (3.25). The number of unknown coefficients in (3.25) is 2n+2. The number of boundary conditions (stress and displacement continuity for 'n+1' boundaries) is also 2n+2. Applying the displacement and stress continuity boundary conditions, we get a matrix equation

$$[A]\{x\} = \{B\} \quad , \tag{3.26}$$

where $[A]$ and $\{B\}$ are given (Appendix C), and $\{x\}$ are the scattering-coefficients vector which can be solved. $\{x\}$ can be written as

$$\{x\} = \begin{Bmatrix} A_{m0} \\ A_{m1} \\ B_{m1} \\ | \\ | \\ | \\ | \\ A_{mn} \\ B_{mn} \\ B_m \end{Bmatrix} \quad , \tag{3.27}$$

and that $\{x\}$ is a (2n+2) vector. Rewrite Equation (3.26) as

$$\{x\} = [A]^{-1}\{B\} = \frac{1}{|A|}\begin{pmatrix} A_{11} & A_{21} & \cdots & A_{n1} \\ A_{12} & A_{22} & \ddots & \vdots \\ \vdots & \ddots & \ddots & A_{n,n-1} \\ A_{1n} & \cdots & A_{n-1,n} & A_{nn} \end{pmatrix}\{B\} \quad . \tag{3.28}$$

Here A_{ij} is the cofactor of the matrix [A] and |A| is the determinant of [A]. The scattering coefficient in the matrix region of the composite, B_m, is therefore:

$$B_m = \frac{1}{|A|}\left[A_{n-1,n}J_m(ka_n) + A_{n,n}\mu k J_m'(ka_n)\right] i^m e^{ikR\cos\Phi} \quad . \tag{3.29}$$

Apparently if (3.29) is rewritten as

$$B_m = b_m i^m e^{ikR\cos\Phi} \quad ,$$

$$\text{where } b_m = \frac{1}{|A|}\left[A_{n-1,n}J_m(ka_n) + A_{n,n}\mu k J_m'(ka_n)\right], \tag{3.30}$$

then the multiple scattering equation for the multiple-interfacial-layers composite (as in the last of Equation 3.10) is simply

$$F_{mi} = e^{ik_1 R_i \cos\phi_i} i^m + \sum_{j\neq i}^{N}\sum_{n=-\infty}^{\infty} F_{n+m,j}\, b_{n+m} H_n(k_1 r_{ij}) e^{in\theta_{ij}} \quad . \tag{3.31}$$

The determinant $|A|$, the cofactor $A_{n-1,n}$ and A_{nn} can easily be computed to obtain the property of b_m. As in Equation (3.11), u_1 and u_0 can be calculated from b_m for wave lengths large compared to the fiber radius a_n. Consequently b_1 can be approximated as

$$b_1 = \frac{i\pi}{4}(ka_n)^2 u_1 \quad , \tag{3.32}$$

where $u_1 = \frac{A_1}{A_2}$. A_1 is the determinant of a (2n+1)×(2n+1) matrix $[A_1]$, and A_2 is the determinant of a (2n+2)×(2n+2) matrix $[A_2]$ (Appendix C).

For b_0, different asymptotic values would be used for determinant |A|, $A_{n-1,n}J_m(ka_n)$, and $A_{n,n}\mu k J_m'(ka_n)$ in Equation (3.30). Consequently the 'b_0' becomes

$$b_0 = \frac{\pi i}{4}(ka_1)^2 u_0 \quad , \tag{3.33}$$

where $u_0 = \left(\frac{\rho_1}{\rho} - \left(\frac{a_0}{a_1}\right)^2\left(\frac{\rho_1-\rho_0}{\rho}\right) - 1\right)$ for fibers with 1-layer-interface,

$$= \left(\frac{\rho_2}{\rho} - \left(\frac{a_1}{a_2}\right)^2\left(\frac{\rho_2-\rho_1}{\rho}\right) - \left(\frac{a_0}{a_2}\right)^2\left(\frac{\rho_1-\rho_0}{\rho}\right) - 1\right)$$ for fibers with 2-layer-interface,

$$= \left(\frac{\rho_3}{\rho} - \left(\frac{a_2}{a_3}\right)^2\left(\frac{\rho_3-\rho_2}{\rho}\right) - \left(\frac{a_1}{a_3}\right)^2\left(\frac{\rho_2-\rho_1}{\rho}\right) - \left(\frac{a_0}{a_3}\right)^2\left(\frac{\rho_1-\rho_0}{\rho}\right) - 1\right)$$ for fibers with 3-layer-interface. Generally

$$u_0 = \left[\frac{\rho_n}{\rho} - \left(\frac{a_{n-1}}{a_n}\right)^2\left(\frac{\rho_n-\rho_{n-1}}{\rho}\right) - \left(\frac{a_{n-2}}{a_n}\right)^2\left(\frac{\rho_{n-1}-\rho_{n-2}}{\rho}\right) - \left(\frac{a_{n-3}}{a_n}\right)^2\left(\frac{\rho_{n-2}-\rho_{n-3}}{\rho}\right)\right.$$
$$\left. \cdots - \left(\frac{a_2}{a_n}\right)^2\left(\frac{\rho_3-\rho_2}{\rho}\right) - \left(\frac{a_1}{a_n}\right)^2\left(\frac{\rho_2-\rho_1}{\rho}\right) - \left(\frac{a_0}{a_n}\right)^2\left(\frac{\rho_1-\rho_0}{\rho}\right) - 1\right] \tag{3.34}$$

for fibers with a n-layer-interface. Thus the u_1 and u_0 terms are established for the fiber-reinforced composite with multiple interfacial layers.

3.6 Numerical Results

A computer program, based on Equations (3.20-3.22), (C3), (C4) and (3.34), has been created to calculate the overall effective normalized axial shear modulus (M/μ_1), the normalized axial shear wave phase speed (B/β_1) and the axial shear wave specific damping capacity (Ψ) of a multiphase fiber-matrix composite. Note that the subscript '1' indicates the mechanical property of the matrix material. Apparently when the wave frequency becomes zero, i.e. in static state, the I_n terms in Equation (3.20) become zero. Then (3.21) degenerates to (3.22), from which it can be further simplified to (3.23) and M/μ_1 can be obtained. For the low-frequency dynamic state (our equation applies only when the frequencies are such that $k_1a_n<0.1$), B/β_1 and Ψ can be obtained as previously described. The u_0 and u_1 terms in (3.21) depend on the material

properties (shear moduli and density) of the constituent materials in the composite. For the sake of demonstrating the applicability of our program, we assume that the material properties of the interfacial region possess either a linear or exponential distribution between the fiber core and the matrix. Thus

$$\frac{\mu_i}{\mu_2} = 1 - \left(1 - \frac{\mu_1}{\mu_2}\right)\left(\frac{f_i}{f}\right)^{kface}$$
$$\frac{\rho_i}{\rho_2} = 1 + \left(\frac{\rho_1}{\rho_2} - 1\right)\left(\frac{f_i}{f}\right)^{kface} . \qquad (3.35)$$

Here again the subscripts '1' and '2' indicate the material properties in the matrix and in the fiber core respectively, and '*i*' indicates those in the interfacial region. The 'f_i' indicates the distance from the fiber core to the individual interfacial layer and 'f' is the whole thickness of the interfacial region. The thickness of the interfacial layer is evenly divided. Finally the '*kface*' indicates the exponential order of the material property distribution. Apparently when *kface*=1, the interfacial zone is a linear distribution, otherwise it is an exponential distribution (Figure 12). Note that the composites for our case are such that the fiber core is more stiff and less weighted than those of the matrix. Specifically, μ_1=1.28e^{10} Pa, μ_2=8.08e^{10} Pa, ρ_1=801 Kg/m^3, ρ_2 =234.7 Kg/m^3. In Figure 13, the damping capacity as a function of wave frequencies for various cases of different interfacial thickness is shown. As expected, the thinner the interfacial depth, the less damped the composites. In Figure 14, the damping capacity of a linear distribution of the interfacial region is calculated for various cases of different numbers of divisions. The Figure shows that if the number of divisions of the interfacial region increase, the composites is less damped. This can be explained by the scattering of energy due to the mismatch of impedance when waves propagate between the fiber core and matrix. More interphase divisions mean that the composite has smoother change of material properties and less impedance mismatch. Therefore less energy is scattered and the composite has a lower damping capacity. The same phenomenon can be observed for an exponential distribution case in Figure 15. Finally in Figure 16, damping capacity is calculated for various cases of the different exponential order distributions of the interfacial regions. Figure 16 shows that the exponential order cases are more damped than the linear distribution case. Again the unevenly distributed material properties in the interphase area cause more damping for the composite.

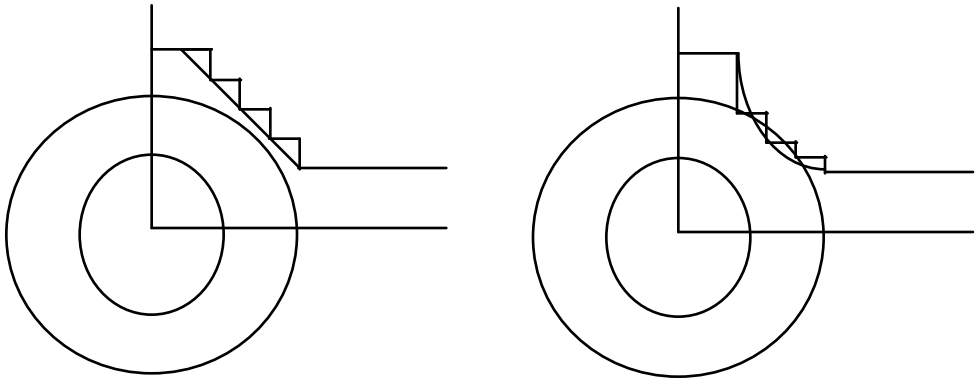

Figure 12. Schematic representation of the interfacial material properties (μ and ρ). When kface=1, the material properties are linear distributed. When kface=2,3..., they are exponential distributed.

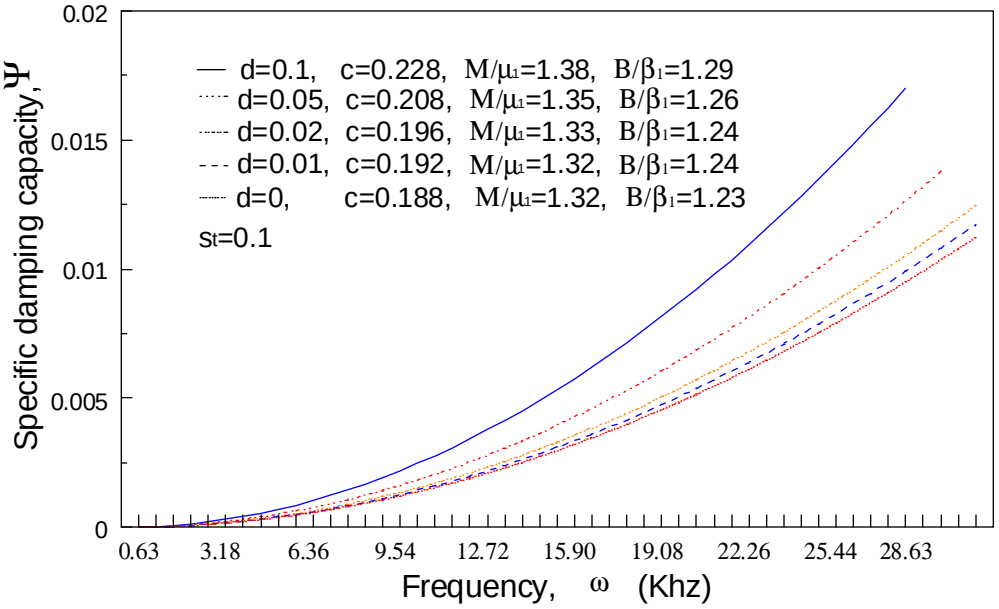

Figure 13. Specific damping capacity as a function of wave frequency for various cases of interfacial length ('d', the percentage of the fiber radius). 'c' is the fiber vol. fraction. M/μ_1 is the normalized static shear modulus. B/β_1 is the normalized shear wave phase speed. Note that the normalized shear wave phase speed does not change for the low frequencies ranges and the statistical parameter s_t is given as 0.1.

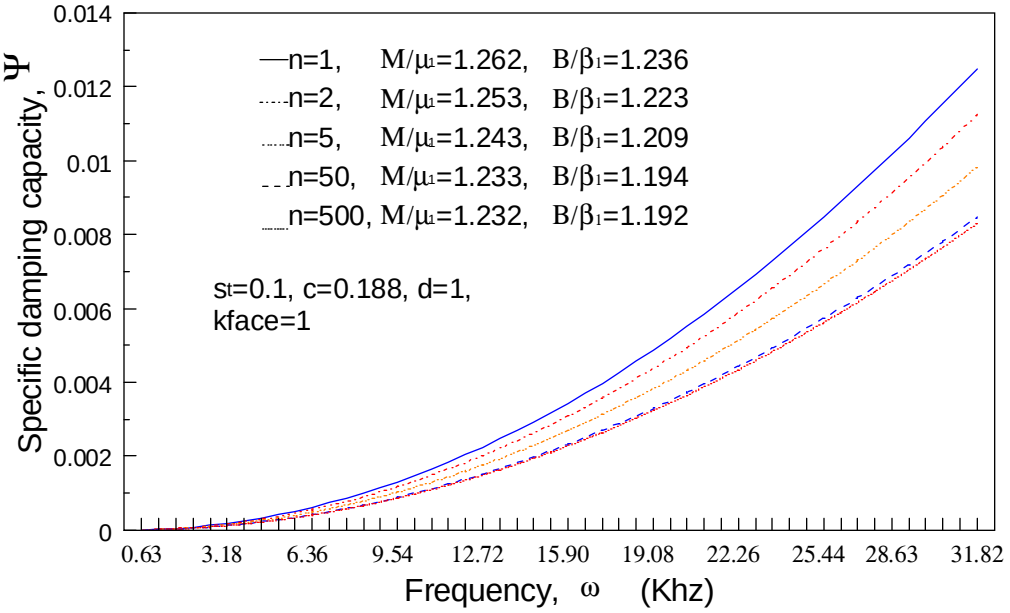

Figure 14. Specific damping capacity for different numbers of interfacial layers. 'n' is the number of layers. 'kface' is the exponential order of the division. For ‘kface’=1, the interfacial material properties are distributed linearly throughout the interfacial region.

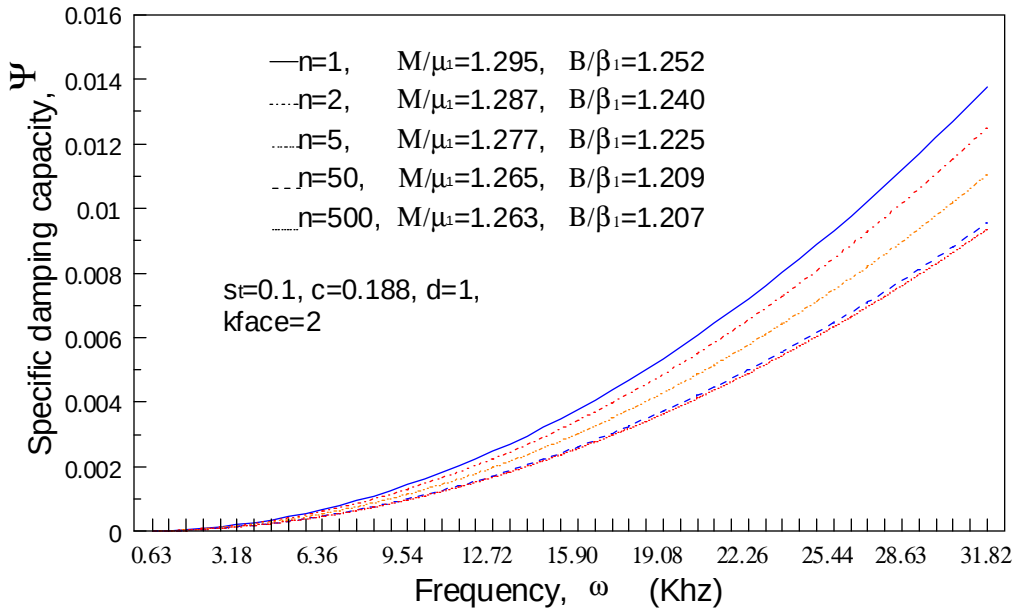

Figure 15. Specific damping capacity for different numbers of divisional interfacial layers. All the parameters are the same as in Figure 14 except that the exponential order of the division is 'kface'=2.

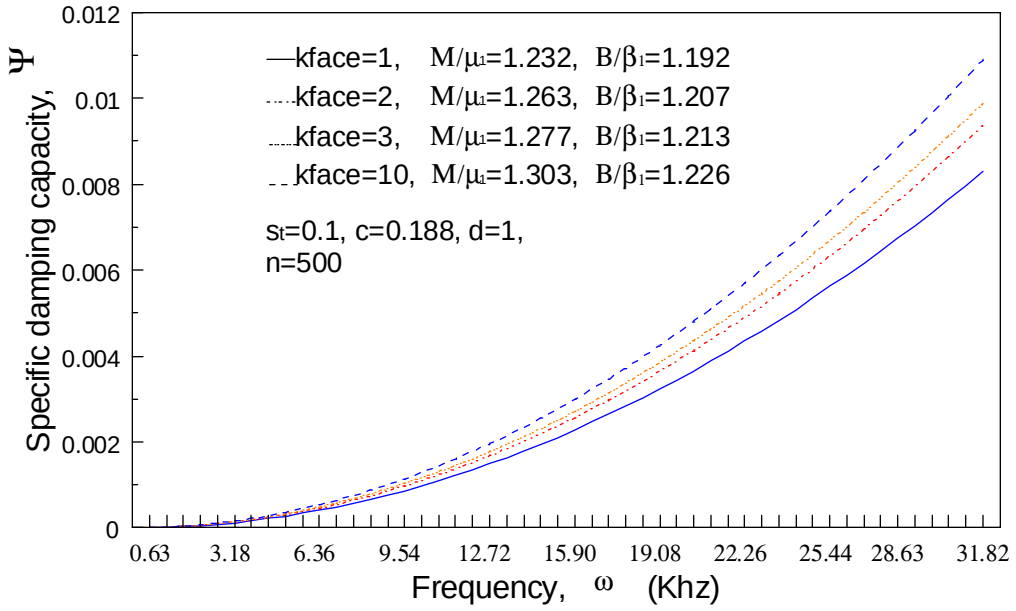

Figure 16. Specific damping capacity for various cases of different exponential orders of divisions. The number of divisional layers is 'n=500'.

3.7 Summary

The effects of interfacial material properties on the overall mechanical behavior of a multiphase fiber-matrix composite are investigated through the use of wave theories. The fiber-matrix composite consists of identical fibers which are imbedded in a matrix. Multiphase interfacial regions are assumed to exist between the fiber core and the matrix, and their material properties are assumed to have linear or exponential order distributions between the fiber core and the matrix. Only the case of axial shear waves is studied, therefore the effective global axial shear modulus (M), the axial shear wave phase speed (B) and the axial shear wave specific damping capacity (Ψ) are obtained. The analyses indicate that the effective global material properties of the multiphase composite depend on (in addition to the fiber volume fraction, c, and the dynamic parameters I_n) two parameters u_0 and u_1. u_1 can be represented by a division for which both the dividend and divisor are determinants of square matrices (3.32). u_0 is a series summation (3.34). The numerical computations show, among others, that the smoother (more divisional layers), or thinner, the interfacial region the less damped the composite material. And the composites with exponential order distribution of the interfacial region are more damped than the one with a linear distribution. For all cases, waves in the composites are indispersive for the low frequency range. Finally the statistical number s_t in Equation (3.13) is given as 0.1 for each dynamic case. The computations show that the change of s_t (for the same order) does not have a significant effect on the results.

CHAPTER 4. AXIAL SHEAR WAVES IN FIBER-REINFORCED COMPOSITES WITH INTERFACIAL CRACKS

4.1 Background

Theories of elastic waves in a variety of debonded situations have been studied extensively [62-78]. Solution techniques include the integral equation method [65,67,69,] and the perturbation method [84-85]. A more straightforward approach is the employment of the eigenfunction expansion of solutions which are subjected to boundary conditions [72]. With various solution techniques and points of emphasis, elastic wave propagation in composites with the presence of imperfect bonding has been studied by many researchers [75-78]. In this chapter, we adopt the method used by Bose and Mal [35], combined with the approach by Yang and Norris [72], in dealing with fiber-reinforced composites with interfacial cracks. For simplicity, an idealistic situation is assumed where all fibers in a composite have the same radius and bonding situations. The bonding situations are determined by the half crack length, δ, and the orientation, α, of the crack face (Figure 17). The approach we use is straightforward but mathematically rigorous. Starting with the eigenfunction expansion (Bessel functions) of the wave equation, we seek to obtain the scattering coefficients as functions of the geometrical and crack parameters and as the dynamic response of the waves in the composites. The scattering coefficients thus obtained are functions of themselves. By performing the asymptotic analyses and, through statistical averaging procedures, assuming the existence of an effective plane wave, a system of simultaneous linear equations emerges. Both the static property (shear modulus μ) and the dynamic properties (shear wave phase velocity B and specific damping capacity Ψ) can be deduced from this matrix equation. The calculated average properties are generally complex numbers for the dynamic case and real numbers for the static case. For the dynamic case, the complex numbers of the mechanical properties correspond to the visco-elasticity of the material. The real numbers for the static case correspond to the elasticity of the material.

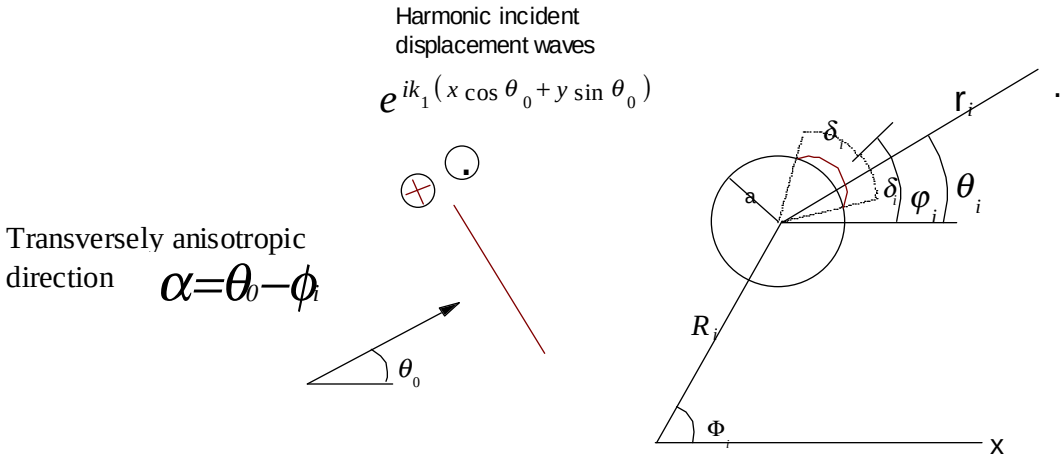

Figure 17. Schematic representation of the incident shear displacement waves and the polar coordinate of the fiber 'i' in the composite system.

4.2 Boundary value problem

4.2.1 Single fiber scattering

Consider a single-fiber-matrix composite where the interface between the fiber and the matrix has a debonded crack length of $2\delta_i$ radians (Figure 17). The center line of the crack face has an orientation of an angle of φ_i radians away from the horizontal radius line of the fiber. The location of the fiber '*i*' and a field point of interest as referenced to the center of the fiber are expressed by the polar coordinate system. The radius of the fiber is 'a'. As before, the material properties associated with the matrix will be denoted as '1', and those associated with the fiber will be denoted as '2'.

Let a plane axially shear displacement wave, $e^{ik_1(x\cos\theta_0+y\sin\theta_0)}$, be incident upon the composite. The incident waves are time-harmonic with a frequency of ω. The time factor, $e^{-i\omega t}$, will be omitted because of the steady state condition. Then the displacement in both the matrix and in the fiber can be written as

$$u_i = \begin{cases} u^{in} + u_{1,i}, r_i > a \\ u_{2,i}, r_i < a \end{cases} , \tag{4.1}$$

where u^{in} is the incident wave, $u_{1,i}$ is the scattering wave in the matrix, and $u_{2,i}$ is the scattering wave inside the fiber. Since they are solutions of the Helmholtz equation, $\nabla^2 u_i + k^2 u_i = 0$, they can be expressed as the series representation of Bessel and Hankel functions:

$$u^{in} = e^{ik_1 R_i \cos(\Phi_i-\theta_0)} \sum_{m=-\infty}^{\infty} i^m J_m(k_1 r_i) e^{im(\theta_i-\theta_0)}$$

$$u_{1,i} = \sum_{m=-\infty}^{\infty} A_{mi} H_m(k_1 r_i) e^{im(\theta_i-\theta_0)} \tag{4.2}$$

$$u_{2,i} = \sum_{m=-\infty}^{\infty} B_{mi} J_m(k_2 r_i) e^{im(\theta_i-\theta_0)}.$$

Here k_1 is the wave number in the matrix, k_2 in the fiber. The coordinate system (r_i,θ_i) refers to the center of the fiber '*i*'. Note that $k_1=\omega/\beta_1$, $k_2=\omega/\beta_2$, $\beta_1 = \sqrt{\mu_1/\rho_1}$, $\beta_2 = \sqrt{\mu_2/\rho_2}$. β is the wave speed, μ is the shear modulus and ρ is the material density. From the stress boundary condition on the matrix-fiber interface:

$$\mu_1 \frac{\partial}{\partial r_i}\left(u^{in} + u_{1,i}\right)_{r_i=a} = \mu_2 \frac{\partial}{\partial r_i}\left(u_{2,i}\right)_{r_i=a} \quad . \tag{4.3}$$

Substitute the relevant terms (Equation 4.2) into Equation 4.3 and simplify,

$$e^{ik_1 R_i \cos(\Phi_i-\theta_0)} i^n \mu_1 k_1 J_n'(k_1 a) + A_{ni}\mu_1 k_1 H_n'(k_1 a) = B_{ni}\mu_2 k_2 J_n'(k_2 a) \quad . \tag{4.4}$$

For displacement boundary conditions we have

$$\begin{cases} \left(u^{in}+u_{1,i}-u_{2,i}\right)_{r_i=a}=\Delta U_i(\theta_i), & -\delta_i+\varphi_i<\theta_i<\delta_i+\varphi_i \\ \left(u^{in}+u_{1,i}-u_{2,i}\right)_{r_i=a}=0, & other \end{cases}, \tag{4.5}$$

where $\Delta U_i(\theta_i)$ is the dynamic crack opening displacement (COD) of fiber '*i*'. From elasticity, the COD must be satisfied by the crack edge condition which is explained in the following. Let x be the amount of radians measured from the center line of the crack face. x is positive if it is measured counterclockwise, negative if measured clockwise. Thus from Figure 17, x=0 corresponds to the center line of the crack face, x=±1 to the broken lines indicated. Obviously, x can be expressed as $x=\frac{\theta_i-\varphi_i}{\delta_i}$. The crack edge condition requires (and can be shown) that the COD around the crack edge decreases proportionally as $O\left(\varepsilon^{1/2}\right)$, where $1-|x|\rightarrow\varepsilon$ (a small number) [67]. Since the Chebychev functions of the second kind $V_n(x)$ (appendix D) decrease proportionally as $O\left(\varepsilon^{1/2}\right)$ when $1-|x|\rightarrow\varepsilon$, i.e. when near the crack tip, it is reasonable to use $V_n(x)$ as our base function for the series expansion of COD. The COD, $\Delta U_i(\theta_i)$, can then be expressed as

$$\Delta U_i(\theta_i)=\sum_{n=1}^{\infty}\beta_{n,i}\phi_{n,i}(\theta_i) \quad , \tag{4.6}$$

where $\beta_{n,i}$ is the coefficient of the COD series and

$$\phi_{n,i}(\theta_i)=\frac{1}{n}V_n\left(\frac{\theta_i-\varphi_i}{\delta_i}\right)=\frac{1}{n}\sin\left(\frac{n\pi}{2}-n\sin^{-1}\frac{\theta_i-\varphi_i}{\delta_i}\right), \quad n=1,2,3\cdots \quad . \tag{4.7}$$

Substitute the relevant terms into the displacement boundary condition (Equation 4.5) and simplify

$$\begin{aligned} &e^{ik_1R_i\cos(\Phi_i-\theta_0)}i^nJ_n(k_1a)+A_{ni}H_n(k_1a)=B_{ni}J_n(k_2a)+\frac{e^{in(\theta_0-\varphi_i)}}{2n}\sum_{n'=1}^{\infty}\beta_{n',i}i^{n'+1}J_{n'}(-n\delta_i), n\neq 0 \\ &e^{ik_1R_i\cos(\Phi_i-\theta_0)}J_0(k_1a)+A_{0i}H_0(k_1a)=B_{0i}J_0(k_2a)+\frac{1}{4}\beta_{1,i}\delta_i, n=0. \end{aligned} \tag{4.8}$$

Combining Equations (4.4) and (4.8), yields

$$\begin{aligned} A_{mi}&=\frac{E_m}{D_m}F_{mi} \\ B_{mi}&=\frac{2i}{\pi k_1a}\frac{F_{mi}}{D_m}+\frac{J_m'(k_1a)}{2mE_m}e^{im(\theta_0-\varphi_i)}\sum_{n'=1}^{\infty}\beta_{n',i}i^{n'+1}J_{n'}(-m\delta_i) \quad , \quad m\neq 0 \\ F_{mi}&=e^{ik_1R_i\cos(\Phi_i-\theta_0)}i^m-\frac{zJ_m'(k_2a)}{2mE_m}e^{im(\theta_0-\varphi_i)}\sum_{n'=1}^{\infty}\beta_{n',i}i^{n'+1}J_{n'}(-m\delta_i) \end{aligned} \tag{4.9}$$

and

$$A_{0i} = \frac{E_0}{D_0} F_{0i}$$

$$B_{0i} = \frac{2i}{\pi k_1 a} \frac{F_{0i}}{D_0} + \frac{J_0'(k_1 a)}{4E_0} \beta_{1,i} \delta_i \quad , \tag{4.10}$$

$$F_{0i} = e^{ik_1 R_i \cos(\Phi_i - \theta_0)} - \frac{z J_0'(k_2 a)}{4E_0} \beta_{1,i} \delta_i$$

where

$$E_m = z J_m(k_1 a) J_m'(k_2 a) - J_m(k_2 a) J_m'(k_1 a)$$

$$D_m = J_m(k_2 a) H_m'(k_1 a) - z J_m'(k_2 a) H_m(k_1 a)$$

$$z = \frac{\mu_2 k_2}{\mu_1 k_1}.$$

The β terms (coefficients of the COD) in the above equations can be solved by requiring that, at fiber '*i*', the stress on the crack face be vanished. Therefore, at fiber '*i*',

$$\frac{\partial}{\partial r_i}\left(u_{2,i}\right)_{r_i = a} = 0, -\delta_i + \varphi_i < \theta_i < \delta_i + \varphi_i \,. \tag{4.11}$$

The equation above becomes

$$B_{0,i} J_0'(k_2 a) \frac{(-1)^m \pi \delta_i}{2m} \delta_{1m} = \sum_{p \neq 0}^{\infty} B_{pi} J_p'(k_2 a) e^{-ip(\theta_0 - \varphi_i)} \frac{\pi}{-p} i^{m+1} J_m(p\delta_i), -\delta_i + \varphi_i < \theta_i < \delta_i + \varphi_i \,. \tag{4.12}$$

Substitute B_{mi} terms from (4.9) and (4.10) into Equation 4.12 and multiply both sides by $\phi_m(\theta_i)$ of Equation 4.7. Then integrate both sides with respect to θ_i from $-\delta_i+\varphi_i$ to $\delta_i+\varphi_I$, and we get

$$\begin{aligned} &\frac{i}{\pi k_1 a} J_0'(k_2 a) \frac{(-1)^m \delta_i}{m D_0} \delta_{1m} F_{0i} + \sum_{p \neq 0}^{\infty} \frac{2i}{\pi k_1 a} J_p'(k_2 a) e^{-ip(\theta_0 - \varphi_i)} \frac{i^{m+1}}{p D_p} J_m(p\delta_i) F_{pi} \\ &= \frac{J_0'(k_1 a)}{8E_0} \delta_i^2 J_0'(k_2 a) \frac{(-1)^{m+1}}{m} \delta_{1m} \beta_{1,i} - \sum_{p \neq 0}^{\infty} \frac{J_p'(k_1 a) J_p'(k_2 a)}{2p^2 E_p} i^{m+1} J_m(p\delta_i) \sum_{n=1}^{\infty} \beta_{n,i} i^{n+1} J_n(-p\delta_i). \end{aligned} \tag{4.13}$$

Simplify Equation 4.13 further and rearrange, and we get the matrix equation in β as $\left[Q_{mn,i}\right]\left\{\beta_{n,i}\right\} = \left\{N_{m,i}\right\}$, where

$$Q_{mn,i} = \left(\frac{iz}{\pi k_1 a} J_0'(k_2 a) \frac{(-1)^m}{D_0} + \frac{J_0'(k_1 a)}{2} (-1)^{m+1} \right) \frac{\delta_i^2}{m} \frac{J_0'(k_2 a)}{4E_0} \delta_{1m} \delta_{1n} +$$

$$i^{n+1} \left[J_n(-m\delta_i) \frac{-i^m}{\pi k_1 a} \frac{z J_m'(k_2 a)}{m E_m} e^{im(\theta_0 - \varphi_i)} \sum_{p \neq 0}^{\infty} J_p'(k_2 a) e^{-ip(\theta_0 - \varphi_i)} \frac{J_m(p\delta_i)}{D_p p} - i^{m+1} \sum_{p \neq 0}^{\infty} \frac{J_p'(k_1 a) J_p'(k_2 a)}{2p^2 E_p} J_n(-p\delta_i) J_m(p\delta_i) \right]$$

$$N_{m,i} = \left[J_0'(k_2 a) \frac{\delta_i}{m D_0} \delta_{1m} + \sum_{p \neq 0}^{\infty} J_p'(k_2 a) e^{-ip(\theta_0 - \varphi_i)} \frac{2i}{D_p p} J_m(p\delta_i) \right] \frac{i}{\pi k_1 a} (-1)^m e^{ik_1 R_i \cos(\Phi_i - \theta_0)} \quad . \tag{4.14}$$

Note that δ_{mn}'s are the Kronecker deltas. The β terms can then be solved numerically in light of the above equation. Equation (4.14) can be simplified further for the quasi-static case, i.e., when the wave length is large compared with the fiber radius. In this case, it is assumed that both k_1a and k_2a are small compared to 1 and that the order of k_1a and k_2a are approximately the same. Therefore if the wave length is large compared with the fiber radius,

$$Q_{m,i} \cong i^{n+1}\left[zJ_n(-m\delta_i)J_m(\delta_i)\frac{k_1}{k_2}\frac{i^{m+1}e^{im(\theta_0-\varphi_i)}e^{-i(\theta_0-\varphi_i)}}{\left(\frac{\mu_2}{\mu_1}-1\right)\left(\frac{\mu_2}{\mu_1}+1\right)}\frac{(m-1)!}{\left(\frac{k_1a}{2}\right)^{m-1}} - \frac{i^{m+1}}{2\left(\frac{\mu_2}{\mu_1}-1\right)}\sum_{p\neq 0}^{\infty}\frac{J_n(-p\delta_i)J_m(p\delta_i)}{p}\right] \quad \text{and}$$

$$N_{m,i} \cong \frac{i(-1)^m e^{-i(\theta_0-\varphi_i)}}{\left(\frac{\mu_2}{\mu_1}+1\right)}J_m(\delta_i)e^{ik_1R_i\cos(\Phi_i-\theta_0)}k_1a \quad . \tag{4.15}$$

It is apparent that, judging from Equation 4.15, the order of β terms is $O(k_1a)$ in the quasi-static case.

4.2.2 Multiple wave scattering

For a composite in which there are *N* fibers embedded in the matrix, the effect of multiple wave scattering should be considered. The scattering coefficients A_{mi} and B_{mi} in Equation 4.9 and 4.10 for multiple scattering case are the same as in the single fiber scattering, except that F_{mi} terms should include the multiple scattering effects. Thus for the multiple wave scattering case, the displacement both in the matrix and in the fibers is

$$u_i = \begin{cases} u^{in} + \sum_{i=1}^{N} u_{1,i}, r_i > a \\ u_{2,i}, r_i < a \end{cases} \quad . \tag{4.16}$$

Introducing the stress and displacement boundary conditions for all the fibers, we have, for each fiber '*i*'

$$A_{mi} = \frac{E_m}{D_m}F_{mi}$$

$$B_{mi} = \frac{2i}{\pi k_1 a}\frac{F_{mi}}{D_m} + \frac{J_m'(k_1a)}{2mE_m}e^{im(\theta_0-\varphi_i)}\sum_{n'=1}^{\infty}\beta_{n',i}i^{n'+1}J_{n'}(-m\delta_i)$$

$$F_{mi} = e^{ik_1R_i\cos(\Phi_i-\theta_0)}i^m - \frac{zJ_m'(k_2a)}{2mE_m}e^{im(\theta_0-\varphi_i)}\sum_{n'=1}^{\infty}\beta_{n',i}i^{n'+1}J_{n'}(-m\delta_i) \quad ,m\neq 0 \tag{4.17}$$

$$+\sum_{j\neq i}^{N}\sum_{n=-\infty}^{\infty}\frac{E_{m+n}}{D_{m+n}}F_{m+n,j}e^{in(\theta_{ij}-\theta_0)}H_n(k_1r_{ij})$$

and

$$A_{0i} = \frac{E_0}{D_0} F_{0i}$$

$$B_{0i} = \frac{2i}{\pi k_1 a} \frac{F_{0i}}{D_0} + \frac{J_0'(k_1 a)}{4E_0} \beta_{1,i} \delta_i \tag{4.18}$$

$$F_{0i} = e^{ik_1 R_i \cos(\Phi_i - \theta_0)} - \frac{z J_0'(k_2 a)}{4E_0} \beta_{1,i} \delta_i + \sum_{j \neq i}^{N} \sum_{n=-\infty}^{\infty} \frac{E_n}{D_n} F_{n,j} e^{in(\theta_{ij} - \theta_0)} H_n(k_1 r_{ij}).$$

At this point, the general expression for $\beta_{n,i}$ will not be derived as we did in Equation (4.14) and (4.15). Rather the expectation values of $\beta_{n,i}$ are more useful for obtaining the effective wave properties for the composite systems, as will be shown in section 4.5.

4.3 Statistical considerations

4.3.1 Random distribution of the fibers

As stated in Equation 3.13, the correlation probability of the fibers (which is randomly distributed in space) in a composite is a function of three parameters-'n_0', 'a', and 's_t' (again we assign the number 0.1 for all the dynamic cases). For fiber-reinforced composites with interfacial cracks, other parameters which in practice may affect the correlation probability include the half crack length (δ) and the orientation (α). Yet for simplicity, we assume that all interfacial cracks possess the same orientations and half crack length. A mathematical model to accommodate the cracks distribution, if possible in a limited fashion, will be studied in the future. The statistical treatments are similar to those in chapter 3. Again the definition of statistical notation and the probability Equations (2.41-2.45) in chapter 2 still apply for the application in this chapter. And quasi-crystalline approximation (2.40) will be used again.

4.3.2 Use of the properties of indistinguishability of fibers and quasi-crystalline approximation

Observing the third equation of (4.17) and that of (4.18), F_{mi}'s are functions of themselves. They contain the multiple scattering information associated with each fiber '*i*', and the geometrical information of all the fibers other than fiber '*i*'. Therefore they are the terms on which we perform the averaging procedures in order to obtain an overall effective material property for the composite system. The rationale for performing the averaging process is based on the fact that 1) all the fibers are indistinguishable from a random point of view, as stated in the first two equations of (2.42); and 2) the multiple scattering in the composite system is the dual combination of the coherent waves and incoherent waves. Apparently, the averaging material property is the overall effective quantity due to the coherent waves. And the incoherent waves are the non-constructive part of the multiple scattering waves in the composites. Before the averaging process, we follow the elasticity of materials to obtain the displacement fields in the composites. After the averaging process, the contributions from the incoherent waves are lost in the calculation of the effective property of the composite. Hence, the visco-elasticity emerges as

the end result to reflect the fact that part of the multiple scattering energy, i.e., those of the non-coherent waves, is lost.

Due to the indistinguishability of the fibers, one can choose any fiber to investigate the expectation value of F_{mi} without loss of generality. Thus, for fiber '1',

$$
\begin{aligned}
F_{m1} &= e^{ik_1R_1\cos(\Phi_1-\theta_0)}i^m - \frac{zJ_m'(k_2a)}{2mE_m}e^{im(\theta_0-\varphi_1)}\sum_{n=1}^{\infty}\beta_{n,1}i^{n+1}J_n(-m\delta_1) \\
&+\sum_{j=2}^{N}\sum_{n=-\infty}^{\infty}\frac{E_{m+n}}{D_{m+n}}F_{n+m,j}H_n(k_1r_{1j})e^{in(\theta_{1j}-\theta_0)}, m\neq 0 \\
F_{01} &= e^{ik_1R_1\cos(\Phi_1-\theta_0)} - \frac{zJ_0'(k_2a)}{4E_0}\beta_{1,1}\delta_1 \\
&+\sum_{j=2}^{N}\sum_{n=-\infty}^{\infty}\frac{E_n}{D_n}F_{n,j}H_n(k_1r_{1j})e^{in(\theta_{1j}-\theta_0)}.
\end{aligned}
\tag{4.19}
$$

By using Equation 2.41-2.42, the correlation probability defined in the 'well-stirred' approximation (Equation 3.13), the quasi-crystalline approximation (Equation 2.40) and considering a large sample (i.e. the number of fibers N is large), $\langle F_{m1}\rangle_1$ become

$$
\begin{aligned}
\langle F_{m1}\rangle_1 &= e^{ik_1R_1\cos(\Phi_1-\theta_0)}i^m - \frac{zJ_m'(k_2a)}{2mE_m}e^{im(\theta_0-\varphi_1)}\sum_{n=1}^{\infty}\langle\beta_{n,1}\rangle_1 i^{n+1}J_n(-m\delta_1) + \\
&n_0\sum_{n=-\infty}^{\infty}\frac{E_{m+n}}{D_{m+n}}\int_{|\bar{r}_2-\bar{r}_1|\geq 2a}\left(1-e^{2a-r_{12}/(a/n_0)^{s_t}}\right)\langle F_{n+m,2}\rangle_2 H_n(k_1r_{12})e^{in(\theta_{12}-\theta_0)}d\tau_2, m\neq 0 \\
\langle F_{01}\rangle_1 &= e^{ik_1R_1\cos(\Phi_1-\theta_0)} - \frac{zJ_0'(k_2a)}{4E_0}\langle\beta_{1,1}\rangle_1\delta_1 + \\
&n_0\sum_{n=-\infty}^{\infty}\frac{E_n}{D_n}\int_{|\bar{r}_2-\bar{r}_1|\geq 2a}\left(1-e^{2a-r_{12}/(a/n_0)^{s_t}}\right)\langle F_{n,2}\rangle_2 H_n(k_1r_{12})e^{in(\theta_{12}-\theta_0)}d\tau_2.
\end{aligned}
\tag{4.20}
$$

4.4 Extinction theory

The extinction theorem states that the incident wave vanishes upon entering the composite [35], or that the incident wave is canceled by waves generated at the boundary [31]. By applying this theorem, we appeal to the physics, not the mathematics, of Equation (4.20). The setup of the boundary value problems and the solutions of the displacement fields are for obtaining the multiple scattering information inherited by the presence of the fibers and interfacial cracks. Once the scattering formula is established (Equations 4.17 and 4.18), statistical-averaging procedures need to be introduced (Equations 4.19 and 4.20) to obtain the overall effective property of the composite system. By applying the extinction theorem, the energy of incident waves is assumed to be 'transformed' into the scattering waves in the system and all the scattering waves traveling to the infinite boundary of the system are canceled by the

incident wave. Thus in Equation (4.20) the quantities associated with the infinite boundary of the composite, i.e. the upper limit of the integral term on the right hand side of both equations, are canceled by the incident wave. Finally by assuming the existence of an average wave such that $\langle F_{mi} \rangle_i = i^m F_m e^{iKR_i \cos(\Phi_i - \theta_0)}$, where K represents the overall effective wave number in the composite system, Equation (4.20) becomes

$$i^m F_m e^{iKR_1\cos(\Phi_1-\theta_0)} \cong \frac{-zJ_m'(k_2a)}{2mE_m} e^{im(\theta_0-\varphi_1)} \sum_{n=1}^{\infty} \langle \beta_{n,1} \rangle_1 i^{n+1} J_n(-m\delta_1) +$$

$$2\pi n_0 e^{iKR_1\cos(\Phi_1-\theta_0)} i^m \sum_{n=-\infty}^{\infty} \frac{E_{m+n}}{D_{m+n}} F_{n+m} \left[\frac{a}{k_1^2 - K^2} \left(J_n(2Ka) \frac{\partial}{\partial a} H_n(2k_1a) - H_n(2k_1a) \frac{\partial}{\partial a} J_n(2Ka) \right) - \right.$$

$$\left. \int_{2a}^{0} e^{\frac{2a-r_{12}}{(a/n_0)^{st}}} J_n(Kr_{12}) H_n(k_1 r_{12}) r_{12} dr_{12} \right], m \neq 0 \qquad (4.21)$$

$$F_0 e^{iKR_1\cos(\Phi_1-\theta_0)} \cong \frac{-zJ_0'(k_2a)}{4E_0} \delta_1 \langle \beta_{1,1} \rangle_1 +$$

$$2\pi n_0 e^{iKR_1\cos(\Phi_1-\theta_0)} \sum_{n=-\infty}^{\infty} \frac{E_n}{D_n} F_n \left[\frac{a}{k_1^2 - K^2} \left(J_n(2Ka) \frac{\partial}{\partial a} H_n(2k_1a) - H_n(2k_1a) \frac{\partial}{\partial a} J_n(2Ka) \right) - \right.$$

$$\left. \int_{2a}^{0} e^{\frac{2a-r_{12}}{(a/n_0)^{st}}} J_n(Kr_{12}) H_n(k_1 r_{12}) r_{12} dr_{12} \right].$$

4.5 Construction of the linear system of equations

4.5.1 Asymptotic analyses

Asymptotic analyses are needed if Equation (4.21) is to be mathematically manageable. Thus we resort to the fact that, for wave lengths large compared to the radius of the fibers (low frequencies waves, or $k_ia \to \varepsilon$ (a small number), i=1,2), the Bessel functions can be approximated as quantities with power order of k_ia. Therefore by asymptotic approximations of the Bessel functions and Equation (4.21), and assuming that the order of magnitude of the β's terms are $\beta \sim O(k_1a)^t$, then the order of magnitude of F's becomes $F_0 \sim O(k_1a)^{t-1}$ and $F_m \sim O(k_1a)^{t-|m|}$. The statistical average of β terms in Equation 4.21 can be obtained by using boundary conditions which require that the stress on the crack face of each fiber be vanished. Thus for the multiple scattering case we use Equation 4.13 (with '*i*' substitute with '1') as the boundary conditions for vanished stress on the interfacial crack. Bear in mind that for the multiple scattering case, the *F*'s terms in 4.13 are referred to as in Equations 4.19. By performing the low frequencies analyses on Equation 4.13 for the multiple scattering case and considering the order of magnitude of the *F*'s terms ($F_0 \sim O(k_1a)^{t-1}$ and $F_m \sim O(k_1a)^{t-|m|}$), we get

$$\sum_{n=1}^{\infty}\sum_{p=1}^{\infty}\frac{J_m(p\delta_i)J_n(p\delta_i)}{p}i^{n+1}\left((-1)^m+(-1)^n\right)\beta_{n,i}$$
$$=4\frac{\mu_2-\mu_1}{\mu_2+\mu_1}\sum_{p=1}^{\infty}\frac{J_m(p\delta_i)}{p!}\left(\frac{k_1a}{2}\right)^p\left((-1)^{p+m}e^{ip\alpha}F_{-pi}-e^{-ip\alpha}F_{pi}\right) \quad (4.22)$$

Note that in obtaining (4.22), $\alpha=\theta_0-\varphi_i$ (defined as the transversely anisotropic direction) and the first term on the left and right hand side of Equation 4.13 are neglected. Equation (4.22) can be rewritten as $\left[Q_{mn,i}\right]\left\{\beta_{n,i}\right\}=\left\{N_{m,i}\right\}$, where

$$Q_{mn,i}=i^{n+1}\left[(-1)^m+(-1)^n\right]\sum_{p=1}^{\infty}\frac{J_m(p\delta_i)J_n(p\delta_i)}{p}$$
$$N_{m,i}=4\frac{\mu_2-\mu_1}{\mu_2+\mu_1}\sum_{p=1}^{\infty}\frac{J_m(p\delta_i)}{p!}\left(\frac{k_1a}{2}\right)^p\left[(-1)^{p+m}e^{ip\alpha}F_{-pi}-e^{-ip\alpha}F_{pi}\right]. \quad (4.23)$$

Take the conditional statistical average of the above equation and consider the fact that $\left\langle F_{pi}\right\rangle_i=i^pF_pe^{iKR_i\cos(\Phi_i-\theta_0)}$, yields

$$\left\langle\beta_{n,i}\right\rangle_i=\sum_{p=1}^{\infty}\left(\sum_{m=1}^{\infty}q_{nm,i}X_{mp}\right)i^{-p}F_{-p}e^{iKR_i\cos(\Phi_i-\theta_0)}(k_1a)^p+$$
$$\sum_{p=1}^{\infty}\left(\sum_{m=1}^{\infty}q_{nm,i}Y_{mp}\right)i^pF_pe^{iKR_i\cos(\Phi_i-\theta_0)}(k_1a)^p, \quad (4.24)$$

where

$$\left[q_{nm,i}\right]=\left[Q_{mn,i}\right]^{-1}$$
$$X_{mp}=4\frac{\mu_2-\mu_1}{\mu_2+\mu_1}\frac{J_m(p\delta_i)}{p!2^p}(-1)^{p+m}e^{ip\alpha} \quad (4.25)$$
$$Y_{mp}=4\frac{\mu_2-\mu_1}{\mu_2+\mu_1}\frac{J_m(p\delta_i)}{p!2^p}(-1)e^{-ip\alpha}.$$

It will be beneficial, as will be seen later, to transform the *F*'s terms in Equation 4.24 to a new set of quantities. That is, let

$$\overline{F_0}=F_0\times(k_1a)\sim O(k_1a)^t$$
$$\overline{F_p}=F_p\times(k_1a)^p\sim O(k_1a)^t$$
$$\overline{F_{-p}}=F_{-p}\times(k_1a)^p\sim O(k_1a)^t. \quad (4.26)$$

Note that '*p*' in the above equation is a positive integer. Thus the order of magnitude of the $\overline{F}$'s terms are asymptotically the same and (4.24) becomes

$$\left\langle \beta_{n,i} \right\rangle_i = \sum_{p=1}^{\infty}\left(\sum_{m=1}^{\infty} q_{nm,i} X_{mp}\right) i^{-p}\overline{F}_{-p} e^{iKR_i\cos(\Phi_i-\theta_0)} + \sum_{p=1}^{\infty}\left(\sum_{m=1}^{\infty} q_{nm,i} Y_{mp}\right) i^{p}\overline{F}_{p} e^{iKR_i\cos(\Phi_i-\theta_0)} (k_1 a)^p . \tag{4.27}$$

Finally substituting (4.27) to (4.21) and consider the low frequencies limit, we get a homogeneous linear equations in $\overline{F}$'s. Thus for m≥2,

$$\overline{F_{-m}} = \frac{z e^{-im\alpha}(-i)^m}{(m-1)!\left(\frac{\mu_2}{\mu_1}-1\right)}\frac{k_1}{k_2} 2^{m-1}\sum_{n=1}^{\infty}\left\{\sum_{p=1}^{\infty}\left(\sum_{m'=1}^{\infty} q_{nm',i} X_{m'p}\right) i^{-p}\overline{F_{-p}} + \sum_{p=1}^{\infty}\left(\sum_{m'=1}^{\infty} q_{nm',i} Y_{m'p}\right) i^{p}\overline{F_p}\right\} i^{n+1} J_n(m\delta_i),$$

$$\overline{F_m} = \frac{-z e^{im\alpha} i^{-m}}{(m-1)!\left(\frac{\mu_2}{\mu_1}-1\right)}\frac{k_1}{k_2} 2^{m-1}\sum_{n=1}^{\infty}\left\{\sum_{p=1}^{\infty}\left(\sum_{m'=1}^{\infty} q_{nm',i} X_{m'p}\right) i^{-p}\overline{F_{-p}} + \sum_{p=1}^{\infty}\left(\sum_{m'=1}^{\infty} q_{nm',i} Y_{m'p}\right) i^{p}\overline{F_p}\right\} i^{n+1} J_n(m\delta_i)(-1)^n . \tag{4.28}$$

In obtaining the above equation, the positive and negative of '*m*' in the first equation of (4.21) need to be considered separately. Also, in obtaining (4.28) when m≥2, the second term of the right hand side of both equations in (4.21) is neglected. For *m*=-1,

$$\frac{-ze^{-i\alpha}}{\left(\frac{\mu_2}{\mu_1}-1\right)}\frac{k_1}{k_2}\sum_{n=1}^{\infty}\sum_{p=2}^{\infty}\left(\sum_{m'=1}^{\infty} q_{nm',i} X_{m'p}\right) i^{n-p}\overline{F}_{-p} J_n(\delta_i) +$$

$$\left[\frac{cu_1}{1-\left(\frac{K}{k_1}\right)^2} + 1 + \frac{\pi i}{2} cu_1 I_0 - \frac{ze^{-i\alpha}}{\left(\frac{\mu_2}{\mu_1}-1\right)}\frac{k_1}{k_2}\sum_{n=1}^{\infty}\left(\sum_{m'=1}^{\infty} q_{nm',i} X_{m'1}\right) i^{n-1} J_n(\delta_i)\right]\overline{F}_{-1} +$$

$$\left[\frac{cu_0}{1-\left(\frac{K}{k_1}\right)^2}\frac{K}{k_1} + \frac{\pi i}{2} cu_0 I_1\right]\overline{F}_0 + \left[\frac{cu_1}{1-\left(\frac{K}{k_1}\right)^2}\left(\frac{K}{k_1}\right)^2 + \frac{\pi i}{2} cu_1 I_2 - \frac{ze^{-i\alpha}}{\left(\frac{\mu_2}{\mu_1}-1\right)}\frac{k_1}{k_2}\sum_{n=1}^{\infty}\left(\sum_{m'=1}^{\infty} q_{nm',i} Y_{m'1}\right) i^{n+1} J_n(\delta_i)\right]\overline{F}_1 +$$

$$\frac{-ze^{-i\alpha}}{\left(\frac{\mu_2}{\mu_1}-1\right)}\frac{k_1}{k_2}\sum_{n=1}^{\infty}\sum_{p=2}^{\infty}\left(\sum_{m'=1}^{\infty} q_{nm',i} Y_{m'p}\right) i^{n+p}\overline{F}_p J_n(\delta_i) = 0. \tag{4.29}$$

For *m*=0, the first term in the second equation of (4.21) is neglected, therefore

$$\left[\frac{cu_1}{1-\left(\frac{K}{k_1}\right)^2}\left(\frac{K}{k_1}\right)+\frac{\pi i}{2}cu_1I_1\right]\overline{F}_{-1}+\left[\frac{cu_0}{1-\left(\frac{K}{k_1}\right)^2}+1+\frac{\pi i}{2}cu_0I_0\right]\overline{F}_0+\left[\frac{cu_1}{1-\left(\frac{K}{k_1}\right)^2}\left(\frac{K}{k_1}\right)+\frac{\pi i}{2}cu_1I_1\right]\overline{F}_1=0\quad . \tag{4.30}$$

For m=1,

$$\frac{ze^{i\alpha}}{\left(\frac{\mu_2}{\mu_1}-1\right)}\frac{k_1}{k_2}\sum_{n=1}^{\infty}\sum_{p=2}^{\infty}\left(\sum_{m'=1}^{\infty}q_{nm',i}X_{m'p}\right)i^{n-p}\overline{F}_{-p}J_n(\delta_i)(-1)^n+$$

$$\left[\frac{cu_1}{1-\left(\frac{K}{k_1}\right)^2}\left(\frac{k_1}{k_2}\right)^2+\frac{\pi i}{2}cu_1I_2+\frac{ze^{i\alpha}}{\left(\frac{\mu_2}{\mu_1}-1\right)}\frac{k_1}{k_2}\sum_{n=1}^{\infty}\left(\sum_{m'=1}^{\infty}q_{nm',i}X_{m'1}\right)i^{n-1}J_n(\delta_i)(-1)^n\right]\overline{F}_{-1}+\left[\frac{cu_0}{1-\left(\frac{K}{k_1}\right)^2}\frac{K}{k_1}+\frac{\pi i}{2}cu_0I_1\right]\overline{F}_0+$$

$$\left[\frac{cu_1}{1-\left(\frac{K}{k_1}\right)^2}+1+\frac{\pi i}{2}cu_1I_0+\frac{ze^{i\alpha}}{\left(\frac{\mu_2}{\mu_1}-1\right)}\frac{k_1}{k_2}\sum_{n=1}^{\infty}\left(\sum_{m'=1}^{\infty}q_{nm',i}Y_{m'1}\right)i^{n+1}J_n(\delta_i)(-1)^n\right]\overline{F}_1+$$

$$\frac{ze^{i\alpha}}{\left(\frac{\mu_2}{\mu_1}-1\right)}\frac{k_1}{k_2}\sum_{n=1}^{\infty}\sum_{p=2}^{\infty}\left(\sum_{m'=1}^{\infty}q_{nm',i}Y_{m'p}\right)i^{n+p}\overline{F}_pJ_n(\delta_i)(-1)^n=0. \tag{4.31}$$

Note that in (4.29-4.31),

$c=\pi a^2n_0$

$$u_0=\frac{\rho_2}{\rho_1}-1$$

$$u_1=\frac{1-\mu_2/\mu_1}{1+\mu_2/\mu_1} \tag{4.32}$$

$$I_n=\int_{2k_1a}^{0}e^{\frac{2a-\frac{x}{k_1}}{(a/n_0)^{st}}}J_n\left(\frac{K}{k_1}x\right)H_n(x)xdx,n=0,1,2.$$

The I_n terms in the above equation must have an order of magnitude equal to or less than O(1) in order for the asymptotic analyses to be applicable. Thus Equations 4.28-4.31 form a homogeneous linear equation system in $\overline{F}$. By stipulating that the coefficients of $\overline{F}$ terms form a linear matrix and that the determinant of the matrix is equal to zero, the quantity of K/k_1 can be evaluated.

4.5.2 Computational technique

By performing column and row operations (addition, subtraction and multiplication) for the elements of the determinant mentioned previously, a simple equation of the effective wave number K emerges:

$$\left(\frac{K}{k_1}\right)^2 = 1 + cu_0 + \left(cu_1 + cu_0 cu_1\right)\frac{\begin{vmatrix} a_{11} & a'_{12} \\ a'_{21} & a'_{22} \end{vmatrix}}{\begin{vmatrix} a_{11} & a_{12} \\ a_{21} & a_{22} \end{vmatrix}} \quad . \tag{4.33}$$

The numerator of the right-hand side of the above equation is a (2m-1)×(2m-1) determinant and the denominator is a (2m×2m) determinant. More specifically, the a's in Equation 4.33 are all sub-elements structures (see appendix E for the list of a's). The overall effective wave number K in Equation 4.33 is a complex number, i.e.,

$K = \mathrm{Re}(K) + i\,\mathrm{Im}(K)$

where $\mathrm{Re}(K) = \dfrac{\omega}{\mathrm{B}}$. B is the overall effective shear wave phase speed in the composite. A measurement of wave attenuation in the composite is the specific damping capacity, which is defined as $\Psi = 4\pi\dfrac{\mathrm{Im}(K)}{\mathrm{Re}(K)}$.

A Fortran program has been written to perform the computation of $(K/k_1)^2$ in (4.33). Note that for the static case, the probability correlation terms I_n vanishes. In this case the normalized wave number (with respect to the material property of matrix) in (4.33) can be transformed to obtain the normalized shear modulus (as in Equations 3.22 and 3.23). The double summation in the computation of elements of a's (4.33) needs to be carried out for the same number of terms (for our case, we give each summation 30 terms). Also for the Q's terms in (4.23) to be definite, ten-thousand terms are used for the case where the crack length is larger than 0.01 radians. For crack lengths less than or equal to 0.01 radians, we resort to the analytic calculation in the following.

When δ is small ($\delta \le 0.01$) the summation of Q's terms in the first equation of (4.23) can be rewritten as

$$\sum_{p=1}^{\infty} \frac{J_m(p\delta)J_n(p\delta)}{p} = \sum_{p=1}^{\infty} \frac{J_m(p\delta)J_n(p\delta)}{p\delta}\delta \ .$$

Let $\delta \to \Delta x$, a differential form of x, then $p\delta = x_i$. The above summation then becomes

$$\lim_{k\to\infty}\sum_{i=1}^{k} \frac{J_m(x_i)J_n(x_i)}{x_i}\Delta x = \int_0^{\infty} \frac{J_m(x)J_n(x)}{x}dx \quad . \tag{4.34}$$

Using the Weber-Schafheitlin formula [86], the integral in (4.34) can be written as

$$\frac{\Gamma\left[\frac{1}{2}(m+n)\right]}{2\Gamma(n+1)\Gamma\left[\frac{1}{2}(m-n+2)\right]}\times F\left[\frac{1}{2}(n-m),\frac{1}{2}(n+m),(n+1),1\right] \quad , \tag{4.35}$$

where Γ is the Gamma function and F is the hypergeometric function

$$F(\alpha,\beta,\gamma,z)=\left\{1+\frac{\alpha\beta z}{1!\gamma}+\frac{\alpha(\alpha+1)\beta(\beta+1)z^2}{2!\gamma(\gamma+1)}+\cdots\right\}. \tag{4.36}$$

Note that F is one of the solutions of Gauss's equation:

$z(1-z)\frac{d^2y}{dz^2}+\{\gamma-z(\alpha+\beta+1)\}\frac{dy}{dz}-\alpha\beta y=0$, and that

$$F(\alpha,\beta,\gamma,1)=\frac{\Gamma(\gamma)\Gamma(\gamma-\alpha-\beta)}{\Gamma(\gamma-\alpha)\Gamma(\gamma-\beta)} \quad . \tag{4.37}$$

Using Equations (4.34), (4.35) and (4.37), we find that if the crack length is small ($\delta \leq 0.01$ in our program),

$$\sum_{p=1}^{\infty}\frac{J_m(p\delta)J_n(p\delta)}{p}=\frac{\delta_{mn}}{2n} \quad . \tag{4.38}$$

For the dynamic case, where the frequencies of the incident wave are such that $k_1 a$ is less than 0.1 in our program, an iterative scheme needs to be employed. Because the I_n terms of Equation (4.32) are functions of K/k_1, Equation (4.33) cannot be solved explicitly. Hence, similar to chapter 3, an iterative method is used starting with the static value of K/k_1. By substituting the static value of K/k_1 in the last equation of (4.32), initial values of I_n are obtained. Then using these initial values for (4.33), we can get the initial value of K/k_1. Following the same procedures, converging values of K/k_1 are then obtained.

4.6 Numerical results and discussions

In our program, we test the applicability of a fiber-reinforced composite where the fibers have stiffer shear modulus and lighter weight than the matrix (μ_1=1.28e^{10} Pa, μ_2=8.08e^{10}, ρ_1=801 Kg/m^3, ρ_2=234.7 Kg/m^3). Two extreme debonded situations are when 1) there is no crack (δ=0); and 2) the fibers are totally debonded from the matrix ($\delta=\pi$, regarded as the case that the space originally occupied by the fibers is void). For these two extreme cases, the resultant computational shear moduli from our program coincide with those obtained by Hashin and Rosen [27]. Obviously, these two extreme cases render the composites as transversely isotropic material systems. The composite systems become transversely anisotropic when the fibers are partially bonded, as can be seen in Figures 18, 19, 20 and 21.

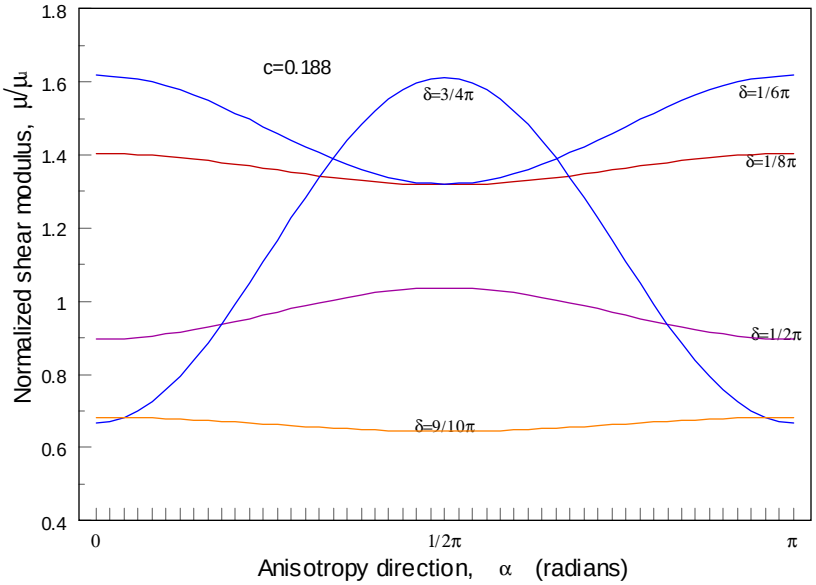

Figure 18. Using normalized shear modulus as a function of anisotropic direction to demonstrate the transverse anisotropy properties for various cases of half crack length at 0.188 fiber vol. fraction.

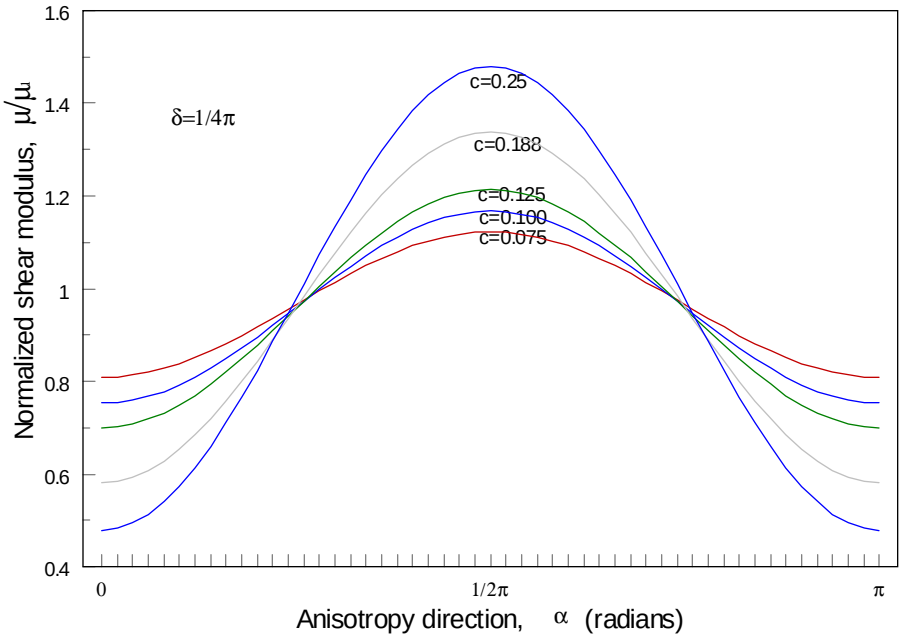

Figure 19. Using normalized shear modulus as a function of anisotropic direction to demonstrate the transverse anisotropy properties for various cases of fiber vol. fraction at 1/4π half crack length.

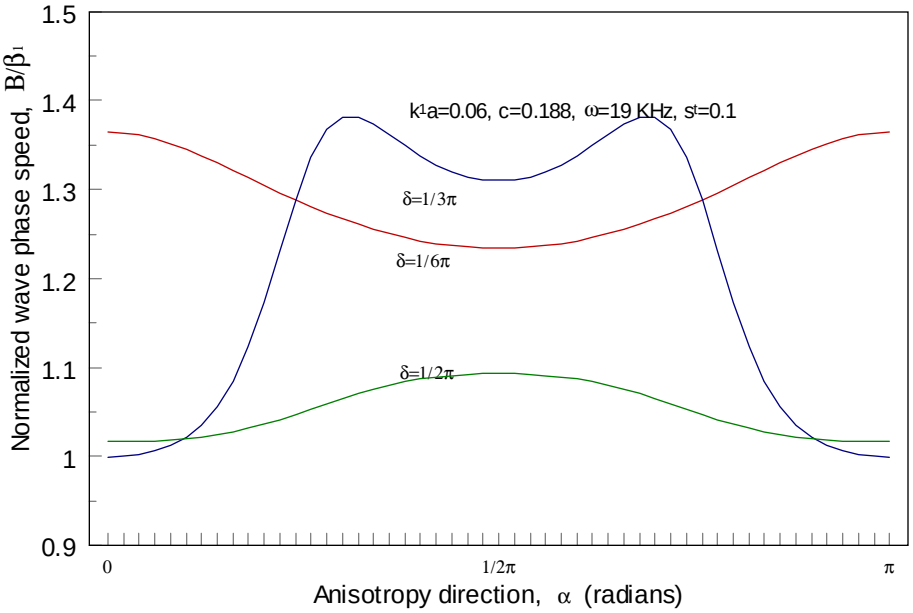

Figure 20. Using normalized shear wave phase speed as a function of anisotropic direction to demonstrate the transverse anisotropy properties for various cases of half crack length at 0.188 fiber vol. fraction.

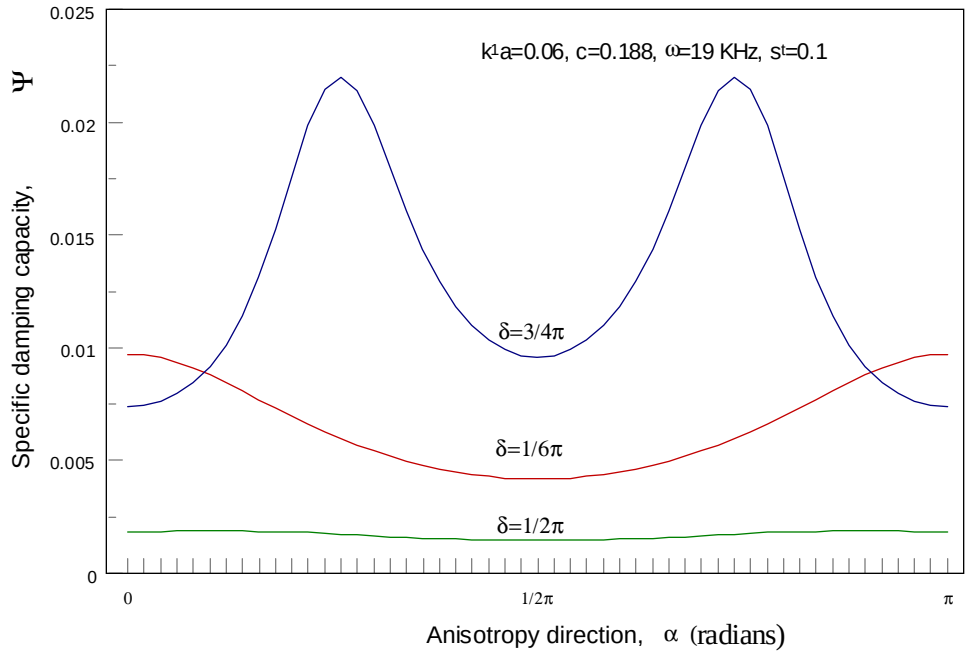

Figure 21. Using specific damping capacity as a function of anisotropic direction to demonstrate the transverse anisotropy properties for various cases of half crack length at 0.188 fiber vol. fraction.

The computational quantities obtained, using Equation (4.33), are normalized wave numbers and are generally complex. For normalized axially shear modulus in the static case, the magnitude of the imaginary part of μ/μ_1 (obtained from the normalized wave number K/k_1) is extremely small compared to that of the real part. Hence for the static case, the shear modulus is a real number and it corresponds to the elasticity of the composite system. For the dynamic case, the magnitude of the imaginary part of K/k_1 is significant compared to that of the real part and it corresponds to the energy dissipation of the composite systems. Only the fact that the calculated shear moduli, the shear wave phase speeds and specific damping capacities are negative numbers or extremely high in some ranges of half crack length conflict with the physics of the composite systems (Figures 22, 23, 24 and 25). These 'jumps' occur in some particular ranges of half crack length for a variety of cases. As the computational results show, the increase of the number of summation terms in our program does not change the resultant magnitude associated with those jumps (i.e., the summation terms are convergent). Therefore the mathematical facts of these 'anomalies' are confirmed and those jumps are finite.

An interesting phenomenon of the transverse anisotropy of the composite system is that it is less pronounced near three ranges of the half crack length. Two of them are, as expected, near $\delta=0$ and $\delta=\pi$. The other one is near, surprisingly, $\delta=\pi/2$ (Figures 18, 20, 21). The fiber volume fraction 'c' also affects the transverse anisotropy of the composite system. As expected, the less the fiber volume concentration, the less anisotropic is the system. These can be observed in Figures 19 and 22 where if the fiber volume fraction is small, then the quantity of μ/μ_1 will be near 1 and the function line will tend to be 'flat' and near 1.

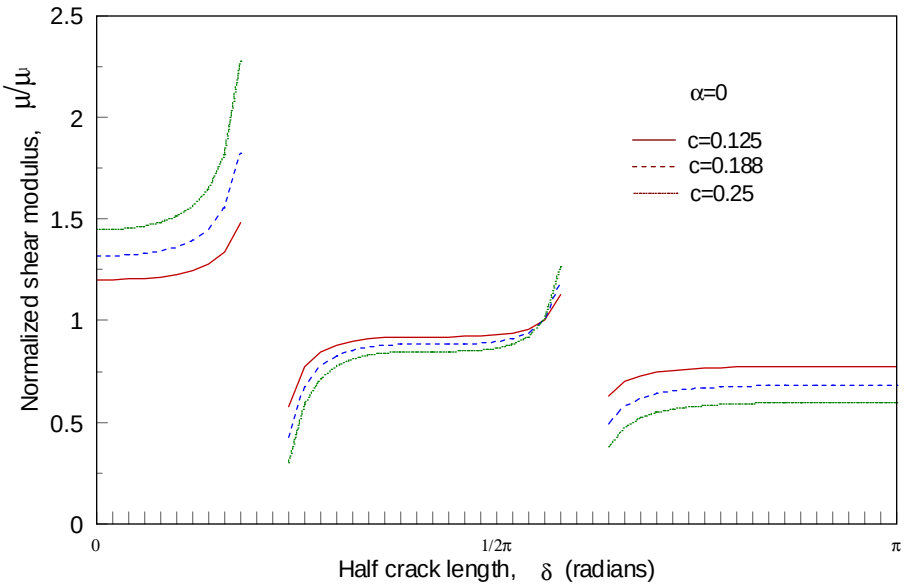

Figure 22. Normalized shear modulus as a function of half crack lengths for various cases of fiber vol. fraction at zero anisotropic direction. Note the 'decreasing steps' fashion as the half crack length increases. Also, the jumps occur near 11/50π, 31/50π.

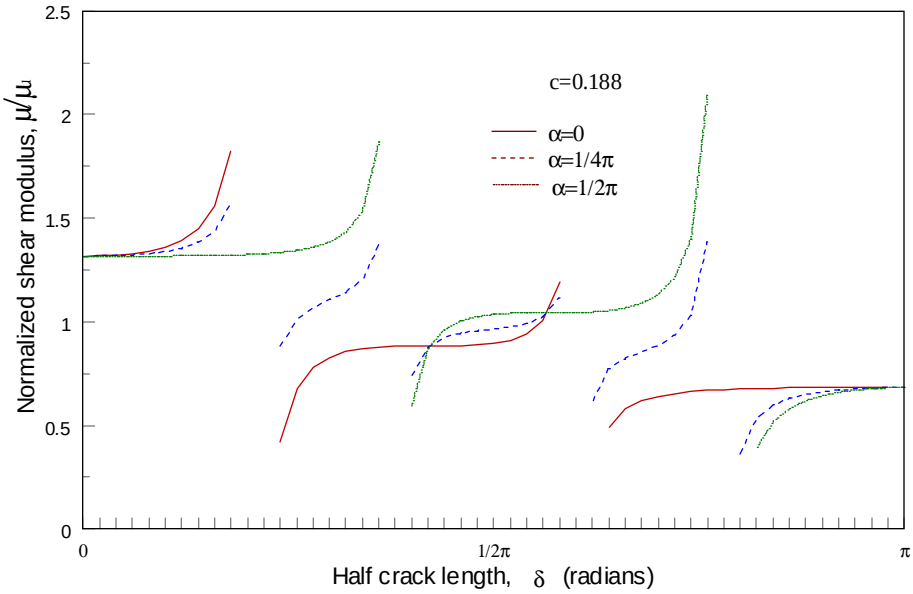

Figure 23. Normalized shear modulus as a function of half crack lengths for various cases of anisotropic direction at 0.188 fiber vol. fraction. Note the 'decreasing steps' fashion as the half crack length increases. Also, for $\alpha=1/2\pi$, jumps occur near $19/50\pi$, $39/50\pi$. For $\alpha=1/4p$, jumps occur near $11/50\pi$, $19/50\pi$, $31/50\pi$, $39/50\pi$. For $\alpha=0$, jumps occur near $11/50\pi$, $31/50\pi$.

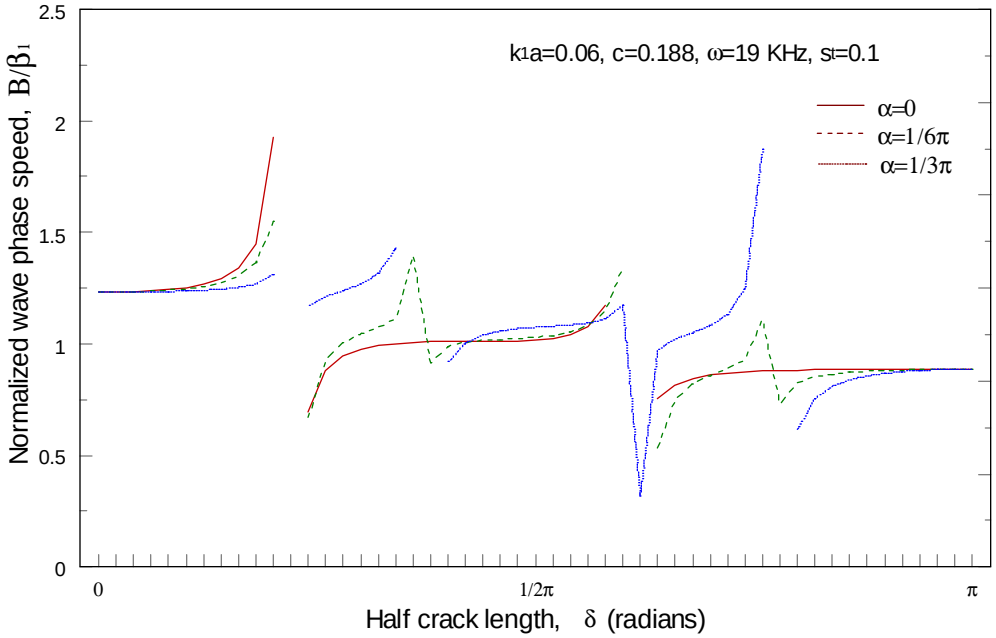

Figure 24. Normalized shear wave phase speed as a function of half crack lengths for various cases of anisotropic direction at 0.188 fiber vol. fraction. The 'decreasing steps' fashion has the same properties as those of the shear modulus. Note that for $\alpha=1/3\pi$, jumps occur near $11/50\pi$, $19/50\pi$, $39/50\pi$. For $\alpha=1/6\pi$, jumps occur near $11/50\pi$, $31/50\pi$. For $\alpha=0$, jumps occur near $11/50\pi$, $31/50\pi$.

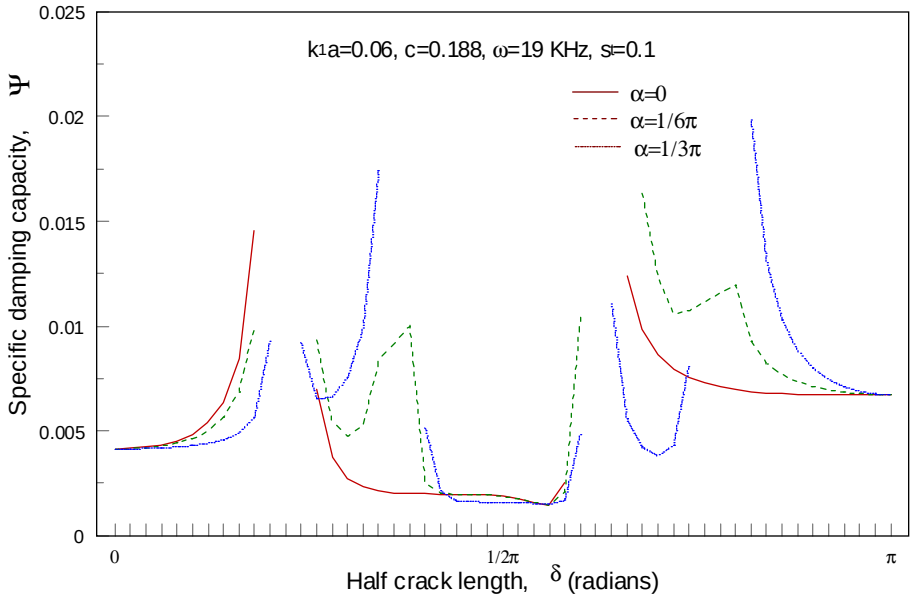

Figure 25. Specific damping capacity as a function of half crack lengths for various cases of anisotropic direction at 0.188 fiber vol. fraction. Note that the least damped range is near the mid-ranges of half crack length. Also, for $\alpha=1/3\pi$, jumps occur near $11/50\pi$, $19/50\pi$, $31/50\pi$, $39/50\pi$. For $\alpha=1/6\pi$, jumps occur near $11/50\pi$, $31/50\pi$. For $\alpha=0$, jumps occur near $11/50\pi$, $31/50\pi$.

Another interesting phenomenon is about the decreasing step tendencies (as functions of half crack length) of the normalized shear modulus and wave speed, as can be observed in Figures 22, 23 and 24. For each step, the function lines are generally leveled before they reach the jump area. This feature, however, cannot be found for the damping capacity as in Figure 25 where the minimum quantity of the damping capacity occurs at the middle step where $1/2\pi$ half crack length locates. This means that for a fiber-reinforced composite with interfacial cracks, the composite system with $1/2\pi$ half crack length is the least attenuated (this fact can also be observed in Figures 21, 30). Finally the locations of the jumps do not correlate with the amount of fiber volume fraction (Figure 22). Rather, they are functions of anisotropic directions (Figures 23, 24 and 25).

The influences of fiber volume fraction ('*c*') on the normalized shear modulus have different trends for different ranges of anisotropic direction (α) and half crack length (δ), as can be seen from Figures 19 and 22, respectively. Roughly speaking, there exist 'critical pairs' of δ and α that the quantity of μ/μ_1 stays approximately constant for any '*c*' (as long as '*c*' is low - $c \leq 0.25$ is sufficient for our case). More specifically, in Figure 22, a normalized shear modulus of approximate magnitude of 1 exists when $\alpha=0$ and δ is near $28/50\pi$. This means that the shear stiffness of a composite system, with zero anisotropic direction and $\delta \cong 28/50\pi$, stays constant for any fiber volume fraction if $c \leq 0.25$. Two other critical pairs of α and δ exist in the 'jump area' where different constant quantities of μ/μ_1 exist. Similarly in Figure 19, two critical pairs of δ and α ($\delta=1/4\pi$, α near$12/50\pi$ or $38/50\pi$) render a normalized shear modulus of approximately 0.94 for $0.075 \leq c \leq 0.25$. These 'critical pair' phenomena can also be seen in Figures 26 and 27. In Figure 26, the influence of 'c' on μ/μ_1 is in an inverse fashion for $\alpha=0$ curve and not for $\alpha=1/6\pi$ curve. Therefore we predict that, given a known half-crack length of $1/3\pi$, there exists an α between 0 and $1/6\pi$ where the magnitude of the fiber volume fraction (for $c \leq 0.25$, at least) does not have any influence on the stiffness of the composite. Similarly in Figure 27, there exists a δ between $1/2\pi$ and $1/3\pi$ where the change of 'c' (for $c \leq 0.25$) does not affect the shear stiffness of the composite. For dynamic mechanical properties, Figure 28 shows that the higher the fiber volume fraction (we fix the magnitude of the fiber radius and vary the number of fibers per unit cross sectional area) the more damping of the composite and the faster the shear wave phase speed. Figure 29 shows that, given a fixed half crack length, the shear wave phase speeds are roughly the same for various anisotropic direction and the change of damping capacity as a function of α is an inverse relationship when $\delta=1/8\pi$. In Figure 30, the change of the wave speeds, given a fixed anisotropic direction of $\alpha=0$, also show the 'decreasing step' fashion as a function of the half crack length. Also in Figure 30, the damping capacity has the lowest quantity in the middle section of δ (where δ is near $1/2\pi$, this reflects the same trends as in Figure 25). Finally, from Figures 28, 29 and 30, the influence of frequencies (low frequencies such that $k_1 a<0.1$) on the wave speeds is non-existent, while it is significant on the damping capacity. Therefore the composite system is non-dispersive and highly visco-elastic in the low frequencies range.

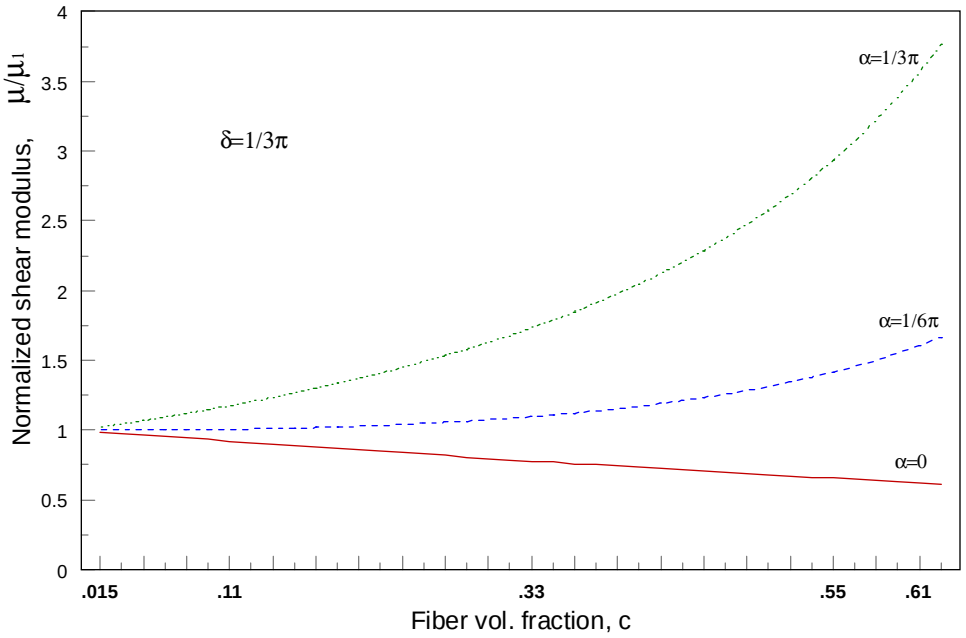

Figure 26. Normalized shear modulus as a function of fiber vol. fraction for various cases of anisotropic directions at 1/3π half crack length. Note that a 'critical pair' exists when $\delta=1/3\pi$ and when a specific anisotropic direction α is between 0 and 1/6 π.

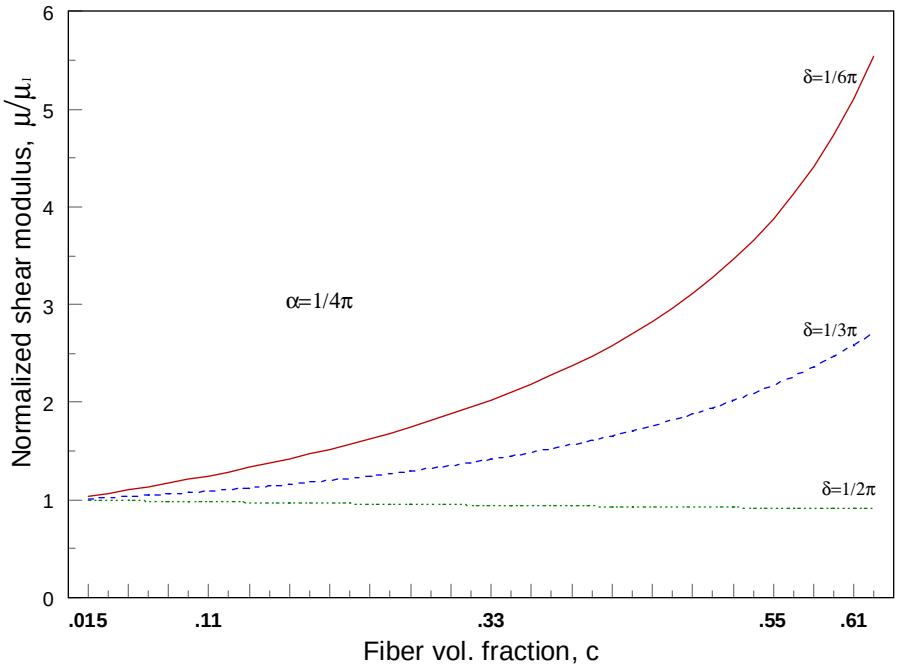

Figure 27. Normalized shear modulus as a function of fiber vol. fraction for various cases of half crack lengths at 1/4π anisotropic direction. Note that a 'critical pair' exists when $\alpha=1/4\pi$ and when a specific half crack length δ is between $1/3\,\pi$ and $1/2\,\pi$.

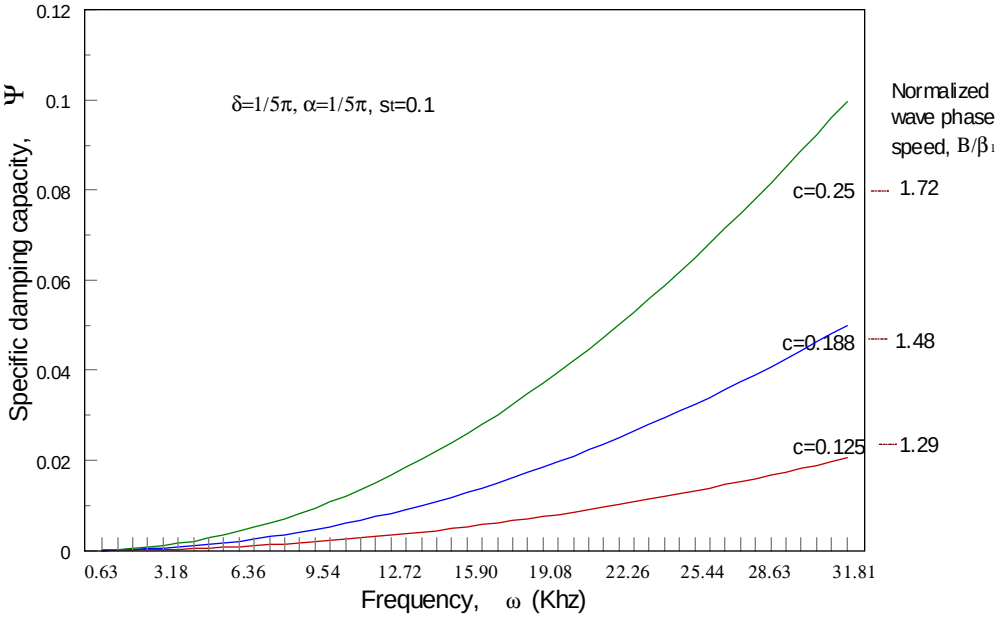

Figure 28. Specific damping capacity as a function of wave frequencies for various cases of fiber vol. fraction at 1/5π half crack length and 1/5π anisotropic direction. Note that the normalized shear wave phase speed does not change for the low frequencies ranges.

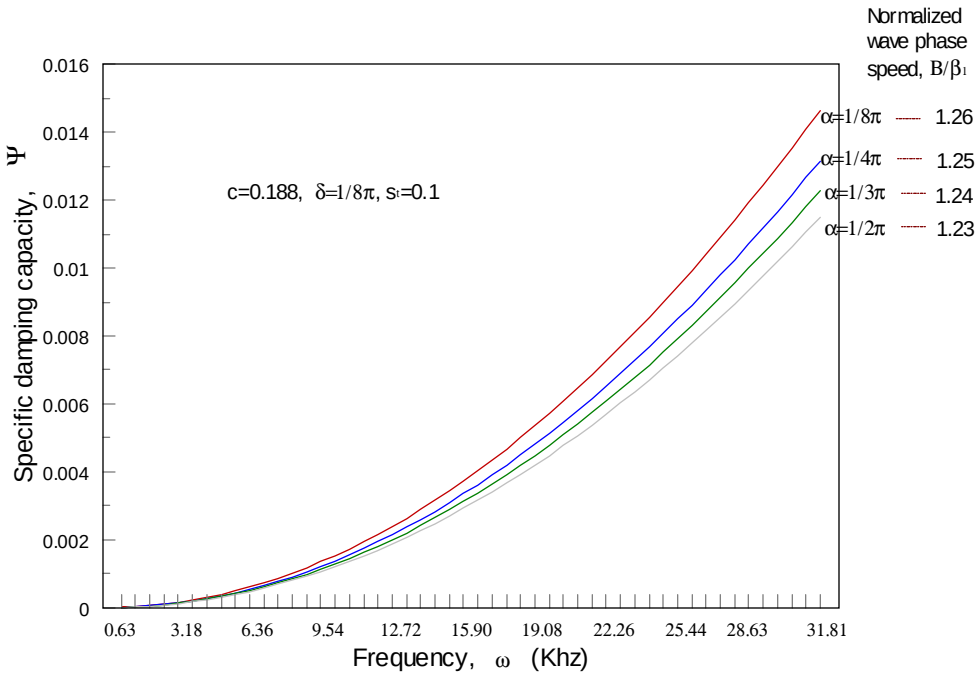

Figure 29. Specific damping capacity as a function of wave frequencies for various cases of anisotropic directions at 1/8π half crack length and 0.188 fiber vol. fraction. Note that the normalized shear wave phase speed does not change for the low frequencies ranges. Also, the change of anisotropic direction does not influence the shear wave phase speed.

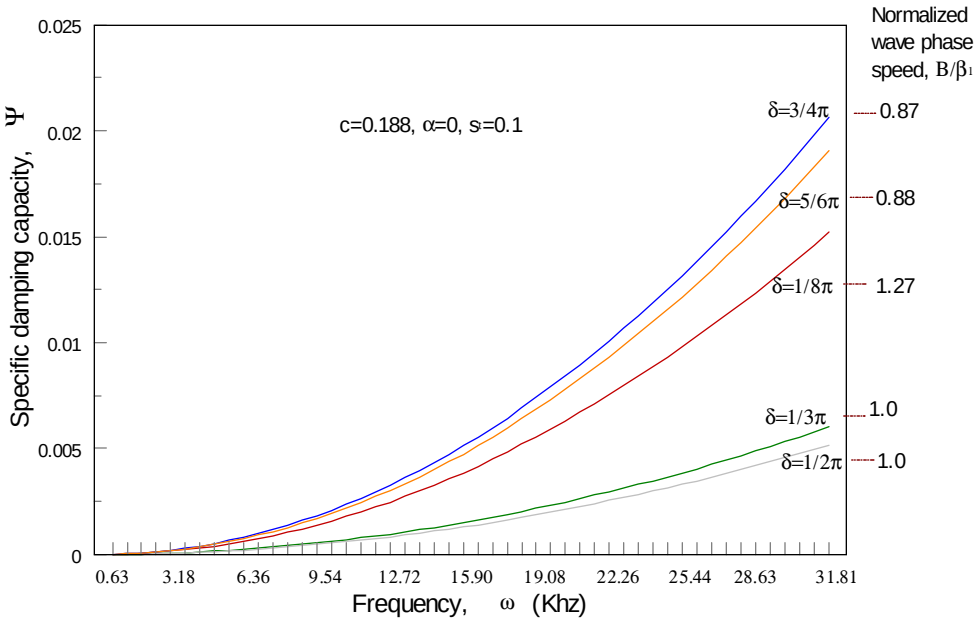

Figure 30. Specific damping capacity as a function of wave frequencies for various cases of half crack lengths at zero anisotropic direction and 0.188 fiber vol. fraction. Note that the normalized shear wave phase speed does not change for the low frequencies ranges. Also, the least damped is near the mid-ranges of half crack length and normalized shear wave speed is in a 'decreasing steps' fashion as the half crack length increases.

4.7 Summary

An ensemble-average statistical method is used to calculate the overall effective mechanical properties of fiber-reinforced composites with interfacial cracks. Specifically cracks are the fiber-matrix interfacial cracks which occur during the manufacturing process or are from inherent material defects. The problem starts with the establishment of the Helmholtz equations and boundary conditions followed by a full scale solution of the multiple scattering equations. Then by considering the low frequencies limit and the statistics of randomly spatial distribution of the fibers, a manageable homogeneous linear matrix equation is obtained. In a homogenized point of view the macroscopic mechanical properties of the composite system are derived. The calculated average mechanical properties include the overall effective shear modulus μ, the average shear wave phase speed B, and the average specific damping capacity Ψ of the composite system. The shear modulus corresponds to the elasticity of the static state, while the shear wave phase speed and damping capacity correspond to the visco-elasticity of the dynamic state of the composite. The results show that, among others:

1. the fiber-reinforced composites with interfacial cracks are transversely anisotropic material systems possessing visco-elastic behavior;
2. as the half crack length (δ) increases, the axial shear modulus of the composite is in a 'decreasing steps' fashion for which finite numerical jumps exist between those steps;
3. for a fiber-reinforced composite with interfacial cracks, the composite system with $1/2\pi$ half crack length is the least attenuated and is nearly transversely isotropic;
4. the composite is a non-dispersed material system in low frequency range.

CHAPTER 5. CONCLUSIONS

Elastic multiple wave scattering problems in time independent steady state condition can be treated by either the many-bodies-single-event approach or the consecutive-events approach. These two approaches have been proven mathematically equivalent in the second chapter. Twersky [52-56] has discussed the same principle, though in problems of electromagnetic nature. In our study, the applications of both approaches have found their use in appropriate situations. While the quasi-crystalline approximation is shown valid in a consecutive-events viewpoint, the effective global material properties of composites can be deduced in an approach combining the many-bodies-single-event and statistical methods. Only in the discussion of the extinction cross-section do we demonstrate some limited physical properties at high frequency (Figure 7). Asymptotic low frequency analyses are essential in solving the boundary value problems and render the equations mathematically manageable, though the wave functions and material properties thus obtained are only satisfied in the Rayleigh (low frequency) limit. Asymptotic analyses in the Rayleigh limit have yielded definitive results from which the physical trends of the fiber-reinforced composites can be simulated. From the consecutive-events viewpoint, a diminishing factor of $\frac{1}{2^4}\left(\frac{\mu_2-\mu_1}{\mu_2+\mu_1}\right)^2$ for the extinction cross-section for the closest arrangement of a two-fibers system is obtained. This can be regarded as a baseline in dealing with the question of whether the effects of higher order scattering need to be taken into account in the case of a dense distribution of fibers. A rough criterion for which the distribution of fibers needs to be considered as 'dense' is whether the higher order scattering effect of the closest two fibers need to be taken into account.

Using the many-bodies-single-event approach and employing statistical methods, effective material properties (axial shear modulus, axial shear wave phase speed and shear wave attenuation) of composite systems can be calculated from Equations 3.21 (for composites with multiple interfacial layers) and 4.33 (for composites with interfacial cracks). For both cases, the modeling has been carried out in straightforward yet rigorous mathematical treatments. Computational results for extreme cases are expectantly reduced to the classical formula obtained by previous researchers. More specifically, normalized shear moduli obtained from Equations 3.21 (when there is no interfacial layers) and 4.33 (when half crack length $\delta=0$ and $\delta=\pi$) reduce to the classical formula in Hashin and Rosen [27]. The main purposes of Equations 3.21 (fiber-reinforced composites with interfacial layers) and 4.33 (fiber-reinforced composites with interfacial cracks) are to predict the dynamic properties of fiber-reinforced composites. Both categories of composite systems are non-dispersive (wave phase speed not being a function of frequencies) yet highly visco-elastic (attenuation of waves) in low frequencies ranges ($k_1 a < 0.1$ for our analyses). For composite systems with elastic interfacial layers, the attenuation is less for those with a more linear and smoothed transition of material properties of layers (Figures 14-16).

For composites with interfacial cracks, as expected, the computational results demonstrate some physical trends yet predict unforeseen results in our cases. Properties of transverse anisotropy are well demonstrated for composites systems with partially bonded fibers, and transverse isotropy is confirmed with extreme situations (when fiber volume fraction 'c' becomes small as in Figure 19, or when the half crack length is $\delta=0$ or $\delta=\pi$). Surprisingly, the computations predict the transverse isotropy of the material system when the half crack length is near $1/2\pi$ (Figures 18, 20 and 21). The stiffness of the composites (shear modulus μ), as the half crack length increases, is decreasing in a step-by-step fashion from the state of perfect bonding ($\delta=0$) to the state of totally debonding ($\delta=\pi$). For each individual step, the quantity of μ is generally leveled until it reaches the jump region. Therefore, in general, the model predicts the weakening of the shear stiffness of the composite as the half crack length grows in spite of the fact that there exists the 'jump anomalies' (Figures 22-24). The wave speeds exhibit the same general trend as the shear moduli do. The damping capacity, generally, has the lowest quantity when half crack length is near $\delta=1/2\pi$. The total debonding case has a higher quantity of damping capacity than the perfect bonding case (Figure 25). Finally for small fiber volume fraction ($c\leq 0.25$), there exist critical pairs of anisotropic direction (α) and half crack length (δ) that the change of c does not influence the magnitude of axially shear modulus of the composite. These critical pairs have not been systematically located; we will do so in the near future.

In retrospect, our model does not claim to be quantitatively precise in predicting the behavior of a composite system, as the finite numerical jumps of the normalized shear moduli clearly show (Figures 22-25). But more importantly, the general trends of the calculated strength and dynamic properties are what we can take into account in designing or inspecting a composite material system. The analyses for composites with interfacial layers would certainly be extended to layers with very low modulus. In this case, a fiber-reinforced composite with totally debonded fibers can be simulated and the results can be compared with the interfacial cracks case in Chapter 4. Finally the visco-elastic effect of the fiber-reinforced composites is only due to the non-constructive (energy scattering by the fibers) wave scattering when waves encounter with the fibers. Throughout the analyses, the fibers and the matrix material are considered as elastic. The visco-elastic material property is resulted from the statistical consideration.

REFERENCES

1. Class note, ESM 5344, 'Wave Propagation in Solids', Virginia Tech, spring semester, 1992.
2. M. J. P. Musgrave, 'On the Propagation of Elastic Waves in Aeolotropic Media. I. General Principle', Proc. Roy. Soc. A226, pp. 339-355, 1954.
3. M. J. P. Musgrave, 'On the Propagation of Elastic Waves in Aeolotropic Media. II. Media of Hexagonal Symmetry', Proc. Roy. Soc. A226, pp. 356-366, 1954.
4. V. T. Buchwald, 'Rayleigh Waves in Transversely Isotropic Media', Q. J. of Mechanics and Applied Mathematics, vol. 14, pt. 3, 1961, pp. 293-317.
5. (1). Edmund G. Henneke II, 'Reflection-Refraction of a Stress Wave at a Plane Boundary between Anisotropic Media', J. Acoust. Soc. Am., vol. 51, no. 1, pp. 210-217, 1972. (2). Edmund G. Henneke II, 'Reflection of an Elastic Wave at a Free Boundary in Hexagonal metals', J. Acoust. Soc. Am., vol. 53, no. 4, pp. 1176-1178, 1973.
6. R. D. Kriz and H. M. Ledbetter, 'Elastic-Wave Surfaces in Anisotropic Media', Rheology of Anisotropic Materials, 1986, pp. 79-91.
7. C. F. Ying and Rohn Truell, 'Scattering of a Plane Longitudinal Wave by a Spherical Obstacle in an Isotropically Elastic Solid', Journal of Applied Physics, vol. 27, no. 9, 1956, pp. 1086-1097.
8. Y.-H. Pao and C. C. Mow, 'Scattering of Plane Compressional Waves by a Spherical Obstacle', Journal of Applied Physics, vol. 34, no. 3, 1963, pp. 493-499.
9. S. K. Datta, 'Diffraction of SH-Waves by an Elliptical Elastic Cylinder', International Journal of Solids and Structures, 1974, vol. 10, pp. 123-133.
10. P. C. Waterman, 'New Formulation of Acoustic Scattering', The Journal of the Acoustical Society of America, vol. 45, no. 6, 1969, pp.1417-1429.
11. Bo Peterson and Staffan Strom, 'Matrix Formulation of Acoustic Scattering from an Arbitrary Number of Scatterers', J. Acoust. Soc. Am., vol. 56, no. 3, 1974, pp. 771-780.
12. Vasundara Varatharajulu and Yih-Hsing Pao, 'Scattering Matrix for Elastic Waves. I. Theory', J. Acoust. Soc. Am., vol. 60, no. 3, 1976, pp. 556-566.
13. Anders Bostrom, 'Multiple Scattering of Elastic Waves by Bounded Obstacles', J. Acoust. Soc. Am., vol. 67, no. 2, 1980, pp. 399-413.
14. Raymond Lim and Roger H. Hackman, 'A Formulation of Multiple Scattering by Many Bounded Obstacles Using a Multi-centered, T Supermatrix', J. Acoust. Soc. Am., vol. 91, no. 2, 1992, pp. 613-638.
15. Raymond Lim, 'Multiple Scattering by Many Bounded Obstacles in a Multilayered Acoustic Medium', J. Acoust. Soc. Am., vol. 92, no. 3, 1992, pp. 1593-1612.
16. Yih-Hsing Pao and Vasundara Varatharajulu, 'Huygens' Principle, Radiation Conditions, and Integral formulas for the Scattering of Elastic Waves', J. Acoust. Soc. Am., vol. 59, no. 6, 1976, pp. 1361-1371.
17. Victor Twersky, 'Multiple Scattering by Arbitrary Configurations in Three Dimensions', Journal of Mathematical Physics, 1962, vol. 3, no. 1, pp. 83-91.

18. T. H. Tan, ‘Theorem on the Scattering and Absorption Cross Section for Scattering of Plane, Time-Harmonic, Elastic Waves’, J. Acoust. Soc. Am., vol. 59, no. 6, 1976, pp. 1265-1267.
19. V. Varatharajulu, ‘Reciprocity Relations and Forward Amplitude Theorems for Elastic Waves’, Journal of Mathematical Physics, vol. 18, no. 4, 1977, pp. 537-543.
20. Jianmin Qu, Jan D. Achenbach and Ronald A. Roberts, ‘Reciprocal Relations for Transmission Coefficients: Theory and Application’, IEEE Transactions on Ultrasonics, Ferroelectrics, and Frequency Control, vol. 36, no. 2, 1989, pp. 280-286.
21. John S. Toll, ‘Causality and the Dispersion Relation: Logical Foundations’, Physical Review, 1956, vol. 104, no. 6, pp. 1760-1770.
22. Richard L. Weaver and Yih-Hsing Pao, ‘Dispersion Relations for Linear Wave Propagation in Homogeneous and Inhomogeneous Media’, J. Math. Phys., 1981, vol 22, no. 9, pp. 1909-1918.
23. Y. C. Angel and J. D. Achenbach, ‘Attenuation and Speed of Antiplane Waves in a Cracked Solid Using the Kramers-Kronig Relations’, J. Acoustic Society of America, 1991, vol. 90(5), pp. 2757-2762.
24. ZVI Hashin, ‘Theory of Mechanical Behavior of Heterogeneous Media’, Applied Mechanics Review, vol. 17, no. 1, 1964, pp. 1-9.
25. ZVI Hashin, ‘Analysis of Composite Materials- A Survey’, Journal of Applied Mechanics, 1983, vol. 50, pp. 481-505.
26. ZVI Hashin, ‘The Elastic Moduli of Heterogeneous Materials’, Journal of Applied Mechanics, March 1962, pp. 143-150.
27. ZVI Hashin and B. W. Rosen, ‘The Elastic Moduli of Fiber-Reinforced Materials’, Jrounal of Applied Mechanics, June 1964, pp. 223-231.
28. ZVI Hashin, ‘Complex Moduli of Viscoelastic Composites-I. General Theory and Application to Particulate Composites’, Int. J. Solids Structures, 1970, vol. 6., pp. 539-552.
29. ZVI Hashin, ‘Complex Moduli of Viscoelastic Composites-II. Fiber Reinforced Materials’, Int. J. Solids Structures, 1970, vol. 6., pp. 797-807.
30. Leslie L. Foldy, ‘The Multiple Scattering of Waves’, Physical Review, 1945, vol. 67, no. 3, pp. 107-119.
31. P. C. Waterman and Rohn Truell, ‘Multiple Scattering of Waves’, Journal of Mathematical Physics, 1961, vol. 2, no. 4, pp. 512-537.
32. Melvin Lax, ‘Multiple Scattering of Waves’, Reviews of Modern Physics, 1951, vol. 23, no. 4, pp. 287-310.
33. Melvin Lax, ‘Multiple Scattering of Waves. II. The Effective Field in Dense Systems’, Physical Review, 1952, vol. 85, no. 4, pp. 621-629.
34. V. Twersky, ‘On Multiple Scattering of Waves’, Journal of Research of the National Bureau of Standards, Section D, Radio Propagation, 1960, vol. 64D, pp. 715-730.
35. (1). S. K. Bose and A. K. Mal, ‘Longitudinal Shear Waves in a Fiber-Reinforced Composite’, International Journal of Solids and Structures, 1973, vol. 9, pp. 1075-1085. (2). S. K. Bose and A. K. Mal, ‘Elastic Waves in a Fiber-Reinforced Composite’, International Journal of Solids and Structures, 1974, vol. 22, pp. 217-229.
36. S. K. Datta, ‘Propagation of SH-Waves Through a Fiber-Reinforced Composites- Elliptic Cylindrical Fibers’, NSF Report, GK-40592x, January 1974.

37. S. K. Datta, H. M. Ledbetter and R. D. Kriz, 'Calculated Elastic Constants of Composites Containing Anisotropic Fibers', International Journal of Solids and Structures, 1984, vol. 20, no. 5, pp. 429-438.
38. J. R. Willis, 'Variational Characterization of Waves in Fiber Reinforced Materials', Mechanics of Composite Material, 1982, pp.191-205.
39. S. K. Datta, H. M. Ledbetter, Y. Shindo and A. H. Shah, 'Phase Velocity and Attenuation of Plane Elastic Waves in a Particle-Reinforced Composite Medium', Wave Motion, vol. 10, 1988, pp. 171-182.
40. Ruey-Bin Yang and A. K. Mal, 'Multiple Scattering of Elastic Waves in a Fiber-Reinforced Composite', J. Mech. Phys. Solids, 1994, vol. 42, no. 12, pp. 1945-1968.
41. R. M. Christensen, 'A Critical Evaluation for a Class of Micro-Mechanical Models', J. Mech. Phys. Solids, 1990, vol. 38, pp. 379-404.
42. J. D. Achenbach and G. Herrmann, 'Dispersion of Free Harmonic Waves in Fiber-Reinforced Composites', AIAA Journal, vol. 6, no. 10, 1968, pp. 1832-1836.
43. J. D. Achenbach, 'Generalized Continuum Theories for Directionally Reinfored solids', Archives of Mechanics, vol. 28, no. 3, 1976, pp. 257-278.
44. A. K. Mal, 'Wave Propagation in Layered Composite Laminates under Periodic Surface Loads', Wave Motion, vol. 10, 1988, pp. 257-266.
45. W. A. Green and E. R. Baylis, 'The Propagation of Impact Stress Waves in Anisotropic Fiber Rein-Forced Laminates', in: Wave Propagation in Structured composites, 1988, ASME/AMD vol. 90, 53-68.
46. E. Rhian Green, 'Transient Impact Response of a Fiber Composite Lamimate', Acta Mechanica, vol. 86, 1991, pp. 153-165.
47. W. Karunasena, A. H. Shah and S. K. Datta, 'Ultrasonic Characterization of Multilayered Thick Composite Plates', Review of Progress in Quantitative Nondestructive Evaluation, vol. 10B, 1991, pp. 1631-1637.
48. W. Anthony Green, 'Reflection and Transmission Phenomena for Transient Stress Waves in Fiber Composite Laminates', Review of Progress in Quantitative Nondestructive Evaluation, vol. 10B, 1991, pp. 1407-1414.
49. W. Anthony Green, 'Surface Wave Propagation in Fiber Composite Laminates', Review of Progress in Quantitative Nondestructive Evaluation, vol. 11, 1992, pp. 185-191.
50. E. R. Baylis and W. A. Green, 'Flexural Waves in Fiber-Reinforced Laminated Plates', Journal of Sound and Vibration, vol. 110, no. 1, 1986, pp. 1-26.
51. E. R. Baylis and W. A. Green, 'Flexural Waves in Fiber-Reinforced Laminated Plates, Part II', Journal of Sound and Vibration, vol. 111, no.2, 1986, pp. 181-190.
52. Vic Twersky, 'Multiple Scattering of Radiation by an Arbitrary Configuration of Parallel Cylinders', The Journal of The Acoustical Society of America, January 1952, vol. 24, no. 1, 42-46.
53. Victor Twersky, 'Multiple Scattering of Radiation by an Arbitrary Planer Configuration of Parallel Cylinders and by Two cylinders', Journal of Applied Physics, April 1952, vol. 23, no. 4, 407-414.
54. V. Twersky, 'On a Multiple Scattering Theory of the Finite Grating and the Wood Anomalies', Journal of Applied Physics, October 1952, vol. 23, no. 10, 1099-1118.

55. Vic Twersky, ‘Multiple Scattering of Waves by Planer Random Distributions of Parallel Cylinders and Bosses’, New York University, Institute of Mathematical Sciences, Division of Electromagnetic Research, Research Report no. EM-58.
56. Vic Twersky, ‘Multiple Scattering of Waves by a Volume Distribution of Parallel Cylinders’, New York University, Institute of Mathematical Sciences, Division of Electromagnetic Research, Research Report no. EM-59.
57. J. D. Achenbach and H. Zhu, ‘Effect of Interfacial Zone on Mechanical Behavior and Failure of Fiber-Reinforced Composites’, J. Mech. Phys. Solids, vol. 37, no. 3, 1989, pp. 381-393.
58. P.-C. Xu and S. K. Datta, ‘Characterization of Fiber-Matrix Interface by Guided Waves: Axisymmetric Case’, J. Acoust. Soc. Am., vol. 89. 1991, pp. 2573-2583.
59. Y. C. Chu and S. I. Rokhlin, ‘Determination of Macro- and Micromechanical and Interfacial Elastic Properties of Composites from Ultrasonic Data’, J. Acoust. Soc. Am., 1992, vol. 92, no. 2, pp. 920-931.
60. Y. C. Chu and S. I. Rokhlin, ‘Determination of Fiber-Matrix Interphase Moduli from Experimental Moduli of Composites with Multi-layered Fibers’, Mechanics of Materials, 1995, vol. 21, pp.191-215.
61. W. Huang, S. Brisuda, and S. I. Rokhlin, ‘Ultrasonic Wave Scattering from Fiber-Matrix Interphases’, J. Acoust. Soc. Am., 1995, vol. 97, no. 2, pp. 807-817.
62. Osamu Tamate and Tetsuyoshi Yamada, ‘Stress in an Infinite Body with a Partially Bonded Circular Cylindrical Inclusion under Longitudinal Shear’, 1969, Technology Report, Tohoku Univ., vol. 34, no. 1, pp. 161-171.
63. M. Toya, ‘ A Crack along the Interface of a Circular Inclusion Embedded in an Infinite Solid’, J. Mech. Phys. Solids, 1974, vol. 22, pp. 325-348.
64. L. B. Freund, ‘The Stress Intensity Factor due to Normal Impact Loading of the Faces of a Crack’, Int. J. Engng. Sci., 1974, vol. 12, pp. 179-188.
65. Y. C. Angel, ‘On the Reduction of Elastodynamic Crack Problems to Singular Integral Equations’, International Journal of Engng. Sci., 1988, vol. 26, no. 7, pp. 757-764.
66. S. Itou, ‘Three-Dimension Wave Propagation in a Cracked Elastic Solid’, Journal of Applied Mechanics, 1978, vol. 45, pp. 807-811.
67. Fred L. Neerhoff, ‘Diffraction of Love Waves by a Stress-Free Crack of Finite Width in the Plane Interface of a Layered Composite’, Applied Scientific Research, 1979, vol. 35, pp. 265-315.
68. A. Bostrom, ‘Elastic Wave Scattering from an Interface Crack: Antiplane Strain’, Journal of Applied Mechanics, 1987, vol. 54, pp. 503-508.
69. S. Krenk and H. Schmidt, ‘Elastic Wave Scattering by a Circular Crack’, Phil. Trans. R. Soc. Lond. A, 1982, vol. 308, pp.167-198.
70. Y. M. Tsai, ‘Dynamic Penny-Shaped Crack in a Transversely Isotropic Material’, Engineering Fracture Mechanics, 1988, vol. 31, no. 6, pp. 977-984.
71. Andrew Norris and Yang Yang, ‘Dynamic Stress on a Partially Bonded Fiber’, Journal of Applied Mechanics, Transactions of the ASME, vol. 58, 1991, pp. 404-409.
72. Y. Yang and A. N. Norris, ‘Shear Wave Scattering from a Debonded Fiber’, J. Mech. Phys. Solids, 1991, vol. 39, no. 2, pp. 273-294.

73. J. D. Achenbach, D. A. Sotiropoulos, and H. Zhu, 'Characterization of Cracks from Ultrasonic Scattering Data', Journal of Applied Mechanics, 1987, vol. 54, pp. 754-760.
74. D. A. Sotiropoulos and J. D. Achenbach, 'Ultrasonic Reflection by a Planar Distribution of Cracks', Journal of Nondestructive Evaluation, 1988, vol. 7, no. 3/4, pp. 123-129.
75. O. Coussy, 'The Influence of Interface Cracks on Wave Motion in Fiber Reinforced Elastic Solids', Journal of Theoretical and Applied Mechanics, 1986, vol. 5, no. 5, pp. 803-823.
76. Jacob Aboudi, 'Wave Propagation in Damaged Composite Materials', International Journal of Solids and Structures, 1988, vol. 24, no. 2, pp. 117-138.
77. A. K. Mal, C.-C. Yin and Y. Bar-Cohen, 'Ultrasonic Nondestructive Evaluation of Cracked Composite Laminates', Composite Engineering, 1991, vol. 1, no. 2, pp. 85-101.
78. Y. C. Angel and Y. K. Koba, 'Propagation of Antiplane Waves in a Multi-Cracked Solid', AMD-vol. 158, Anisotropy and Inhomogenity in Elasticity and Plasticity ASME 1993, pp. 51-57.
79. Luther Pfahler Eisenhart, 'Separable Systems in Euclidean 3-Space', Physical Review, Letter to the Editor, vol. 45, 1934, pp.427-428.
80. Y.-H. Pao and C. C. Mow, Diffraction of Elastic Waves and Dynamic Stress Concentrations(Crane, Russak & Company Inc., New York, 1973), pp. 194-204.
81. A. I. Beltzer, Acoustics of Solids, Springer-Verlag, Berlin; New York, 1988.
82. J. D. Achenbach, A. K. Gautesen and H. Mcmaken, Ray Methods for Waves in Elastic Solids, Boston; London, p. 38-43, 1982.
83. Toshiyuki Oshima, Ronald D. Kriz and Sumio G. Nomachi, 'Simulation and Visualization of Stress Wave Propagation in Composite Laminate with Interphase Layer', Nondestr. Test. Eval., vol. 8-9, pp. 391-403, 1992.
84. Coussy O., Scattering of elastic waves by an inclusion with an interface crack. Wave motion, **6**, 223-236 (1984).
85. Coussy O., Scattering of SH-waves by a rigid elliptic fiber partially debonded from its surrounding matrix. Mech. Res. Communications, **13**, 39-45 (1986).
86. N. W. McLachlan, Bessel functions for engineers, p91, Oxford university press, 1934.
87. George Arfken, Mathematical Methods for Physicists, pp. 67, 2nd ed., Academic Press, 1970.

APPENDIX

Appendix A

In the Rayleigh limit [87], i.e. in the low frequency limit, *ka* is small. That is, as $ka \to \varepsilon$

$$J_0(ka) \to 1 - \frac{(ka)^2}{4}$$

$$J_0'(ka) \to -\frac{ka}{2}$$

$$Y_0(ka) \to \frac{2}{\pi}(\ln ka + \gamma - \ln 2)$$

$$Y_0'(ka) \to \frac{2}{\pi ka}$$

$$J_m(ka) \to \frac{1}{m!}\left(\frac{ka}{2}\right)^m$$

$$J_m'(ka) \to \frac{1}{(m-1)!}\frac{1}{2}\left(\frac{ka}{2}\right)^{m-1}$$

$$H_m(ka) \to \frac{1}{m!}\left(\frac{ka}{2}\right)^m - i\frac{(m-1)!}{\pi}\left(\frac{2}{ka}\right)^m$$

$$H_m'(ka) \to \frac{1}{2(m-1)!}\left(\frac{ka}{2}\right)^{m-1} + i\frac{m!}{ka\pi}\left(\frac{2}{ka}\right)^m \qquad \text{(A1)}$$

where γ is the Euler constant and γ=0.5772156649..., m≥1. From the above, we get

$$E_0 \to O(\varepsilon)$$

$$D_0 \to O(\varepsilon) + iO\left(\varepsilon^{-1}\right)$$

$$\frac{E_0}{D_0} \to iO\left(\varepsilon^2\right)$$

$$E_m \to O\left(\varepsilon^{2m-1}\right) \qquad \text{(A2)}$$

$$D_m \to O\left(\varepsilon^{2m-1}\right) + iO\left(\varepsilon^{-1}\right)$$

$$\frac{E_m}{D_m} \to iO\left(\varepsilon^{2m}\right)$$

.

In the optical limit, i.e. in the high frequency limit, ka is large. That is, as $ka \to \infty$ and $m \geq 0$

$$J_m(ka) \to \sqrt{\frac{2}{\pi ka}}\cos\left(ka - \left(m+\frac{1}{2}\right)\frac{\pi}{2}\right)$$

$$Y_m(ka) \to \sqrt{\frac{2}{\pi ka}}\sin\left(ka - \left(m+\frac{1}{2}\right)\frac{\pi}{2}\right)$$

$$H_m(ka) \to \sqrt{\frac{2}{\pi ka}}\exp\left(i\left(ka - \left(m+\frac{1}{2}\right)\frac{\pi}{2}\right)\right)$$

$$J_m'(ka) \to -\sqrt{\frac{1}{2\pi k^3 a^3}}\cos\left(ka - \left(m+\frac{1}{2}\right)\frac{\pi}{2}\right) - \sqrt{\frac{2}{\pi ka}}\sin\left(ka - \left(m+\frac{1}{2}\right)\frac{\pi}{2}\right) \qquad \text{(A3)}$$

$$Y_m'(ka) \to -\sqrt{\frac{1}{2\pi k^3 a^3}}\sin\left(ka - \left(m+\frac{1}{2}\right)\frac{\pi}{2}\right) + \sqrt{\frac{2}{\pi ka}}\cos\left(ka - \left(m+\frac{1}{2}\right)\frac{\pi}{2}\right)$$

$$H_m'(ka) \to \left(-\sqrt{\frac{1}{2\pi k^3 a^3}} + i\sqrt{\frac{2}{\pi ka}}\right)\exp\left(i\left(ka - \left(m+\frac{1}{2}\right)\frac{\pi}{2}\right)\right)$$

Appendix B

We list the first five orders of scattering coefficients:

$$u_i = \sum_{p=-\infty}^{\infty} A_{pi} H_p\left(k_1 r_i\right) e^{ip\theta_i} \quad \text{where} \quad A_{pi} = u_0 e^{ik_1 R_i \cos\Phi_i} i^p \frac{E_p}{D_p} \tag{B1}$$

$$u_{ij} = \sum_{p=-\infty}^{\infty} A_{pij} H_p\left(k_1 r_i\right) e^{ip\theta_i} \quad \text{where} \quad A_{pij} = u_0 e^{ik_1 R_j \cos\Phi_j} \frac{E_p}{D_p} \sum_{n=-\infty}^{\infty} i^{n+p} \frac{E_{n+p}}{D_{n+p}} H_n\left(k_1 r_{ij}\right) e^{in\theta_{ij}} \tag{B2}$$

$$u_{ijk} = \sum_{p=-\infty}^{\infty} A_{pijk} H_p\left(k_1 r_i\right) e^{ip\theta_i} \quad \text{where}$$

$$A_{pijk} = u_0 e^{ik_1 R_k \cos\Phi_k} \frac{E_p}{D_p} \sum_{m=-\infty}^{\infty} \sum_{n=-\infty}^{\infty} i^{m+n+p} \frac{E_{m+p}}{D_{m+p}} \frac{E_{m+n+p}}{D_{m+n+p}} H_m\left(k_1 r_{ij}\right) H_n\left(k_1 r_{jk}\right) e^{i\left(m\theta_{ij}+n\theta_{jk}\right)} \tag{B3}$$

$$u_{ijkl} = \sum_{p=-\infty}^{\infty} A_{pijkl} H_p\left(k_1 r_i\right) e^{ip\theta_i} \quad \text{where}$$

$$A_{pijkl} = u_0 e^{ik_1 R_l \cos\Phi_l} \frac{E_p}{D_p} \sum_{m=-\infty}^{\infty} \sum_{n=-\infty}^{\infty} \sum_{r=-\infty}^{\infty} i^{m+n+r+p} \frac{E_{m+p}}{D_{m+p}} \frac{E_{m+n+p}}{D_{m+n+p}} \frac{E_{m+n+r+p}}{D_{m+n+r+p}} \times$$
$$H_m\left(k_1 r_{ij}\right) H_n\left(k_1 r_{jk}\right) H_r\left(k_1 r_{kl}\right) e^{i\left(m\theta_{ij}+n\theta_{jk}+r\theta_{kl}\right)} \tag{B4}$$

$$u_{ijklh} = \sum_{p=-\infty}^{\infty} A_{pijklh} H_p\left(k_1 r_i\right) e^{ip\theta_i} \quad \text{where}$$

$$A_{pijklh} = u_0 e^{ik_1 R_h \cos\Phi_h} \frac{E_p}{D_p} \sum_{m=-\infty}^{\infty} \sum_{n=-\infty}^{\infty} \sum_{r=-\infty}^{\infty} \sum_{s=-\infty}^{\infty} i^{m+n+r+s+p} \frac{E_{m+p}}{D_{m+p}} \frac{E_{m+n+p}}{D_{m+n+p}} \frac{E_{m+n+r+p}}{D_{m+n+r+p}} \frac{E_{m+n+r+s+p}}{D_{m+n+r+s+p}} \times$$
$$H_m\left(k_1 r_{ij}\right) H_n\left(k_1 r_{jk}\right) H_r\left(k_1 r_{kl}\right) H_s\left(k_1 r_{lh}\right) e^{i\left(m\theta_{ij}+n\theta_{jk}+r\theta_{kl}+s\theta_{lh}\right)} \tag{B5}$$

Appendix C

$[A]$ is a (2n+2)×(2n+2) matrix which can be represented as

$$
\left[\begin{array}{ccccc}
J_m(k_0a_0) & -J_m(k_1a_0) & -H_m(k_1a_0) & & \\
\mu_0k_0J_m'(k_0a_0) & -\mu_1k_1J_m'(k_1a_0) & -\mu_1k_1H_m'(k_1a_0) & & \\
 & J_m(k_1a_1) & H_m(k_1a_1) & -J_m(k_2a_1) & -H_m(k_2a_1) \\
 & \mu_1k_1J_m'(k_1a_1) & \mu_1k_1H_m'(k_1a_1) & -\mu_2k_2J_m'(k_2a_1) & -\mu_2k_2H_m'(k_2a_1) \\
 & & & \backslash & \backslash \\
 & & & \backslash & \backslash \\
 & & & & \backslash \\
 & & & & \backslash \\
 & & & & \backslash \\
 & & & & \backslash \\
 & & & & \backslash \\
 & & & & \backslash
\end{array}\right.
$$

(C1)

$$
\left.\begin{array}{ccccccc}
\backslash & & & & & & \\
\backslash & & & & & & \\
\backslash & & & & & & \\
\backslash & & & & & & \\
\backslash & & & & & & \\
\backslash & & & & & & \\
J_m(k_{n-2}a_{n-2}) & H_m(k_{n-2}a_{n-2}) & -J_m(k_{n-1}a_{n-2}) & -H_m(k_{n-1}a_{n-2}) & & & \\
\mu_{n-2}k_{n-2}J_m'(k_{n-2}a_{n-2}) & \mu_{n-2}k_{n-2}H_m'(k_{n-2}a_{n-2}) & -\mu_{n-1}k_{n-1}J_m'(k_{n-1}a_{n-2}) & -\mu_{n-1}k_{n-1}H_m'(k_{n-1}a_{n-2}) & & & \\
 & & J_m(k_{n-1}a_{n-1}) & H_m(k_{n-1}a_{n-1}) & -J_m(k_na_{n-1}) & -H_m(k_na_{n-1}) & \\
 & & \mu_{n-1}k_{n-1}J_m'(k_{n-1}a_{n-1}) & \mu_{n-1}k_{n-1}H_m'(k_{n-1}a_{n-1}) & -\mu_nk_nJ_m'(k_na_{n-1}) & -\mu_nk_nH_m'(k_na_{n-1}) & \\
 & & & & J_m(k_na_n) & H_m(k_na_n) & -H_m(ka_n) \\
 & & & & \mu_nk_nJ_m'(k_na_n) & \mu_nk_nH_m'(k_na_n) & -\mu kH_m'(ka_n)
\end{array}\right]
$$

$\{B\}$ is a (2n+2) vector

$$\{B\} = \begin{Bmatrix} 0 \\ 0 \\ 0 \\ | \\ | \\ | \\ 0 \\ 0 \\ e^{ikR\cos\Phi} i^m J_m(ka_n) \\ e^{ikR\cos\Phi} i^m \mu k J_m'(ka_n) \end{Bmatrix} \qquad \text{(C2)}$$

$[A_1]$ is a (2n+1)×(2n+1) matrix

$$\begin{bmatrix}
1 & -\left(\frac{a_0}{a_1}\right)^m & \frac{1}{m}\left(\frac{a_1}{a_0}\right)^m & & \\
0 & \left(\frac{a_0}{a_1}\right)^m(\mu_0-\mu_1) & -\frac{1}{m}\left(\frac{a_1}{a_0}\right)^m(\mu_0+\mu_1) & & \\
 & 1 & -\frac{1}{m} & -\left(\frac{a_1}{a_2}\right)^m & \frac{1}{m}\left(\frac{a_2}{a_1}\right)^m \\
 & 0 & \frac{2}{m}\mu_1 & \left(\frac{a_1}{a_2}\right)^m(\mu_1-\mu_2) & -\frac{1}{m}\left(\frac{a_2}{a_1}\right)^m(\mu_1+\mu_2) \\
 & & & \backslash & \backslash \\
 & & & \backslash & \backslash \\
 & & & & \backslash \\
 & & & & \backslash \\
 & & & & \backslash \\
 & & & & \backslash \\
 & & & & \backslash \\
 & & & & \backslash
\end{bmatrix}$$

(C3)

$$\begin{bmatrix}
\backslash & & & & & \\
\backslash & & & & & \\
\backslash & & & & & \\
\backslash & & & & & \\
\backslash & & & & & \\
\backslash & & & & & \\
\backslash & & & & & \\
1 & -\frac{1}{m} & -\left(\frac{a_{n-2}}{a_{n-1}}\right)^m & \frac{1}{m}\left(\frac{a_{n-1}}{a_{n-2}}\right)^m & & \\
0 & \frac{2}{m}\mu_{n-2} & \left(\frac{a_{n-2}}{a_{n-1}}\right)^m(\mu_{n-2}-\mu_{n-1}) & -\frac{1}{m}\left(\frac{a_{n-1}}{a_{n-2}}\right)^m(\mu_{n-2}+\mu_{n-1}) & & \\
 & & 1 & -\frac{1}{m} & -\left(\frac{a_{n-1}}{a_n}\right)^m & \frac{1}{m}\left(\frac{a_n}{a_{n-1}}\right)^m \\
 & & 0 & \frac{2}{m}\mu_{n-1} & \left(\frac{a_{n-1}}{a_n}\right)^m(\mu_{n-1}-\mu_n) & -\frac{1}{m}\left(\frac{a_n}{a_{n-1}}\right)^m(\mu_{n-1}+\mu_n) \\
 & & & & m(\mu_n-\mu) & \mu_n+\mu
\end{bmatrix}$$

$[A_2]$ is a (2n+2)×(2n+2) matrix

$$
\begin{bmatrix}
1 & -\left(\frac{a_0}{a_1}\right)^m & \frac{1}{m}\left(\frac{a_1}{a_0}\right)^m & & & & & & \\
0 & \left(\frac{a_0}{a_1}\right)^m(\mu_0-\mu_1) & -\frac{1}{m}\left(\frac{a_1}{a_0}\right)^m(\mu_0+\mu_1) & & & & & & \\
 & 1 & -\frac{1}{m} & -\left(\frac{a_1}{a_2}\right)^m & \frac{1}{m}\left(\frac{a_2}{a_1}\right)^m & & & & \\
 & 0 & \frac{2}{m}\mu_1 & \left(\frac{a_1}{a_2}\right)^m(\mu_1-\mu_2) & -\frac{1}{m}\left(\frac{a_2}{a_1}\right)^m(\mu_1+\mu_2) & & & & \\
 & & & \ddots & \ddots & & & & \\
 & & & & 1 \quad -\frac{1}{m} & -\left(\frac{a_{n-2}}{a_{n-1}}\right)^m & \frac{1}{m}\left(\frac{a_{n-1}}{a_{n-2}}\right)^m & & \\
 & & & & 0 \quad \frac{2}{m}\mu_{n-2} & \left(\frac{a_{n-2}}{a_{n-1}}\right)^m(\mu_{n-2}-\mu_{n-1}) & -\frac{1}{m}\left(\frac{a_{n-1}}{a_{n-2}}\right)^m(\mu_{n-2}+\mu_{n-1}) & & \\
 & & & & & 1 & -\frac{1}{m} & -\left(\frac{a_{n-1}}{a_n}\right)^m & \frac{1}{m}\left(\frac{a_n}{a_{n-1}}\right)^m \\
 & & & & & 0 & \frac{2}{m}\mu_{n-1} & \left(\frac{a_{n-1}}{a_n}\right)^m(\mu_{n-1}-\mu_n) & -\frac{1}{m}\left(\frac{a_n}{a_{n-1}}\right)^m(\mu_{n-1}+\mu_n) \\
 & & & & & & m & -1 & 1 \\
 & & & & & & 0 & 2\mu_n & -(\mu+\mu_n)
\end{bmatrix}
\qquad \text{(C4)}
$$

Appendix D

The generating function of Chebyshev polynomial [87] is defined as

$$T_n(x)+iV_n(x)=\left[x+i\left(1-x^2\right)^{1/2}\right]^n, \qquad |x|\le 1 \tag{D1}$$

where

$$T_n(x)=x^n-\binom{n}{2}x^{n-2}\left(1-x^2\right)+\binom{n}{4}x^{n-4}\left(1-x^2\right)^2-\cdots$$

$$V_{n+1}(x)=\sqrt{1-x^2}\,U_n(x) \tag{D2}$$

$$U_n(x)=\left[\binom{n+1}{1}x^n-\binom{n+1}{3}x^{n-2}\left(1-x^2\right)+\binom{n+1}{5}x^{n-4}\left(1-x^2\right)^2-\cdots\right]$$

$T_n(x)$ is the Chebyshev function of type I and $U_n(x)$ is the Chebychev function of type II. Rewrite $V_n(x)$ as

$$V_n(x)=\sqrt{1-x^2}\left[\binom{n}{1}x^{n-1}-\binom{n}{3}x^{n-3}\left(1-x^2\right)+\binom{n}{5}x^{n-5}\left(1-x^2\right)^2-\cdots\right], \text{ n=1,2,3...} \tag{D3}$$

Note that for $x\to\pm1$, $V_n(x)\to O\left(\sqrt{1-(1-\varepsilon)^2}\right)$, i.e., $V_n(x)\to o\left(\varepsilon^{1/2}\right)$ as x approach ±1.

Let $x=\cos\theta$ in equation (D1), then

$$T_n(x)+iV_n(x)=e^{in\theta}.$$

Consequently,

$$\begin{aligned} T_n(x)&=\cos n\theta=\cos\left(n\cos^{-1}x\right)\\ V_n(x)&=\sin n\theta=\sin\left(n\cos^{-1}x\right)\end{aligned} \tag{D4}$$

Furthermore, let $\theta=\pi/2-\alpha$. Thus $x=\cos\theta=\cos(\pi/2-\alpha)=\sin\alpha$. Accordingly

$$V_n(x)=\sin n\theta=\sin n\left(\pi/2-\alpha\right)=\sin\left(n\pi/2-n\sin^{-1}x\right) \qquad \text{n=1,2,3...} \tag{D5}$$

The following formulae are used to perform integration involving Chebychev function:

$$\begin{aligned} &\int_0^{2\pi}e^{iz\cos\theta}\cos n\theta\,d\theta=2\pi i^nJ_n(z)\\ &\int_0^{2\pi}e^{iz\cos\theta}\sin n\theta\,d\theta=0\\ &\int_0^{2\pi}e^{iz\cos\theta}e^{in\theta}\,d\theta=2\pi i^nJ_n(z)\\ &J_{n-1}(x)+J_{n+1}(x)=\frac{2n}{x}J_n(x)\end{aligned} \tag{D6}$$

The integration of Chebychev function is performed as the following

$$\phi_n(\theta_i)=\frac{1}{n}V_n\left(\frac{\theta_i-\varphi_i}{\delta_i}\right)=\frac{1}{n}\sin\left(\frac{n\pi}{2}-n\sin^{-1}\frac{\theta_i-\varphi_i}{\delta_i}\right), \qquad \text{n=1,2,3...}$$

$$\int_{-\delta_i+\varphi_i}^{\delta_i+\varphi_i} \phi_n(\theta_i) e^{-ip(\theta_i-\theta_0)} d\theta_i$$

$$= e^{ip\theta_0} \frac{1}{n} \int_{-\delta_i+\varphi_i}^{\delta_i+\varphi_i} sin\left(n\pi/2 - n \sin^{-1} \frac{\theta_i - \varphi_i}{\delta_i} \right) e^{-ip\theta_i} d\theta_i \quad \text{(D7)}$$

Let $\sin^{-1} \frac{\theta_i - \varphi_i}{\delta_i} = \tau'$, then $\sin\tau' = \frac{\theta_i - \varphi_i}{\delta_i}$, and $d\theta_i = \delta_i \cos\tau' \, d\tau'$. In addition let

$\tau' = \tau - \pi/2$

then equation (D7) becomes

$$e^{ip\theta_0} \frac{1}{n} \int_{-\pi/2}^{\pi/2} \sin\left(n\pi/2 - n\tau' \right) e^{-ip(\varphi_i + \delta_i \sin\tau')} \delta_i \cos\tau' \, d\tau'$$

$$= (-1)^{n+1} e^{ip(\theta_0 - \varphi_i)} \frac{\delta_i}{n} \frac{1}{4} \int_{-\pi}^{\pi} e^{ip\delta_i \cos\tau} \left[\cos(n-1)\tau - \cos(n+1)\tau \right] d\tau \quad \text{(D8)}$$

Summarily, the integration of Chebychev function is

$$\int_{-\delta_i+\varphi_i}^{\delta_i+\varphi_i} \phi_n(\theta_i) e^{-ip(\theta_i-\theta_0)} d\theta_i$$

$$= \begin{cases} \frac{(-1)^{n+1} \pi \delta_i}{2n} \delta_{1n}, \; p = 0 \\ e^{ip(\theta_0 - \varphi_i)} \frac{\pi}{p} i^{n+1} J_n(-p\delta_i), \; p \neq 0 \end{cases} \quad \text{, n=1,2,3…} \quad \text{(D9)}$$

Appendix E

$$a_{11}=\begin{bmatrix} a_{11,mm} & & & a_{11,m1} \\ & \ddots & & \vdots \\ & & \ddots & \vdots \\ & & a_{11,22} & a_{11,21} \\ a_{11,1m} & \cdots & \cdots & a_{11,12} \quad a_{11,11} \end{bmatrix} \tag{E1}$$

where

$$a_{11,rm}=\begin{cases} \dfrac{z}{\left(\dfrac{\mu_2}{\mu_1}-1\right)}\dfrac{k_1}{k_2}\displaystyle\sum_{n=1}^{\infty}\sum_{p=1}^{\infty}q_{np,i}J_n(\delta_i)\left[e^{-i\alpha}+e^{i\alpha}(-1)^n\right]\left(X_{p1}i^{n-3}+Y_{p1}i^{n+1}\right)+2(1+cu_1)+\pi icu_1(I_0-I_2), r=m=1 \\ \dfrac{z}{(m-1)!\left(\dfrac{\mu_2}{\mu_1}-1\right)}\dfrac{k_1}{k_2}2^{m-1}\displaystyle\sum_{n=1}^{\infty}\sum_{p=1}^{\infty}q_{np,i}J_n(m\delta_i)\left[e^{-im\alpha}+e^{im\alpha}(-1)^n\right]\left(X_{pm}i^{n+2m-1}+Y_{pm}i^{n+1}\right)+2, r=m\neq 1 \\ \dfrac{z}{(m-1)!\left(\dfrac{\mu_2}{\mu_1}-1\right)}\dfrac{k_1}{k_2}2^{m-1}\displaystyle\sum_{n=1}^{\infty}\sum_{p=1}^{\infty}q_{np,i}J_n(m\delta_i)\left[e^{-im\alpha}+e^{im\alpha}(-1)^n\right]\left(X_{pr}i^{n-r-m-1}+Y_{pr}i^{n+r-m+1}\right), r\neq m \end{cases} \tag{E2}$$

$$a_{12}=\begin{bmatrix} a_{12,m1} & & & a_{12,mm} \\ \vdots & & \iddots & \\ \vdots & \iddots & & \\ a_{12,21} & a_{12,22} & & \\ a_{12,11} & a_{12,12} & \cdots\ \cdots & a_{12,1m} \end{bmatrix},\quad a'_{12}=\begin{bmatrix} a_{12,m2} & & a_{12,mm} \\ \vdots & \iddots & \\ \vdots & \iddots & \\ a_{12,22} & & \\ a_{12,12} & \cdots\ \cdots & a_{12,1m} \end{bmatrix} \tag{E3}$$

where

$$a_{12,rm}=\begin{cases} \dfrac{z}{\left(\dfrac{\mu_2}{\mu_1}-1\right)}\dfrac{k_1}{k_2}\displaystyle\sum_{n=1}^{\infty}\sum_{p=1}^{\infty}q_{np,i}Y_{p1}i^{n-1}J_n(\delta_i)\left[e^{-i\alpha}+e^{i\alpha}(-1)^n\right]-(1+cu_1)+\frac{\pi}{2}icu_1(I_2-I_0), r=m=1 \\ \dfrac{z}{(m-1)!\left(\dfrac{\mu_2}{\mu_1}-1\right)}\dfrac{k_1}{k_2}2^{m-1}\displaystyle\sum_{n=1}^{\infty}\sum_{p=1}^{\infty}q_{np,i}Y_{pm}i^{n-1}J_n(m\delta_i)\left[e^{-im\alpha}+e^{im\alpha}(-1)^n\right]-1, r=m\neq 1 \\ \dfrac{z}{(m-1)!\left(\dfrac{\mu_2}{\mu_1}-1\right)}\dfrac{k_1}{k_2}2^{m-1}\displaystyle\sum_{n=1}^{\infty}\sum_{p=1}^{\infty}q_{np,i}Y_{pr}i^{n+r-m-1}J_n(m\delta_i)\left[e^{-im\alpha}+e^{im\alpha}(-1)^n\right], r\neq m \end{cases} \tag{E4}$$

$$a_{21}=\begin{matrix} a_{21,1m} & \cdots & \cdots & a_{21,12} & a_{21,11} \\ & & & a_{21,22} & a_{21,21} \\ & & \iddots & \vdots & \vdots \\ & \iddots & & \vdots & \vdots \\ a_{21,mm} & & & a_{21,m1} & \end{matrix},\quad a'_{21}=\begin{matrix} a_{21,2m} & \cdots & \cdots & a_{21,22} & a_{21,21} \\ & & \iddots & & \vdots \\ & \iddots & & & \vdots \\ & & & & \end{matrix} \tag{E5}$$

where

$$a_{21,rm}=\begin{cases} \dfrac{ze^{i\alpha}}{\left(\dfrac{\mu_2}{\mu_1}-1\right)}\dfrac{k_1}{k_2}\displaystyle\sum_{n=1}^{\infty}\sum_{p=1}^{\infty}q_{np,i}J_n(\delta_i)(-1)^n\left(X_{p1}i^{n-1}+Y_{p1}i^{n-1}\right)-(1+cu_1)+\frac{\pi}{2}icu_1(I_2-I_0), r=m=1 \\ \dfrac{ze^{im\alpha}}{(m-1)!\left(\dfrac{\mu_2}{\mu_1}-1\right)}\dfrac{k_1}{k_2}2^{m-1}\displaystyle\sum_{n=1}^{\infty}\sum_{p=1}^{\infty}q_{np,i}J_n(m\delta_i)(-1)^n\left(X_{pm}i^{n-2m+1}+Y_{pm}i^{n-1}\right)-1, r=m\neq 1 \\ \dfrac{ze^{im\alpha}}{(m-1)!\left(\dfrac{\mu_2}{\mu_1}-1\right)}\dfrac{k_1}{k_2}2^{m-1}\displaystyle\sum_{n=1}^{\infty}\sum_{p=1}^{\infty}q_{np,i}J_n(m\delta_i)(-1)^n\left(X_{pr}i^{n-r-m+1}+Y_{pr}i^{n+r-m-1}\right), r\neq m \end{cases} \tag{E6}$$

$$a_{22}=\begin{matrix} a_{22,11} & a_{22,12} & \cdots & \cdots & a_{22,1m} \\ a_{22,21} & a_{22,22} & & & \\ \vdots & & \ddots & & \\ \vdots & & & \ddots & \\ a_{22,m1} & & & a_{22,mm} & \end{matrix},\quad a'_{22}=\begin{matrix} a_{22,22} & \cdots & \cdots & a_{22,2m} \\ \vdots & \ddots & & \\ \vdots & & \ddots & \\ a_{22,m2} & & & a_{22,mm} \end{matrix} \tag{E7}$$

where

$$a_{22,rm}=\begin{cases} \dfrac{ze^{i\alpha}}{\left(\dfrac{\mu_2}{\mu_1}-1\right)}\dfrac{k_1}{k_2}\displaystyle\sum_{n=1}^{\infty}\sum_{p=1}^{\infty}q_{np,i}Y_{p1}i^{n+1}J_n(\delta_i)(-1)^n+1+\frac{\pi}{2}icu_1I_0, r=m=1 \\ \dfrac{ze^{im\alpha}}{(m-1)!\left(\dfrac{\mu_2}{\mu_1}-1\right)}\dfrac{k_1}{k_2}2^{m-1}\displaystyle\sum_{n=1}^{\infty}\sum_{p=1}^{\infty}q_{np,i}Y_{pm}i^{n+1}J_n(m\delta_i)(-1)^n+1, r=m\neq 1 \\ \dfrac{ze^{im\alpha}}{(m-1)!\left(\dfrac{\mu_2}{\mu_1}-1\right)}\dfrac{k_1}{k_2}2^{m-1}\displaystyle\sum_{n=1}^{\infty}\sum_{p=1}^{\infty}q_{np,i}Y_{pr}i^{n+r-m-1}J_n(m\delta_i)(-1)^n, r\neq m \end{cases} \tag{E8}$$

VITA

Wenlung Liu

was born on November 21, 1961 in Taipei City, Taiwan. He entered college in 1980 and studied Industrial Engineering for two years. In 1982, he continued his college education at Chung-Yuan University where he studied Civil Engineering for 3 years and earned his Bachelor of Science degree in Civil and Hydraulic Engineering. After finishing the college education, he served in the military as a commissioned officer with the rank of second lieutenant for two years to fulfill the obligations as a male citizen of Taiwan. In 1989, he came to the United States to start graduate studies in Aerospace Engineering in Mississippi State University and obtained his Master of Science degree in the summer of 1991. Armed with the knowledge of the Finite element method and wave propagation, he then sought to enter the Ph. D. program in the Engineering Science and Mechanics Department at Virginia Tech. He completed his Ph. D. degree in May of 1997. Wenlung will start his career as a research engineer specialized in waves and NDE method.